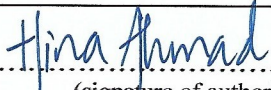




Universitetet
i Stavanger

FACULTY OF SCIENCE AND TECHNOLOGY

MASTER'S THESIS

Study programme/specialisation: Biological Chemistry	Spring semester, 2018 Open/Confidential
Author: Hina Ahmad	 (signature of author)
Programme coordinator: Supervisor(s)	Peter Ruoff Hanne R. Hageland / Tia Tidwell / Steinar Evje
Title of master's thesis: Modelling 3D Cancer Growth and Extracellular Matrix Properties <i>In Vitro</i>	
Credits: 60 ECTS	
Keywords: Extracellular Matrix (ECM), Tumor Microenvironment (TME), Young's Modulus (YM), Hooks Law, Darcy's Law, Colorectal Cancer, Cancer Metabolism, Glycolysis, Oxidative Phosphoraylation (OXPHOS), Gel Contraction Assay (GCA), Interstitial Fluid Flow	Number of pages:101..... + supplemental material/other:10..... Stavanger, August 15, 2018 date/year

UNIVERSITY OF STAVANGER

MASTER THESIS

**Modelling 3D Cancer Growth and
Extracellular Matrix Properties *In Vitro***

by

Hina Ahmad

A thesis submitted in partial fulfillment for the
degree of Master of Science in Biological Chemistry

in the

Department of Mathematics and Natural Sciences
Faculty of Science and Technology

Faculty Supervisor: Hanne R. Hagland

Co-supervisor: Tia Tidwell / Steinar Evje

August 2018

Declaration of Authorship

I, HINA AHMAD, declare that this thesis titled, 'Modelling 3D Cancer Growth and Extracellular Matrix Properties *In Vitro*' and the work presented in it is my own. I confirm that:

- This work was done wholly or mainly while in candidature for a research degree at this University.
- It is clearly stated if and where any part of this thesis has previously been submitted for a degree or any other qualification at this University or any other institution.
- It is clearly attributed where I have consulted the published work of others.
- The source is provided where I have quoted from the work of others. Apart from such quotations, this thesis is entirely my own work.
- I have acknowledged all main sources of help.
- Where the thesis is based on work done by myself jointly with others, I have made clear exactly what was done by others and what I have contributed myself.

Signed:

Hina Ahmad

Date:

15 August 2018

“Research is formalized curiosity. It is poking and prying with a purpose.”

Zora Neale Hurston

Abstract

BACKGROUND: Cancer can be defined as loss of normal behavior of cellular components thus losing tissue organization and giving rise to a tumor microenvironment (TME). Increased matrix stiffness, strain and elevated interstitial fluid flow and/or pressure of extracellular matrix (ECM) in TME is characterized as the cause of initiation and progression of tumorigenesis. The purpose of this study is to develop an understanding of physical and mechanical forces that contribute in remodeling of extracellular matrix in a cancerous environment to promote cancer development using a 3D cell culture model with collagen to mimic in-vivo microenvironment.

METHODS: Type I collagen was used to create a 3D model to investigate the mechanical properties under various conditions like changes in concentration, polymerization pH and temperature, and presence of colorectal cancer cell lines, SW948 and SW1116, were used that exhibit differential metabolic phenotypes. Co-culture with fibroblast, CCD-18Co was evaluated to recapitulate the stromal environment that the cells encounter in vivo to elucidate the changes ECM go through during tumor progression. A microfluidic cell culture system was used to apply fluid flow and pressure gradient to a 3D collagen scaffold to understand the role of interstitial flow in matrix organization, cancer growth and migration during cancer progression.

RESULTS: Mechanical testing of acellular collagen showed Young's Modulus of 44 KPa in 2 mg/ml while 88 KPa in 4 mg/ml collagen gel. Collagen with polymerization pH range of 7.4-6.1 showed a 73% decrease in collagen stiffness in 2 mg/ml acellular collagens while 26% decrease in 4 mg/ml sample. Independent co-culture with fibroblast (CCD-18Co) of cancer cells SW948 and SW1116 showed an increase in YM by 39% and 37% in 2mg/ml collagen while a decrease in YM by 85% and 43% respectively in 4 mg/ml gel. Fibroblast mono-culture gel showed most contraction (79%) in 2 mg/ml while among cancer cells, co-cultured SW1116 (78%) with fibroblast showed most contraction then SW948 (60%) in 2 mg/ml sample. Highest cell migration under normal interstitial flow with fibroblast embedded collagen resulting in 734 migrated cell of SW948 and 350 cells of SW1116.

CONCLUSIONS: The study has established that pure biophysical forces from cancer or fibroblast cells can optimize the mechanical properties of extracellular matrix. Young's Modulus increased with increasing gel concentration. Collagen cancer and fibroblast co-cultured gel showed an increase in stiffness in 2mg/ml collagen while a decrease in YM in 4 mg/ml gel. Gel contraction assay showed highest contraction in fibroblast mono-culture gel samples while SW1116 gel co-cultured with fibroblast showed most contraction. Highest cell migration was observed by SW948 under normal flow with fibroblast embedded 2 mg/ml collagen. In summary it can be concluded that it is important to consider both tumor microenvironment and phenotype of cancer cells when considering regulation of extracellular matrix.

Acknowledgements

Foremost, I would like to express my sincere gratitude to my advisor Prof. Hanne R. Hagland for her expert guidance, continuous support and encouragement to improve my knowledge and understanding throughout the thesis work.

I would like to thank Tia Tidwell for her patience and stimulating discussions to steer me in the right direction. Her guidance helped me throughout the research and writing of this thesis. I could not have imagined having a better advisor and mentor. I would also like to thank Prof. Steinar Evje for his insightful comments and suggestions for my work.

My sincere thanks also go to Sigurd Øines from Nofima for training me to use Texture Analyser and being patient with all my questions. Thanks to my fellow lab mates, Cecilie Lindseth, Sam Danby, Alexandra Szwedó and Leena Shinde for being there to discuss and support each other during the master program. Thanks to Abdelnour Alhourani for his support towards the end of my thesis with his vast knowledge in data analysis. Thanks to CORE team for their help and assistance throughout the thesis work.

Last but not the least, I would like to thank my family for their unconditional love and support, especially my husband who have been so understanding and encouraged me to accomplish my goals.

Contents

Declaration of Authorship	i
Abstract	iii
Acknowledgements	v
List of Figures	ix
List of Tables	xi
Abbreviations	xii
1 Introduction	1
1.1 Colorectal Cancer	1
1.2 Extracellular Matrix	4
1.2.1 Tumor Microenvironmnet	5
1.2.2 Metabolism	7
1.3 Biomechanical Properties of Extracellular Matrix	8
1.3.1 Mechanical properties of cellular environment	9
1.3.2 Interstitial fluid flow in cellular environment	11
1.4 Aim and Objectives	12
2 Materials and Methods	14
2.1 Materials	14
2.1.1 Colorectal cell lines	14
2.1.2 Reagents	15
2.1.3 Prepared solutions	16
2.1.3.1 3D Culture Media	16
2.1.3.2 Cell Culture Media	17
2.1.3.3 100 mM HEPES with 2x PBS	17

2.1.3.4	5N and 0,5N NaOH	18
2.1.3.5	3,7 % and 1,85 % HCl	18
2.1.3.6	1x PBS	18
2.1.3.7	Fluorospheres microspheres Beads	18
2.1.4	Consumables	19
2.1.5	Instruments	19
2.2	Methods	20
2.2.1	Cell Culture	20
2.2.2	Collagen Gel Preparation	20
2.2.3	Collagen Gel Preparation with Cell Co-Culture	21
2.2.4	Characterization of Mechanical Properties of Collagen Gel	22
2.2.4.1	Collagen Mechanical Test Protocol	22
2.2.5	Structural Analysis of Collagen Gel with Confocal Reflection Microscopy (CRM)	26
2.2.5.1	Preparation	26
2.2.5.2	Confocal Imaging	27
2.2.6	Cell-Matrix Interaction Analysis with Collagen Gel Contraction Assay (GCA)	27
2.2.7	Interstitial Fluid Flow and Cell Migration Analysis in 3D Model	28
2.2.7.1	Preparation	28
2.2.7.2	Testing Volumetric flow (Q), and Collagen Permeability, k	30
2.2.7.3	Testing interstitial flow and cell migration through collagen	30
2.2.7.4	Fixation of Cell culture Chips	32
2.2.7.5	Confocal imaging	32
2.2.8	Data Analysis	33
2.2.8.1	Mechanical testing of collagen	33
2.2.8.2	Structural analysis of collagen gel – Confocal Reflection Microscopy (CRM)	36
2.2.8.3	Cell-Matrix Interaction Analysis with Collagen Gel Contraction Assay (GCA)	37
2.2.8.4	Interstitial Fluid flow and Cell Migration Analysis in 3D Model	37

3	Results	40
3.1	Characterization of Mechanical Properties of Collagen Gel	40
3.1.1	Collagen Control Test	40
3.1.2	Collagen Gel Polymerization Temperature Test	41
3.1.3	Collagen Test with Different Polymerization pH	43
3.1.4	Collagen test with colorectal cancer cell suspension and co-culture	45
3.1.5	Structural Analysis of Collagen Gel with Confocal Reflection Microscopy (CRM)	50
3.2	Cell-Matrix Interaction Analysis with Collagen Gel Contraction Assay	54
3.3	Interstitial Fluid Flow and Cell Migration Analysis in 3D Model . . .	58
3.3.1	Volumetric Fluid Flow & Permeability	58
3.3.2	Interstitial Fluid Flow and Cell Migration	60
4	Discussion	67
4.1	Type I Collagen as model system for ECM, close but not exact. . . .	67
4.1.1	Acellular Collagen Gel Properties	68
4.1.1.1	Acellular collagen gel matrix formation	69
4.1.2	Colorectal cells remodel the matrix dependent on the initial collagen concentration	70
4.2	Fibroblast promotes cell-mediated contraction of Collagen Gel depending on CRCs phenotype	72
4.3	Interstitial Fluid Flow and Cell Migration Analysis in 3D Model . . .	73
4.3.0.1	Collagen gel permeability	73
4.3.0.2	Fibroblast promote cancer cell migration	74
4.3.0.3	Data Analysis and limitations	75
4.4	Challenges and Future Perspectives	76
4.4.1	Technical Challenges	76
4.4.2	Future Considerations	76
5	Conclusion	78
	References	87
	Appendix A	88
	Appendix B	96

List of Figures

1.1	Epithelial Extracellular Matrix	3
1.2	Metabolic Pathways	8
1.3	Elastic/Young's Modulus in Stress vs Strain curve	10
2.1	Texture Analyser instrument	22
2.2	Force Vs Distance curve of Collagen gel	23
2.3	Force Vs Distance curve of Collagen gel with smooth line feature	24
2.4	3D cell culture chip overview	29
2.5	Interstitial fluid flow through collagen gel test condition illustration	31
2.6	Confined compressive indentation testing of collagen	34
2.7	Force-Displacement and Stress-Strain curve	36
2.8	Structural analysis of collagen gel	37
2.9	Interstitial fluid flow analysis	39
3.1	Young's Modulus (YM) of acellular collagen gel	41
3.2	Young's Modulus (KPa) of 2 mg/ml acellular collagen gel polymerized with two different methods	42
3.3	Young's Modulus (KPa) of 4 mg/ml acellular collagen gel polymerized with two different methods	43
3.4	Young's Modulus (KPa) of 2 mg/ml acellular collagen gel at pH 6.1, 6.8 and 7.4	44
3.5	Young's Modulus (KPa) of 4 mg/ml acellular collagen gel at pH 6.1, 6.8 and 7.4	45
3.6	Young's Modulus of 2 mg/ml cellularized collagen gel with colorectal cancer cell lines (SW948 & SW1116) and colorectal fibroblast (CCD-18Co)	47
3.7	Young's Modulus of 4 mg/ml cellularized collagen gel with colorectal cancer cell lines (SW948 & SW1116) and colorectal fibroblast (CCD-18Co)	49
3.8	Visual presentation of confocal reflectance binary image of 2 and 4 mg/ml acellular collagen gel	50

3.9	Fiber density of 2 mg/ml cellularized collagen gel with colorectal cancer cell lines (SW948 & SW1116) and colorectal fibroblast (CCD-18Co)	51
3.10	Fiber density of 4 mg/ml cellularized collagen gel with colorectal cancer cell lines (SW948 & SW1116) and colorectal fibroblast (CCD-18Co)	53
3.11	Visual presentation of gel contraction assay	54
3.12	Gel contraction of 2 mg/ml cellularized collagen gel with colorectal cancer cell lines (SW948 & SW1116) and colorectal fibroblast (CCD-18Co)	56
3.13	Gel contraction of 4 mg/ml cellularized collagen gel with colorectal cancer cell lines (SW948 & SW1116) and colorectal fibroblast (CCD-18Co)	57
3.14	Permeability of 4 mg/ml	59
3.15	Measured volumetric fluid flow, $Q(m^3/s)$ through 4mg/ml collagen gel over a period of 2 hours with measurements taken every 30 mins	60
3.16	Interstitial fluid flow test apparatus	60
3.17	Confocal fluorescence images of SW948 under normal flow through 2 and 4 mg/ml	61
3.18	Confocal fluorescence images of SW948 under reverse flow through 2 and 4 mg/ml	62
3.19	Confocal fluorescence images of SW1116 under normal flow through 2 and 4 mg/ml	62
3.20	Confocal fluorescence images of SW1116 under reverse flow through 2 and 4 mg/ml	63
3.21	Cell migration distribution overview of SW948 and SW1116	64
3.22	Overview of total migration of SW948 and SW1116	64
3.23	Confocal fluorescence images of SW948 & SW1116 under normal flow through 2 mg/ml	66
1	Texture Analyser calibration of height and force	91
2	Texture Analyser calibration of height and force	92
3	Texture Analyser test settings	92
4	Texture Analyser test configuration	93
5	Texture Analyser test smooth line feature	93
6	Texture Analyser Young's Modulus test macro settings	94
7	Texture Analyser Young's Modulus test macro project	95
8	Fluid flow test calculations for initial flow, permeability and volumetric flow rate of 4 mg/ml collagen gel	97
9	Interstitial fluid flow cell migration test calculations	97

List of Tables

2.1	Cell culture lines	14
2.2	Reagents used in experiments	15
2.3	Consumables used in experiments	19
2.4	Instruments used in experiments	19
2.5	Collagen gel mechanical test conditions	26
2.6	Collagen gel contraction assay test conditions	28
2.7	Interstitial fluid flow test conditions	31

Abbreviations

ATP	Adenosine tri-phosphate
ATTC	American Type Culture Collection
CAF	Cancer-Associated Fibroblast
CORE	Centre for Organelle Research
CRC	Colorectal Cancer
CRM	Confocal Reflectance Microscopy
CRN	Cancer Registry of Norway
ECM	Extracellular matrix
ECACC	European Collection of Authenticated Cell Culture
EMT	Epithelial to Mesenchymal Transition
GCA	Gel Contraction Assay
GLUT	Glucose transporter
MMP	Matrix Metalloproteinases
OXPHOS	Oxidative phosphorylation
TAF	Tumor-Associated Fibroblast
TCA	Tricarboxylic acid cycle
TME	Tumor Microenvironment
YM	Young's Modulus

Dedicated to the ones close to my heart

Chapter 1

Introduction

1.1 Colorectal Cancer

With over a million cases worldwide every year, colorectal cancer (CRC) is the second and third most occurring cancer in women and men, respectively [1]. In Norway in 2016, 1415 cases were recorded for men and 1588 cases for women in colorectal cancer making it one of the most prevalent cancers in the world, affecting millions of people every year, and the rate continues to grow. According to the Cancer Registry of Norway (CRN) the rate of colon cancer has increased by 3% in men while 7% in women in 2016 .

While the root cause of development of most colorectal cancers is unknown, there are many risk factors and associated conditions. Risk of developing CRC has been linked to genetic mutations, but is mostly not hereditary and thought to be due to epigenetic alterations and environmental factors such as lifestyle and diet [2].

Colorectal cancer (CRC) is highly treatable if detected in early stage but it is essential to establish adequate insight of tumor localization with regards to morphology and clinical criteria to identify the aggressiveness of the tumor to plan possible treatment and therapeutic strategies. Primary solid tumors rarely cause death as this is usually caused from spread of cancerous cells from the original tumor to more distant locations in the body by invading in to extracellular matrix and migrate toward the blood or lymph vessels [3], known as metastasis.

Colorectal cancer originates from epithelial cells of the intestinal tract in the colon or rectum. Intestinal epithelium consists of layers of simple columnar epithelial cells that form the lining of both small and large intestine and have apical-basal polarity. Apical side of the epithelial cell faces the lumen of the intestine while

the basal side contacts the basement membrane which in turn is in contact with mesenchymal/interstitial stromal extracellular matrix, ECM [4] as shown in figure 1.1.

It is important to rationalize the fundamental biological capabilities the cancer cells need to acquire during tumor progression as described by Hanahan and Weinberg [5], to be the hallmarks of cancer. They include, sustained proliferation, dysregulated cellular metabolism, death resistance, replicative immortality, evasion of immune destruction, initiation of invasion and metastasis. Many of the characterized hallmarks above are regulated by ECM making consideration of biophysical and biochemical properties of ECM an important step in understanding tumor behaviors and plan of therapeutic interventions [6, 7].

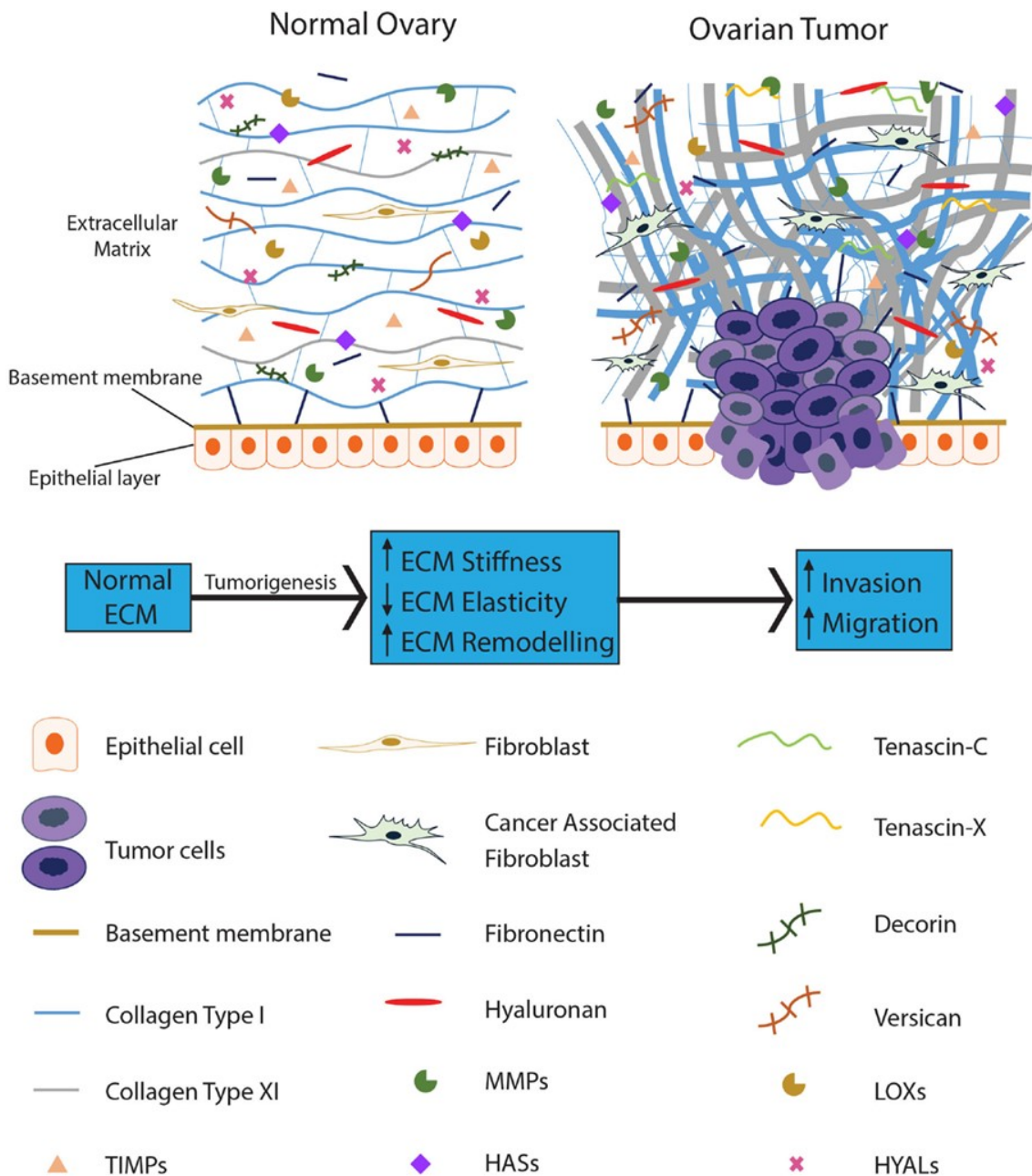


FIGURE 1.1: Epithelial Extracellular Matrix. Normal epithelium ECM consists of tightly packed epithelial cell layer, basement membrane and extracellular matrix with collagen and other stromal components like fibroblasts and MMPs (left). Collagen with loose and wavy fibrils give elasticity and resistance from physical forces. In contrast (right), rigid fibrotic ECM due to tumor formation causes reorientation of collagen fibrils perpendicular to tumor cell by increased cross-linking increasing stiffness and decreasing elasticity of ECM. Moreover, fibroblast having bimodal effect on cancer cells initially work against malignant progression during early tumorigenesis but subvert to promote tumor growth as malignancy advances transforming into cancer-promoting fibroblasts referred to as cancer-associated fibroblasts [8]. Reprinted with permission from Creative Commons Attribution 4.0 International License [9]

1.2 Extracellular Matrix

The extracellular matrix is a noncellular highly dynamic structure consisting of large collection of biologically distinct component and is under constant production, degradation and remodeling to ensure the normal function and development of the tissue or organ giving it its tensile and compressive strength and elasticity [10, 11]. In recent years, the study on composition, structure, and function of ECM has provided essential insight in its role to hold critical importance in cellular growth [12], survival, differentiation [13], tissue morphogenesis [14], migration [15] and homeostasis making ECM microenvironment a key regulator in the arrangement of cellular behavior [16]. ECM provides the structural foundation for its cellular constituents and initiates important biochemical and biomechanical processes [11, 17, 18]. It is this proximal structure that tumor cells need to disrupt for invasion and cell migration [19]. As stated by Goetz et al. “*Mechanotransduction is a key determinant of tissue homeostasis and tumor progression. It is driven by intercellular adhesions, cell contractility, and forces generated within the microenvironment and is dependent on extracellular matrix composition, organization, and compliance*” [20]. Therefore, biophysical and biomechanical properties of ECM have made it an interesting area to study to investigate its potential role in cancer tumorigenesis in the last decade [21].

To hold this dynamic architecture and tissue integrity, ECM undergoes complex biochemical and biophysical process. Biochemical properties of ECM include direct and indirect signaling, regulation of growth factors and cytokines to allow the cell to interact with its environment which results in gene expression and other changes in cell behavior. The biophysical properties of ECM such as rigidity, porosity, insolubility, spatial arrangement and orientation determines its mechanical integrity and role as a barrier, anchoring site, and movement tracking during cell adhesion and migration in three-dimensional structure [6, 17].

Under normal, nonpathological conditions, ECM consist of three general classes of macromolecules i.e. fibrous glycoproteins like collagens; elastin and fibronectin; proteoglycans and non-collagenous accessory glycoproteins. These macromolecules interact in homotypic and heterotypic class associations to develop a dynamic three-dimensional scaffolding/matrix for regulating cell behavior and tissue homeostasis [22, 23].

Fibrillar glycoproteins like type I collagen are transcribed and secreted by mesenchymal cells called fibroblasts present in ECM [24, 25]. To date, collagen constitutes of 28 different forms in vertebrates, adding up to 30% of total protein mass of an

organism making it the most abundant fibrous protein present in interstitial ECM. Combinations of different types of collagen forms the cytoskeletal fibril network giving ECM its structural backbone which regulates cell adhesion and migration [11]. Type I collagen is the most abundant collagen type found in human body, providing the resistance to tensile, shear and compression forces. Type I Collagen is composed of three α polypeptide chains forming a long triple helix fibrils that undergo post-translational modification for stability of its structure by forming covalent intermolecular and interfibrillar cross-links [26]. Hydroxylation of amino acids proline and lysine residues, glycosylation of lysine and the cleavage of N- and C-terminal pro-peptides are the main enzymatic posttranslational pathways in the synthesis of type I collagen [27, 28].

Fibroblast has elongated, spindle like morphology and has a mesenchymal phenotype with highest abundances in connective tissue as shown in figure 1.1. Fibroblast are the most abundant cells of the connective tissue in animals and synthesis and degrade ECM by expressing collagen, fibronectin, laminin, elastin, proteoglycan, integrin and matrix metalloproteinases (MMPs) making it in control of structural integrity of ECM [8]. Fibroblast play a key role during normal processes like wound healing and inflammation. They are recruited by inflammatory cells during a healing process to mediate local tissue contractility via focal adhesion between ECM and fibroblast by remodeling of collagen which enables closing of the wound. Matrix metalloproteinases are a family of extracellular proteins which are activated by fibroblast and also play an important role in tissue repair and remodeling of extracellular matrix in response to injury to regain the physiological environment of the tissue [8].

1.2.1 Tumor Microenvironment

A tumor microenvironment is composed of cancer cells, stromal cells like fibroblast, immune cells, cytokines and vascular tissues all embedded in extracellular matrix making it a dynamic network [19, 23]. Paget [29] laid a theory in 1880's describing tumor microenvironment with "Seed and Soil theory" where cancer cells are "seeds" while the surrounding environment nourishing the seeds being the "soil", is extracellular matrix. His implication with the theory was that cancer metastasis is multifunctional and one must not only focus on "the seed" but also comprehend "the soil" to understand cancer initiation and progression [30].

Cancer can be defined as loss of normal behavior of cellular components thus losing tissue organization and giving rise to a tumor microenvironment, TME [11].

This results in ECM structure and composition to be disorganized, allowing cellular transformation and metastasis [19].

A normal ECM dynamic is controlled by several regulatory functions to retain homeostatic equilibrium and facilitating normal cell division and proliferation. Contrary to the normal nonpathological microenvironment, a shift in the balance results in disruption and disorganization of the ECM's control mechanism leading to abnormal behavior of stromal cells present in the microenvironment. As a result, cell transformation occurs due to genetic mutation and epigenetics alterations [11, 17].

Due to these mutations, epithelial cells go through a change in morphology from a tightly packed lining and apicobasal characteristic to acquire a motile or mesenchymal phenotype featuring migratory and invasive behavior which is referred to an epithelial to mesenchymal transition, EMT [4]. This transition of epithelial cells requires the acquisition of hallmarks of cancer, as described by Hanahan and Weinburg [5], to survive. Biomarkers indicating this mesenchymal property of epithelial cells is repression of E-cadherin which promotes cell adhesion and upgrading of N-cadherin which promotes loss of apical-basal polarity [3].

With tumor progression, the epithelial cell traverses the basement membrane, which is a normal barrier between the epithelium and interstitial stroma/ECM, by thinning and degrading to come in direct contact with ECM [3, 31, 32]. Activation of stromal cells like immune cells and fibroblasts are prompted by the invading epithelial cells by direct or indirect signaling pathways [17], specifically increased amount of proteases, chemokines and supplementary growth factors which in turn regulates matrix realignment by triggering changes in ECM [20, 33].

Tumors have been compared to “*wounds that never heal*” [34] as wound healing process seems to be coopted by them but unlike normal process the deactivation of the fibroblast does not occur, making fibroblasts the architects of tumor pathogenesis [8].

Inflammation is induced in a tumorous environment through regulatory growth factors and chemokines, activating the inflammatory cells like T lymphocytes [25]. Moreover, tissue inflammation causes reorganization of stromal network by inducing trans-differentiation of fibroblast to Cancer-Associated Fibroblasts, CAFs, or Tumor-Associated Fibroblasts, TAFs. Consequently, the production of CAFs is potentiated which promotes and exacerbate remodeling of collagen fibrils from long wavy and thin fibrils of collagen found in normal epithelium microenvironment, providing elasticity to ECM, to thick and short fibrils, stiffening the ECM and resulting in contraction of the collagen network by covalently cross-linking collagen fibers [3]

as shown in figure 1.1. MMPs released during this process also promotes remodeling and degradation of collagen matrix enhancing permeability [11, 35] which helps cell migration and promotion of cell survival and proliferation by upregulation of integrins [9, 17, 36]. These cellular interactions especially between fibroblast and cancer cell is therefore known to contribute to tumor initiation, progression and metastasis in many cancer types [37, 38]. As reported, cancer associated fibroblast are often found in higher number and heterogeneous in colorectal carcinoma [39].

1.2.2 Metabolism

Metabolism consist of pathways adapted by cells to facilitate uptake and breakdown of nutrients in to fundamental building blocks like nucleotides, amino acids, and lipids needed for cell proliferation [40]. All cells need regulation of cell proliferation and apoptosis for maintenance of tissue integrity and function. Cells need energy to undergo these regulatory processes which is fostered by many different metabolic pathway [41]. Metabolism being the energy source is therefore very important for highly proliferating cancer cells.

Under aerobic conditions, normal cells primarily use mitochondrial oxidative phosphorylation for generation of energy. Glucose is metabolized to pyruvate by glycolysis in cytosol and then glycolytic pyruvate is oxidized in mitochondria producing carbon dioxide and adenosine 5' – triphosphate (ATP) under oxidative phosphorylation (OXPHOS) and Tricarboxylic acid (TCA) cycle. This method of energy production is very effective producing large quantity of ATP. In anaerobic conditions lactic acid conversion from pyruvate is favors by the cells with little amount of pyruvate diverted to mitochondria [42] as shown in figure 1.2.

In contrast, cancer cells, even under highly aerobic conditions, metabolize glucose through aerobic glycolysis, a phenomenon termed as “Warburg Effect”, a property first observed by Otto Warburg (WARBURG 1956). The pyruvate produced from glycolysis is converted to lactate through lactic acid fermentation, as shown in figure 1.2, and is then exported out of the cell. The Warburg effect is an inefficient way of ATP production releasing only small amount of ATP [40]. Therefore to compensate for inefficient ATP production tumor cells have increased glycolytic activity during cell division also leading to increased lactate production.

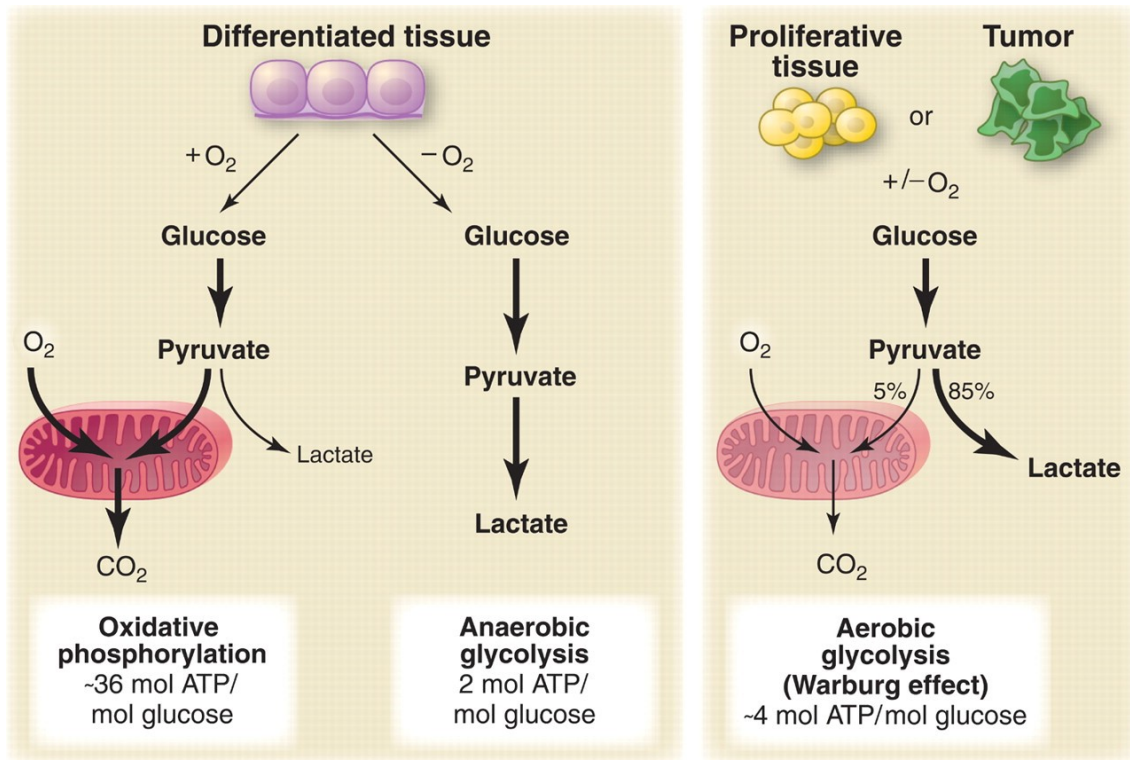


FIGURE 1.2: Metabolic Pathways showing aerobic oxidative phosphorylation carried out by normal cell. In absence of oxygen cells undergo anaerobic glycolysis while cancer cells gain their energy through aerobic glycolysis as called “Warburg Effect” even under well oxygenated conditions. Reprinted with permission from American Association for the Advancement of Science, AAAS [40]

Production of lactic acid through aerobic glycolysis is identified to be the primary cause of acidification of the tumor microenvironment [42–44]. Tumor masses can have a pH of 6.0 to 6.5 [42], a reduction from the normal tissue pH of 7.4. Altered energy metabolism by tumor cells producing an acidic environment have enhanced growth and invasion of tumor cells due to immune destruction and ECM remodeling and degradation [45]. Therefore, the role of metabolism in the ECM interaction is investigated by using two cell lines with differing metabolism, i.e. dependence on glycolysis.

1.3 Biomechanical Properties of Extracellular Matrix

Tumor microenvironment poses a major physiological barrier to the transport and delivery of drugs and reduces the efficiency of radiation therapy and immunotherapy. Increase matrix stiffness, strain and elevated interstitial fluid flow and/or pressure

is characterized as the cause of initiation and progression of tumorigenesis [46]. Resulting mechanical forces can align ECM either by realigning the matrix first or by aligning the cells and then remodeling the matrix around it. Stromal cells exposed to this realignment by surround tumor tissue end up adjusting their cytoskeletal contractility causing an imbalance in stromal ECM architecture [4, 32]. Hence, it is important to understand the evolution of mechanical forces from normal to tumor cells and the barriers they present to lead to better cancer treatments [47]. Increased mechanical stress and strain, due to biophysical forces, contractility, cytoskeletal architecture, permeability and interstitial fluid forces and pressure are important factors to consider when exploring the effect of biomechanical forces in regulation and remodeling of ECM during cancer progression and hence are the focus of this research.

As the major structural component in ECM, type I collagen holds the key to understand structural modifications and biomechanics associated with normal physiology of healthy tissue and malignant processes linked to cancer progression [9, 48]. Collagen type I has the property to self-assemble itself when polymerized in vitro into fibrils similar to what's found in vivo [49] and therefore is widely used in in vitro modeling of ECM and has been the key component used in this research.

1.3.1 Mechanical properties of cellular environment

One dynamic mechanical property of ECM is its elasticity which is threatened in the presence of tumor cell giving ECM a more stiff and rigid structure [19] making it difficult for drug delivery and other treatments. Therefore, a measure of elastic modulus of collagen can give indication of normal and tumorous rigidity of ECM.

Elasticity modulus or Young's modulus is a measure of rigidity or stiffness of a sample, usually reported in Kilopascal (KPa), as described by Hook's law of elasticity. Soft biological tissues exhibit viscoelastic behavior where viscous fluid show a linear trend by resisting shear flow and strain under stress and an elastic solid undergo deformation when stress is applied and rapidly come back to its original state [35].

Considering viscoelastic body in a cylindrical shape, Hook's law, equation 1.1, 1.2, can be defined as normal axial stress being directly proportional to axial strain where Stress, σ , is defined as the force applied on an elastic body with a cross sectional area, A , and strain, ϵ , is the resulting deformation effect due to change in length

[50].

$$\text{Stress}(\sigma) \propto \text{Strain}(\epsilon) \quad (1.1)$$

OR,

$$\frac{F}{A} \propto \frac{\Delta L}{L} \quad (1.2)$$

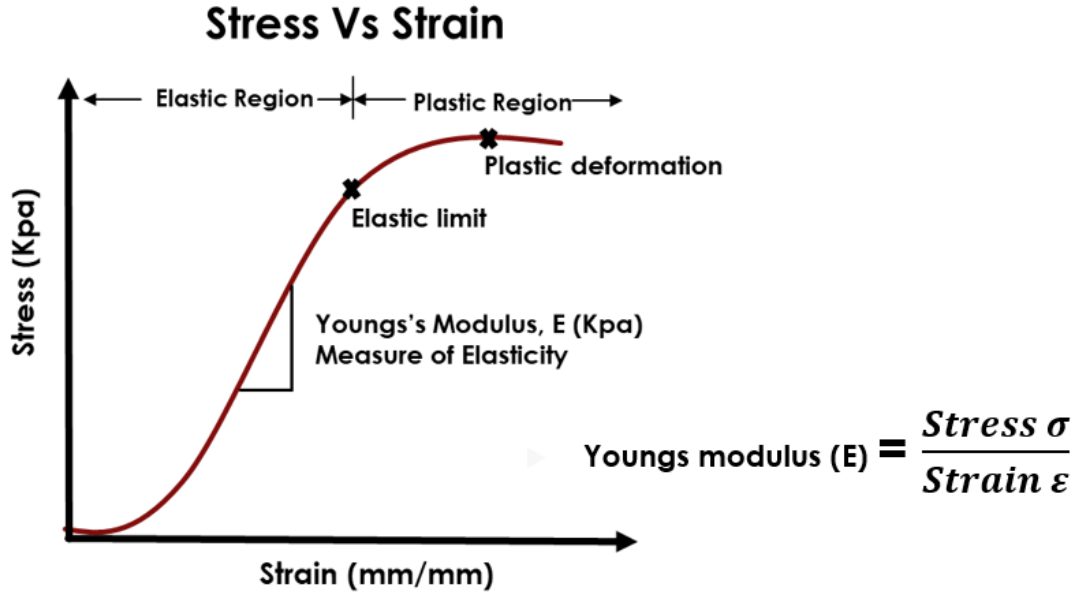


FIGURE 1.3: Elastic/ Young's Modulus in Stress vs Strain curve. In elastic region presenting not permanent deformation while plastic region shows complete deformation of material. Slope of elastic regions gives the Young's modulus of a material.

Two variables are proportional if there is a constant ratio between them. For an elastic body, the proportionality constant is depending on type of material and is called Young's Modulus of Elasticity, E , equation 1.3, 1.4. The constant is equal to the ratio of stress to strain and thus the equation 1.2 can be rewritten as,

$$\frac{F}{A} = E \times \frac{\Delta L}{L} \quad (1.3)$$

$$E = \frac{F}{A} \times \frac{L}{\Delta L} \quad (1.4)$$

$$\text{Young's Modulus, } E = \frac{\text{Stress}(\sigma)}{\text{Strain}(\epsilon)} \quad (1.5)$$

In figure 1.3 the linear regression section of the graph defines the Young's modulus

of a sample, collagen in this case and is called the elastic region. In elastic region the material under stress returns to its original position once the strain is lifted so the deformation is reversible and not permanent. While the plastic region is when the material passes the elastic limit and do not return to its original position due to permanent irreversible deformation.

Several studies have been performed to understand the mechanical properties of collagen when cultures with and without cells and have found that increasing fiber content increase the stiffness of the gel. Furthermore presence of cells and stromal cells like fibroblast can have alternating effect on collagen stiffness based on the morphology and metabolic phenotype of the cell lines [16, 48, 51, 52].

As the biomechanical forces following cell and matrices interactions modify the cellular properties and architecture of surrounding ECM (Harjanto et al. 2012; Palecek et al. 1997), understanding the fiber organisation and contraction of ECM are some of the other properties to measure to understand mechanical nature of collagen.

Despite recent advances in the field, the role of ECM stiffness on tumor pathogenesis is still not clear and needs to be further investigated. Reason being the methods used for deformation studies as based on a method used, the Elastic or Young's modulus of any given tissue can range several orders of magnitude therefore comparison between studies is not always possible [53, 54]. Therefore, the findings from this study should contribute in gaining further understanding of forces that promote remodeling of extracellular matrix in a cancerous environment.

1.3.2 Interstitial fluid flow in cellular environment

Interstitial fluid flow is the movement of fluid, often between blood and lymphatic vessels, through the extracellular matrix of tissues. The function of interstitial fluid is to transport and provide a medium for exchange of substances like nutrients and waste products between extracellular fluid and cell. This makes interstitial fluid flow an important contributor of microcirculation thus have a major effect on drug delivery especially to tumors [55]. The interstitial fluid flow is regulated by lymphatic system. In addition to its role as a mass transporter, providing a specific mechanical environment that is important for physiological activities of interstitial cells is also another trait of interstitial fluid flow [56].

Interstitial fluid flow influences the morphology and migration of cells like fibroblast, cancer cells, epithelial, endothelial and mesenchymal cells thus increasing metastasis potential. An increase of interstitial fluid pressure in neoplastic tissue can function

as a possible stimulus for guiding tumor cells migration and promote metastasis [57–60].

Due to lack of experimental models, the significant biological regulation of interstitial fluid balance is poorly understood. There are very few studies examining the response of cells under interstitial fluid flow and how interstitial fluid flow is regulating the extracellular microenvironment architecture and cell organization [56], hence investigated in this study.

When considering flow of fluid through a porous medium the most fundamental law to consider is the Darcy’s law. Darcy’s law defines the relationship between the instantaneous flow rate through a porous medium, the viscosity of the fluid and the pressure drop over a given distance as presented in equation 1.6.

$$Q = -\frac{k \cdot A}{\mu} \times \frac{\Delta P}{L} \quad (1.6)$$

Where, volumetric fluid velocity, Q (m^3/s) is equal to the product of the permeability of collagen gel, k (m^2), the cross-sectional area to flow, A (m^2), and the total pressure drop ΔP (Pascals, Pa), all divided by fluid viscosity, μ (Pa·s) and the length over which the pressure drop is taking place L (m). the negative value denotes the pressure lose through the column.

The above equation 1.6 can be used as defining equation of measuring absolute permeability as shown below in equation 1.7.

$$k = -\frac{Q \cdot \mu}{A} \times \frac{L}{\Delta P} \quad (1.7)$$

1.4 Aim and Objectives

The main aim of this study is to develop an understanding of how physical and mechanical forces affect the development and spreading of tumor cells by modeling 3D cancer growth and extracellular matrix properties with cancer cells and type I collagen. The objectives of this research were;

The objectives of this research were;

- Characterization of mechanical properties of acellular and cellularized collagen gels by measuring compression resistance of Collagen I ECM model using indentation compression material testing.

-
- Analysis of fiber organization in acellular and cellularized collagen gels by confocal reflectance microscopy.
 - Measurement of the relative mechanical activity of cells on the extracellular matrix in acellular and cellularized collagen gels using gel contraction assay.
 - Determine how fluid flow dynamics mitigate cancer cell migration in extracellular matrix with and without fibroblast.

Chapter 2

Materials and Methods

2.1 Materials

2.1.1 Colorectal cell lines

Colorectal cell lines used in this study with European Collection of Authenticated Cell Culture (ECACC) catalogue numbers and American Type Culture Collection, ATCC, number are stated below in table 2.1.

TABLE 2.1: Cell culture lines with ECACC and ATCC no., tumor grade, source classification and morphology.

Cell Line	ECACC #	ATCC #	Tumor Grade and Source classification	Morphology
SW1116	87071006	CCL-233	Grade III adenocarcinoma 73 year old Caucasian male	Epithelial
SW948	91030714	CCL-237	Grade III adenocarcinoma 81 year old Caucasian female	Epithelial
CCD-18Co	90070503	CRL-1459	Normal Black female infant	Fibroblast

The two colorectal cancer cell line have been used previously in other studies and a profile is established through unpublished work from a research group at CORE, with group leader and thesis supervisor Hanne R. Hagland. It has been established that SW948 have a highly glycolytic profile, while SW1116 have a more oxidative phosphorylation (OXPHOS) dependent profile. Furthermore, SW948 has higher proliferation rate compared to SW1116 with lower proliferation rate.

2.1.2 Reagents

Reagents used during the different experiments are listed below in table 2.2.

TABLE 2.2: Reagents and equipment used in experiments.

Reagents	Manufacturer	Catalog No.	Use
Dulbeccos Modified Eagles Medium (DMEM) (8,3 g/L)	Sigma-Aldrich	D5030	Cell Culture & Collagen preparation
Dulbeccos Modified Eagles Medium (DMEM) (500 mL)	Corning	17-017-CVR	Cell Culture & Collagen preparation
D-(+)-Glucose (1 M)	Sigma-Aldrich	G7021	Cell Culture & Collagen preparation
L-Glutamine Solution (200 mM)	Sigma-Aldrich	59202C	Cell Culture & Collagen preparation
Penicillin-Streptomycin Solution 100X	Biowest	L0022-100	Cell Culture & Collagen preparation
Sodium bicarbonate, NaHCO ₃ (3700 mg/L)	Merck	172577	Cell Culture & Collagen preparation
Sodium chloride, NaCl	Sigma-Aldrich	31434-M	Cell Culture & Collagen preparation
Fetal Bovine Serum, FBS Collagen preparation	Biowest	1810-500	Cell Culture
HEPES 99.5%	Sigma-Aldrich	H4034	Collagen preparation
Type I Collagen (100 mg)	Corning	354249	Collagen preparation
15ml Sodium Hydroxide pellets, NaOH	Scharlau	SO04251000	Cell Culture & Collagen preparation
Phosphate buffered saline tablet, PBS, 50 tablets	Sigma-Aldrich	P4417	Cell Culture, Gel contraction assay & 3D fluid flow
Hydrochloric Acid, HCl 37%	Merck Millipore	1.00317.0510	Cell Culture & Collagen preparation
Bovine Serum Albumin, BSA	VWR Life Science	0332-100G	Gel Contraction assay
FluoSpheres™ Sulfate Microspheres, 4.0 μm, red fluorescent (580/605), 2% solids	ThermoFisher Scientific	F8858	3D fluid flow
CellTracker™ Green BOD-IPY™ Dye	Invitrogen™	C2102	3D fluid flow
CellTracker™ Deep Red Dye	Invitrogen™	C34565	3D fluid flow
Hoechst 33342, 20mM, 5ml	Thermo Scientific	62249	3D fluid flow
Paraformaldehyde, 4%	Sigma-Aldrich	16005	3D fluid flow
Phosphate-Buffered Saline, PBS 1x	ThermoFisher Scientific	18912-014	3D fluid Flow Gel Contraction Assay

Continued on next page

Table 2.2 – Continued from previous page

Reagents	Manufacturer	Catalog No.	Use
Phosphate-Buffered Saline, PBS 5x	Sigma-Aldrich	P4417	3D cell culture media

2.1.3 Prepared solutions

Solutions prepared to be used in different experiments are described below.

2.1.3.1 3D Culture Media

A base 3D culture media was prepared to be used in CO₂ environment for preparation of collagen gel using following formulation with volumes to prepare 50 ml media solution. (Sung 2009; Kopanska 2016)

- 414 mg DMEM powder 8,3 g/L
- 0,09 g NaCl
- 0,185 g Sodium bicarbonate, $NaHCO_3$
- 1,25 ml Glucose 1 M
- 500 μ l L-Glutamine 200 mM
- 5ml FBS (10%)
- 500 μ l antibiotics Penicillin/streptomycin
- Diluted HCl – as needed to achieve 7,4 pH

All reagents were added in a 50 ml tube with double deionized (MilliQ) water to 49 ml, mixed well and pH was adjusted using diluted HCl before more MilliQ water was added to a total of 50 ml. Media was then sterilized using 0,2 μ m sterile filter in to a new sterile tube and stored at 4°C.

2.1.3.2 Cell Culture Media

A base cell culture media was prepared to be used for cell culture and 3D fluid flow experiment. The formulation with volumes to prepare 500 ml media solution is as follows.

- 500 ml DMEM solution
- 50 ml FBS (10
- 5 ml antibiotics Penicillin/streptomycin
- 5 ml L-Glutamine 200 mM

FBS, antibiotics and L-Glutamine was added to DMEM solution, mixed well and stored at 4°C.

2.1.3.3 100 mM HEPES with 2x PBS

- 2,38 g HEPES powder
- 10ml MilliQ water

HEPES powder was mixed in 10 ml MilliQ water to make 1M HEPES. The solution was then sterilized using 0,2 µm sterile filter in to a new sterile tube.

- 1 ml HEPES 1M solution
- 4 ml 5x PBS
- 5 ml MilliQ water

HEPES, 5x PBS and MilliQ water was mixed together and aliquoted in to 1 ml Eppendorf tubes and stored at -20°C.

2.1.3.4 5N and 0,5N NaOH

- 40g NaOH pellets
- 100 ml MilliQ water

Pellets were added in MilliQ water and mixed well to make 5N NaOH solution. Solution stored at room temperature. Furthermore, 0,5N was made by diluting 10 ml of 5N NaOH to 90 ml MilliQ water. Solution were stored in room temperature and used for adjusting pH of media and collagen samples as needed.

2.1.3.5 3,7 % and 1,85 % HCl

- 37% HCl solution
- MilliQ water

100 μ l of 37% HCl was added to 900 μ l of MilliQ water to make 1 ml of 3,7% HCl. Furthermore 1 ml of 1,85% HCl solution was made by adding 50 μ l of 37% HCl to 950 μ l of MilliQ water. Solutions were stored at room temperature and used for adjusting pH of media and collagen samples as needed.

2.1.3.6 1x PBS

- 1 PBS tablet
- 500 ml MilliQ water

Tablet was dissolved in MilliQ water in a bottle and the bottle was autoclaved and stored at 4°C.

2.1.3.7 Fluorospheres microspheres Beads

- Fluorospheres microspheres beads – undiluted conc. $7.2 * 10^5$ beads/ μ l
- 100 mM HEPES with 2x PBS

Mixed undiluted beads in HEPES in a volumetric ratio 1:10 and stored at 4°C.

2.1.4 Consumables

Well plates and other consumables used in the experiments are listed below in table 2.3

TABLE 2.3: Consumables used in different experiments.

Consumables	Manufacturer	Catalog No.	Use
96-Well Microplate	ThermoFisher Scientific	167008	Collagen material test
48 Well Tissue Culture Plates	VWR	10062-898	Gel contraction Assay
DAX-1 3D culture chips	AIM Biotech	DAX-1	3D fluid flow
Luer Connectors	AIM Biotech	LUC-1	3D fluid flow
pH-indicator strips pH 6.5 - 10.0	Merck Millipore	109543	Neutralization of collagen and media
pH-indicator strips pH 4.0 - 7.0	Merck Millipore	109542	Neutralization of collagen and media
Sterile Syringe filter Cellulose Acetate membrane 0.2 μm	VWR	514-0061	Filtration of 3D and cell culture media
Injekt – F Solo Syringes 1 ml	Braun	9166017V	3D Fluid Flow
μ -Dish 35mm, High Grid-500	Ibidi	81166	Confocal Reflection microscopy
25 Culture-Inserts 4 Well for self-insertion	Ibidi	80469	Confocal Reflection microscopy

2.1.5 Instruments

Main instruments used during the different test are listed below in table 2.4

TABLE 2.4: Instruments used in different experiments.

Instruments	Manufacturer	Use
Texture Analyser, TA.XT Plus	Stable Micro Systems Ltd., Surrey, UK version no. 6,1,15,0	Collagen Mechanical testing
Leica TCS SP8 SMD Confocal Laser Microscopy Platform	Leica Microsystem, version no. 3.5.0.18371	Confocal Reflection microscopy and 3D fluid flow
ChemiDoc TM Touch Imaging system	Bio-Rad version no. 2.0	Gel Contraction Assay

2.2 Methods

All the experiments were carried out in dedicated cell culture room requiring use of gowns and shoe covers to avoid contamination and protection. Other aseptic techniques used include,

- Washing hands before and after use of gloves
- Sterilizing gloves with 70% ethanol solution prior to starting work.
- UV sterilized laminar flow cell culture hoods were used for preparation of all samples for all experiments.
- Work surface in the hoods were sterilized with 70% ethanol before and after use.
- All consumables and reagents were sterilized before placing in the hood.
- Disposal of cell culture waste and used consumables in special waste, autoclaved before disposal.

2.2.1 Cell Culture

Cell line as described in table 2.1 are used for this project and aseptic techniques were used throughout handling of cell lines. All the techniques like resuscitation of frozen culture, sub culturing, harvesting and counting of cells is done in a safe manner under cell culture hood. Cell culture of all cell lines used for this project for experiments purposes were handled by a Ph.D. student and were provided on request.

2.2.2 Collagen Gel Preparation

Stock solutions with concentration range of 8-11 mg/ml of collagen I were used to prepare final concentration of acellular 2 and 4 mg/ml gels for mechanical studies. The dilution and neutralization procedure for preparing required volume of 2 and 4 mg/ml hydrated acellular collagen gel proceeded as follows; (Polacheck, Cross) (reference)

1. All the tubes to be used for preparing the sample were kept on ice before and during the procedure.

2. Calculated collagen volume based on desired final concentration and volume was added in a cold tube placed on ice at all times.
3. Collagen was then buffered with 1:1 volume of HEPES in tube and mixed carefully not to introduce bubbles as these will solidify in gel.
4. 3D cell culture media was then added to tube with room to adjust pH to 7,4 using 5N and 0,5N NaOH and mixed carefully.
5. Solution pH was adjusted and tested using Millipore pH strips to be 7,4 before rest of media was added to achieve desired final volume of solution and mixed carefully.
6. Neutralized collagen was polymerized at room temperature for 1 hour and at 37°C at 5% CO_2 thereafter and was considered as “normal polymerization”.

Prepared samples were then used as required by protocols for different experiments.

2.2.3 Collagen Gel Preparation with Cell Co-Culture

2 and 4 mg/ml concentration of collagen gel is prepared with cell co-culture to achieve a final cell concentration of $1 * 10^5$ cell/ml. Collagen gel with cell suspension preparation proceeded as follows;

1. Cell suspension was prepared according to general cell culture techniques for each of 3 cell lines. After counting, the cells were resuspended in cell culture media to a desired density.
2. 6 mg/ml collagen gel was prepared as described in section 2.2.2.
3. For preparing 4 mg/ml collagen and cell suspension solution samples, 2:1 volume ratio of collagen (6 mg/ml) and $1 * 10^5$ cell/ml cell suspension were mixed together.
4. For preparing 2 mg/ml collagen and cell suspension solution samples, 1:2 volume ratio of collagen (6 mg/ml) and $1 * 10^5$ cell/ml cell suspension were mixed together.
5. For samples with co-culture cell suspension, 1:1 volume ratio of each cell line is mixed together to make final sample of cell suspension to be added with collagen gel.

Prepared samples were then used as required by protocols for different experiments.

2.2.4 Characterization of Mechanical Properties of Collagen Gel

2.2.4.1 Collagen Mechanical Test Protocol

Confined compression-stress test was performed on polymerized sample of hydrated acellular 2 and 4 mg/ml collagen gel samples. Mechanical test was performed using instrument called Texture analyzer, TA.XT Plus (section 2.4), as shown in figure 2.1.

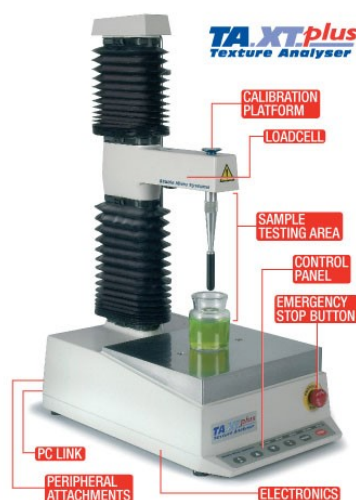


FIGURE 2.1: Texture Analyzer, TA.XT plus by Stable Micro Systems, reprinted with permission from Stable Micro Systems

1. A pre-defined project in the texture analyser, TA.XT plus (TA) based on Kobe method was used to test modulus of elasticity, Young's Modulus E , of collagen gels with different concentrations i.e. 2 and 4 mg/ml using confined compression-stress test. The project info can be found in Appendix A.
2. 5g load cell was used for the experiment. 5 mm diameter cylinder stainless steel probe was used and connected to the arm of the instrument.
3. Height of probe was calibrated by placing an empty 96 well plate on the platform and set to 15 mm from the bottom of the well as start position of the test. Calibration was done before start of each experiment.
4. Calibration of force was done by putting a 2 kg weight on calibration platform. Calibration was done at start of each experiment.
5. Kobe project was opened and T.A. settings were defined. Test speed was defined to be 2 mm/sec as suggested in kobe project. Trigger type "button"

was chosen for the test as the start position of the probe was predefined to be 15 mm from the bottom of the well. This resulted in same distance of compression for each sample with respect to the surface against which the probe was calibrated. Travel distance for the probe was chosen to be 12 mm resulting it to travel 80% of the distance from start position to the bottom of well.

6. Test configuration was defined next by selecting the type of probe and defining parameters like stress area, sample/strain height, data acquisition rate, pre and post test commands.
7. Each sample was then placed under the piston and test was run resulted in a graph with force over distance as shown in figure 2.2.

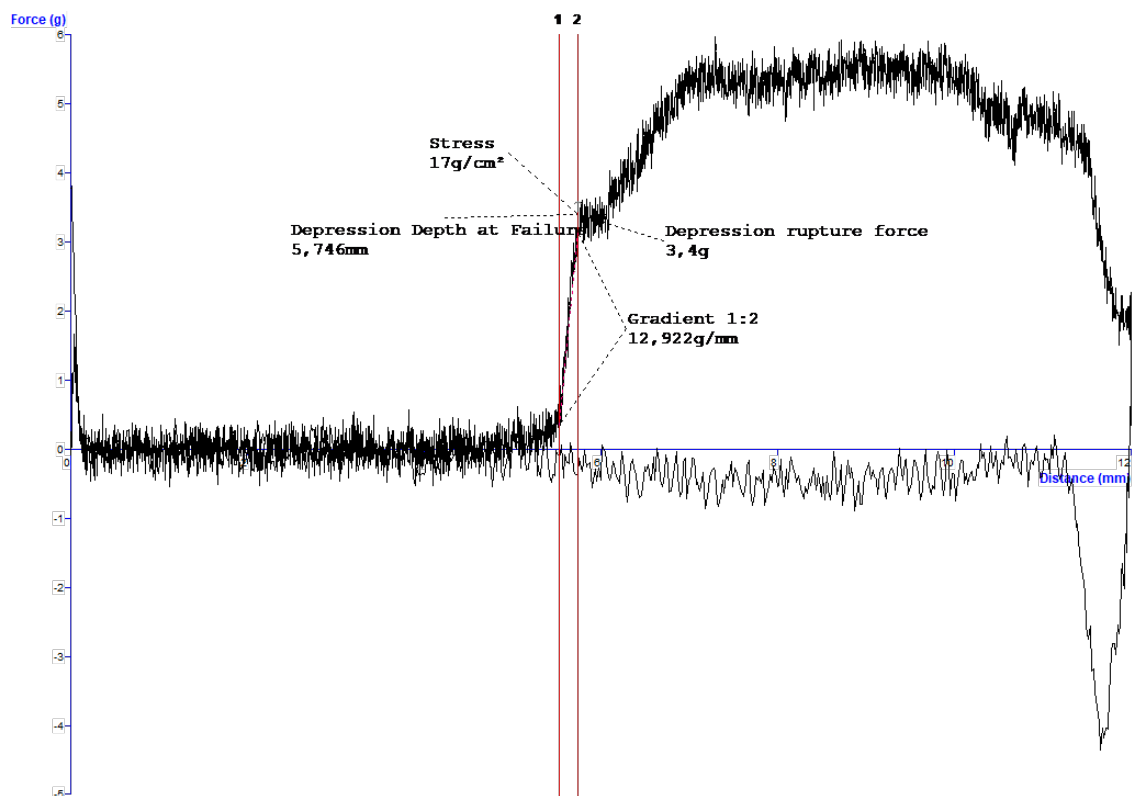


FIGURE 2.2: Graph generated from Texture Analyser representing force vs distance curve of collagen

8. After testing the sample, the graph was refined using a feature “smooth line” in T.A program taking an average of 25 points along the graph. The resulting graph is shown in figure 2.3 and setting used for this feature can be found in Appendix A.

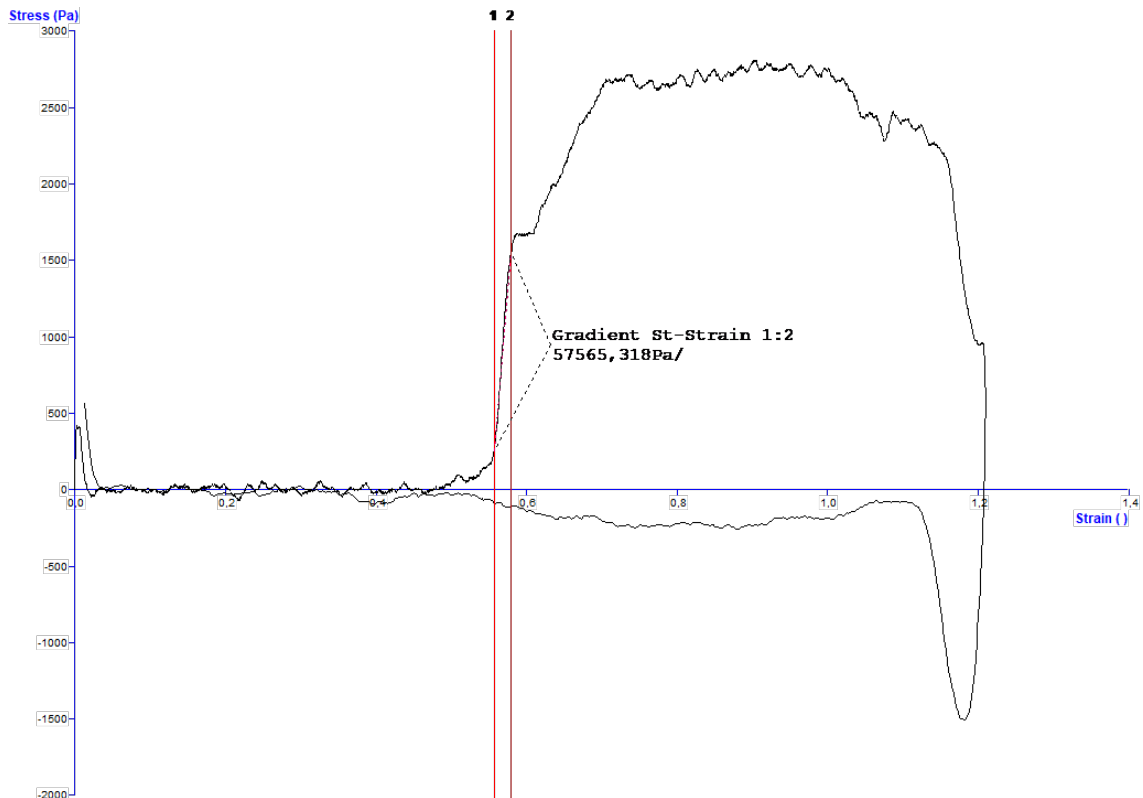


FIGURE 2.3: Graph generated from Texture Analyser representing force vs distance curve of collagen with smooth line feature

9. Next macro settings were run to calculate the gradient of the linear section of the graph representing the elastic region as shown in figure 2.3. gradient in Pascal (Pa) with stress and strain at y and x-axis is acquired via existing project and macro setting in Texture analyser to calculate Young's Modulus (YM). YM Project info and settings can be found in Appendix A.

2.2.4.1.1 Acellular Collagen Gel Mechanical Test This test was performed with 2 and 4 mg/ml collagen gel samples. Same collagen sample preparation procedure was followed as describe in section 2.2.2. Proceeding steps are as follows.

1. 350 μ l/well of the neutralized collagen with desired concentration was immediately added to 96-well plate and allowed to polymerize at room temperature for 1 hour and at 37 °C at 5% CO_2 for 24 hours thereafter before testing. Random available wells were added with sterilized MilliQ water for hydration.
2. Three replicates of each concentration were tested after 1, 2 and 5 days of incubation at 37 °C.

Samples were tested according to procedure described in section 2.2.4.1.

2.2.4.1.2 Collagen Gel Polymerization Mechanical Test This test was performed with 3 replicates of 2 and 4 mg/ml collagen gel samples to investigate the effect of temperature on modeling of collagen in terms of fiber length and density formation and its effect on the strength of collagen gel. Same collagen sample preparation procedure was followed as describe in section 2.2.2 except following;

1. 350 μ l/well of the neutralized collagen with desired concentration was immediately added to 96-well plate and allowed to polymerize directly at 37 °C at 5% CO_2 for 24 hours before testing. Random available wells were added with sterilized MilliQ water for hydration.

Samples were tested according to procedure described in section 2.2.4.1.

2.2.4.1.3 Collagen Mechanical Test in Acidic environment This test was performed to investigate the effect of reduced pH on the strength of collagen gel to imitate the acidic environment caused by aerobic glycolysis and lactate production of CRCs. 3 replicates of each 2 and 4 mg/ml at pH 6.2 and pH 6.8 were tested. Same procedure as described in section 2.2.2 was followed for collagen gel preparation except following;

1. 2 parallel samples were made for each desired concentration of collagen i.e. 2 and 4 mg/ml. During neutralization phase of collagen gel, pH of parallel 1 was adjusted to 6.2 while the pH for parallel 2 was adjust to 6.8 for each concentration of collagen gel.
2. 350 μ l/well of the neutralized collagen with desired concentration was immediately added to 96-well plate and allowed to polymerize at room temperature for 1 hour and at 37 °C at 5% CO_2 for 24 hours thereafter before testing. Random available wells were added with sterilized MilliQ water for hydration

Samples were tested according to procedure described in section 2.2.4.1.

2.2.4.1.4 Collagen Gel with Colorectal Cancer Cell Suspension and Co-Culture This test was performed to see the effect of colorectal cancer cells on elasticity of collagen gel when each cell culture and cell co- culture is mixed with different concentration of collagen gel. Five conditions were tested as illustrated in table 2.5.

TABLE 2.5: Cell suspension test conditions with 2 and 4 mg/ml collagen gel for mechanical testing. P denotes passage number

Collagen Conc.	Condition 1	Condition 2	Condition 3	Condition 4	Condition 5
2mg/ml	SW948 (P14)	SW1116 (P14)	CCD-18Co (P14)	CCD-18Co & SW948	CCD-18Co & SW1116
4mg/ml	SW948 (P14)	SW1116 (P14)	CCD-18Co (P14)	CCD-18Co & SW948	CCD-18Co & SW1116

Collagen gel with cell suspension preparation proceeded as follows;

1. Collagen gel with cell suspension samples were prepared as described in section [2.2.3](#)
2. 350 μ l of sample from each condition for desired collagen gel concentration was immediately added to 96-well plate and allowed to polymerize at room temperature for 1 hour. Random available wells were added with sterilized MilliQ water for hydration.
3. To complete polymerization the samples were incubated at 37 °C at 5% CO_2 for 24 hours.
4. Six replicates for each condition were made for each collagen gel concentration. 3 replicates were tested 2 days after preparation and other 3 replicates were tested 5 days after preparation. Day 2 and day 5 samples were added to separate 96 well plates to avoid unnecessary removal of samples from incubator.

Samples were tested according to procedure described in section [2.2.4.1](#).

2.2.5 Structural Analysis of Collagen Gel with Confocal Reflection Microscopy (CRM)

2.2.5.1 Preparation

Reflection imaging of acellular and cellular collagen gel for structural analysis. The sample preparation was carried out as follows.

1. Samples were prepared as described in section [2.2.2](#) and [2.2.3](#) for 2 and 4 mg/ml collagen gel without and with colorectal cancer cells.

2. Same conditions as described in table 2.6 were used for sample preparation.
3. 100 μl of prepared samples were then added to each well of culture-inserts 4 well plate that was place in a μ -Dish for each condition.
4. Reflection images where taken after 2 days and 6 days of incubation. 10 μl of cell culture media was added for hydration of samples on day 2.

2.2.5.2 Confocal Imaging

Three dimensional images were acquired of the collagen gel samples seeded at 2 time points i.e. 2 days after incubation and 6 days after incubation (Schain et al. 2014). Leica SP8 Confocal microscope (section 2.1.5) using 20x objective (0,55 NA) was used for the purpose. Three image channels were acquired for each day 2 and 6 sample by illuminating the samples with laser light wavelengths 488 nm(green), 638nm (red), 552nm(blue). The reflected light was detected with photomultiplier tube (PMT) for green (486-491 nm) and blue (550-555 nm) channel and with hybrid detector (HyD) for red (636-641 nm) channel with the detection ranges in parentheses. The volumetric Z-stack for each image region covered a range of approx. 70 to 100 microns with 4 stack per z-stack. Image acquisition parameters were kept the same for all gels.

2.2.6 Cell-Matrix Interaction Analysis with Collagen Gel Contraction Assay (GCA)

Gel contraction assay was performed to investigate the physical forces affecting extracellular matrix in the presence of cancer cells. Collagen gel with 2 and 4 mg/ml concentration was prepared with cell suspension as described in table 2.6 below.

TABLE 2.6: Cell suspension test conditions with 2 and 4 mg/ml collagen gel for gel contraction assay (GCA). P denotes passage number

Collagen Conc.	Condition 1	Condition 2	Condition 3	Condition 4	Condition 5	Condition 6
2mg/ml	SW948 (P20)	SW1116 (P19)	CCD-18C (P15)	CCD-18C & SW948	CCD-18C & SW1116	Acellular 2 mg/ml collagen gel
4mg/ml	SW948 (P20)	SW1116 (P19)	CCD-18C (P15)	CCD-18C & SW948	CCD-18C & SW1116	Acellular 4 mg/ml collagen gel

Collagen gel with cell suspension preparation proceeded as follows;

1. 48-well plates were prepared by blocking with 2% BSA in 1 ml/well PBS. The plates were left overnight in incubator at 37 °C.
2. Acellular and cell suspended collagen gel was prepared according to process described in sections 2.2.2 and 2.2.3
3. 175 μ l of sample from each condition for desired collagen gel concentration was immediately added to 48-well plate and allowed to polymerize at room temperature for 1 hour.
4. Collagen gel samples were then floated with 200 μ l of cell culture media by placing the pipette tip on the wall of the well and release the media with one quick press to get the media under the gel.
5. Images of the gels were taken at day 2 and 5.
6. 200 μ l more of cell culture media was added to each well at day 2.
7. Gel diameter for each sample was measured at day 0 and % change of gel diameter at day 2 and 5 is calculated and compared.

2.2.7 Interstitial Fluid Flow and Cell Migration Analysis in 3D Model

2.2.7.1 Preparation

Preparation and testing of interstitial fluid flow through collagen gels with different concentrations was carried out using DAX-1 3D cell culture chips (table 2.3) as

shown in figure 2.4 and the method below. Procedure was prepared by adapting protocols published by AIM Biotech.

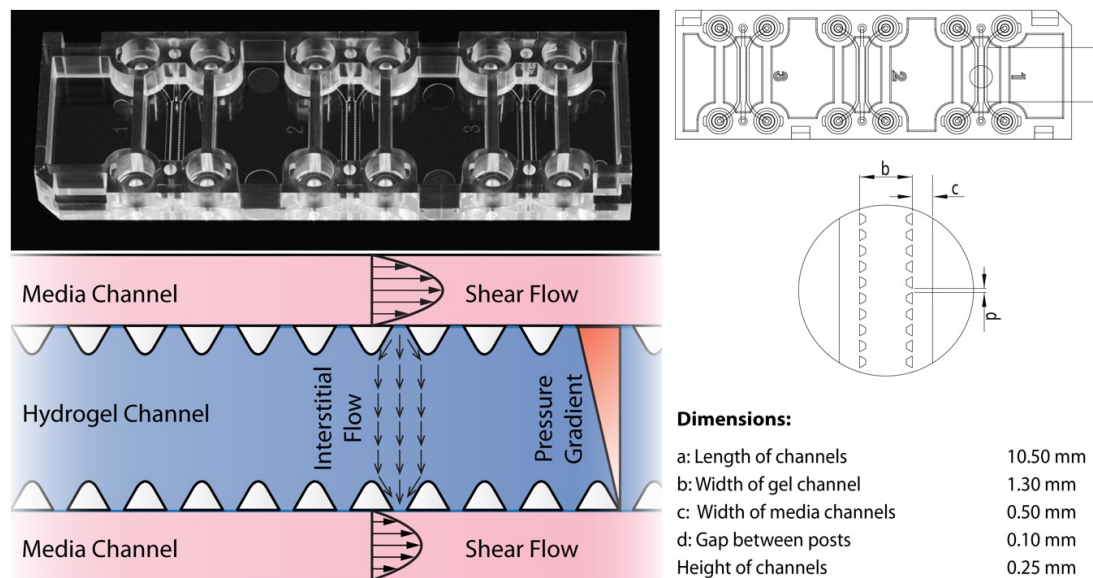


FIGURE 2.4: 3D cell culture chips with presentation of interstitial fluid flow through the media and hydrogel channels with chip dimensions. Reprinted with permission from AIM Biotech

1. Cell culture chips were initially prepared by fitting the connectors into all the 4 inlets of media channels. Chips were then placed in petri dish.
2. Desired volume of collagen gel with 2 and 4 mg/ml concentration was prepared as described in section 2.2.2. 10 μl of gel solution was then carefully injected in the chip from both gel inlets. MilliQ water was added in reservoirs of chip holder for hydration of gel.
3. Chips were left at room temperature to polymerize for 1 hours.
4. Collagen coating solution was prepared by dissolving stock solution to cell culture media to achieve 50 $\mu\text{g}/\text{ml}$ concentration. 30 μl of the coating collagen solution was injected in channels to be seeded with cell suspension. 30 μl of cell culture media was injected in the other channel to keep the gel hydrated. Chips were incubated for an hour at 37 $^{\circ}\text{C}$.
5. 70 μl of cell culture media was added to one connector of a media channel and 50 μl to the other connector of the same media channel to flush out coating solution. This step was repeated twice to remove the coating solution completely. Similarly, the other channel is flushed with fresh media

6. Next cell suspensions were prepared with density of $2,5 \times 10^5$ cell/ml (250 cell/ μ l) and were stained with cytosolic stain CellTracker Green for detection.
7. Media was removed from all the connectors to level above the connector inlet.
8. 20 μ l of cell suspension was injected to one of the connector inlet of the media channel to be seeded with cell suspension and after waiting 2 mins, 20 μ l of cell suspension was added to the other connector inlet attached to the same media channel.
9. 9. Chips were kept in incubator at 37 °C overnight for cell adherence to gel interface and proliferation.

2.2.7.2 Testing Volumetric flow (Q), and Collagen Permeability, k

Volumetric flow, Q and collagen permeability, K was tested after preparation of cell culture chips as described in section [2.2.7.1](#),

1. All connectors where filled with 60 μ l of media and syringe barrels where attached to all connector.
2. Syringes connected to channel with higher volume were filled with 500 μ l of media and syringes connected to low volume media channel were filled with 100 μ l of media causing pressure drop between the channels and resulting in interstitial fluid flow through the collagen gel.
3. Initial difference in volume and height between media channels was recorded.
4. Based on graduation scale on syringe barrels, change in volume and height over every 30 minutes was recorded until the volume equilibrated in all syringes connected to all 4 connectors.

2.2.7.3 Testing interstitial flow and cell migration through collagen

Interstitial flow and cell migration through collagen were tested with different test conditions illustrated below in table [2.7](#) and figure [2.5](#).

TABLE 2.7: Test conditions for Interstitial fluid flow. P denotes passage number

Collagen Conc.	Condition 1 Normal flow	Condition 2 Reverse Flow	Condition 3 Normal flow with Fibroblast	Control No flow
2 mg/ml	SW948 (P26) SW1116 (P23)	SW948 (P26) SW1116 (P23)	CCD-18Co (P16) SW948 (P27) SW1116 (P24)	SW948 SW1116 CCD-18Co
4 mg/ml	SW948 (P26) SW1116 (P23)	SW948 (P26) SW1116 (P23)	Test not Performed	SW948 SW1116 CCD-18Co

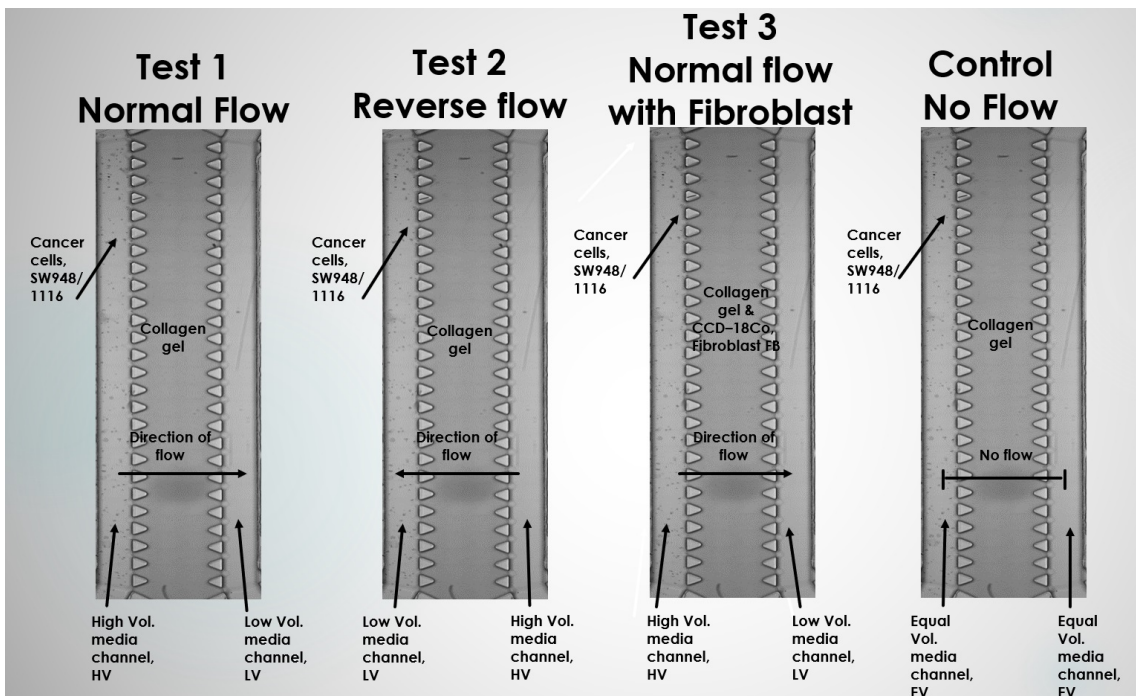


FIGURE 2.5: Interstitial fluid flow through collagen gel test condition illustration

Cell culture chips were prepared as described in section 2.2.7.1 with some additions to step 2 of preparation protocol based on different test conditions. For test condition 1 and 2 as illustrated in table 2.7 and figure 2.5, pre-diluted fluorescent beads (section 2.1.3.7) were added to each concentration of collagen in a volumetric ratio of 1:50. For test condition 3, cancer fibroblast cells, CCD-18Co, were added in a density of 2.5×10^5 cell/ml (250 cell/ μ l) instead of fluorescent beads. Cancer fibroblast cells, CCD-18Co, were stained with cytosolic stain CellTracker Deep Red dye for detection. Succeeding steps are as follows;

1. Day 0 images were taken of the media channel seeded with cells along the gel interface.

2. All connectors were filled with 60 μl of media and syringe barrels were attached to all connector.
3. Syringes connected to channel with higher volume were filled with 200 μl of media and syringes connected to low volume media channel were filled with 50 μl of media causing pressure drop between the channels and resulting in intermittent interstitial fluid flow through the collagen gel.
4. Based on graduation scale on syringe barrels, change in volume over time was recorded and every 3 hours more media was applied to syringes connected to media channel with higher volume to retain 150 μl volume differential between the channels. The application of flow lasted 48 hours out of which flow of media through collagen gel was for 15 hours (Day 1 - 9 hours and day 2 - 6 hours with no flow during the night).
5. After application of flow, cell culture media was removed from syringes to syringe inlet and syringes were carefully removed from all connectors.

2.2.7.4 Fixation of Cell culture Chips

Following the application of flow the cell culture chips were fixed as described below.

1. Both media channels were washed as described in point 7 section [2.2.7.1](#) with PBS for 5 minutes.
2. Next PBS was removed, and chips were treated with 37 °C warm 4% PFA for 15 minutes.
3. After removing 4% PFA, 1 mg/ml nuclear stain Hoechst diluted in PBS in vol. ratio 1:500 was added and left for 30 mins to stain the cancer cells.
4. Hoechst was removed, and chips were flushed with PBS 4 times with 5 min interval between washing.
5. Chips were stored in petri dish covered with aluminum foil at 4 °C before taking 48 hours images.

2.2.7.5 Confocal imaging

Thirteen 3D sections were acquired covering the media channel seeded with cancer cells at gel interface at 2 time points i.e. one day after seeding of cancer cells in

media channel considered as 0 hours and after 48 hours of application of flow using a Leica SP8 Confocal microscope (20x dry objective, 0,55 NA). 3 image channels were acquired for each of the 13 sections at 0 hours, CellTracker Green fluorescence (emission 529 nm) for cancer cells, Red fluorescence (emission 594nm) for fluorescent beads and transmitted light. The fluorescence light was detected with photomultiplier tube (PMT) for green and red channel. Similarly, when imaging after 48 hours, 4 image channels were acquired for each of the 13 sections i.e. Hoechst Blue fluorescence (emission 497nm) for cancer cells, CellTracker Green fluorescence (emission 529 nm) for cancer cells, red fluorescence for fluorescent beads (emission 594 nm) and transmitted light. The fluorescence light was detected with photomultiplier tube (PMT) for green and red channel and with hybrid detector (HyD) for blue channel. For test condition 3 where CCD-18Co fibroblast is used instead of fluorescent beads in collagen gel and the images acquired at both 0 and 48 hours for the red channel were for CellTracker Deep Red fluorescence (emission 660 nm) for fibroblast. The volumetric Z-stack for each image region/section covered a range of approx. 150 to 200 microns with a z-stack step size of 4 microns resulting in over 1000 confocal images due to plurality of test conditions and time points. Image acquisition parameters were kept the same for all gels.

2.2.8 Data Analysis

2.2.8.1 Mechanical testing of collagen

Hook's law of elasticity was used for calculating Young's modulus for different concentrations of collagen gel. Defining hook's law in isotropic form for an unconfined compression of an elastic body, collagen in this case, yield equations 2.1, 2.2, 2.3;

$$E.\epsilon_x = \sigma_x - \nu(\sigma_y + \sigma_z) \quad (2.1)$$

$$E.\epsilon_y = \sigma_y - \nu(\sigma_x + \sigma_z) \quad (2.2)$$

$$E.\epsilon_z = \sigma_z - \nu(\sigma_x + \sigma_y) \quad (2.3)$$

In the above equations, E represents Young's Modulus, σ is stress in x, y and z direction, ϵ is strain in x, y and z direction and ν is Poisson's ratio.

In unconfined compression test, stress in x and y direction is zero, i.e.

$$\sigma_x = \sigma_y = 0 \quad (2.4)$$

So, equation 2.3 can be rewritten as;

$$E \cdot \epsilon_z = \sigma_z \quad \Rightarrow \quad E = \frac{\sigma_z}{\epsilon_z} \quad (2.5)$$

Substituting equation 2.5 in equation 2.1 and 2.2 will generate;

$$E \cdot \epsilon_x = -\nu \sigma_z \quad \Rightarrow \quad E \cdot \epsilon_x = -\nu E \epsilon_z \quad \Rightarrow \quad \nu = -\frac{\epsilon_x}{\epsilon_z} \quad (2.6)$$

$$E \cdot \epsilon_y = -\nu \sigma_z \quad \Rightarrow \quad E \cdot \epsilon_y = -\nu E \epsilon_z \quad \Rightarrow \quad \nu = -\frac{\epsilon_y}{\epsilon_z} \quad (2.7)$$

Confined Compressive Indentation Test

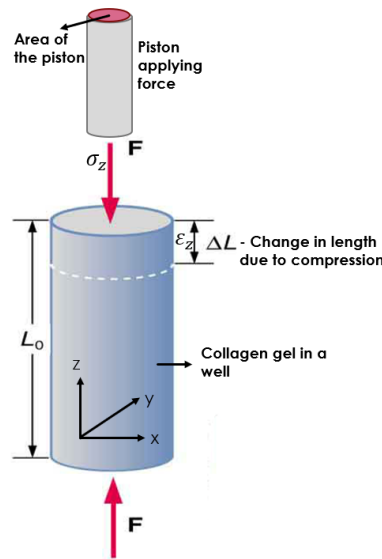


FIGURE 2.6: Confined compressive indentation testing of collagen

However, mechanical strength test of collagen gels was performed in 96 well plates resulting in confinement of material. Therefore, confined compression was considered for characterizing mechanical properties of collagen gel. Considering collagen gel matrix an isotropic viscoelastic material the above equations can be rearranged to define confined compression of collagen gel as shown in figure 2.x. In other words, strain in x and y direction will be zero as the compression is solely in axial direction as shown in equation 2.8, i.e.

$$\epsilon_x = \epsilon_y = 0 \quad (2.8)$$

Therefore, equations 2.1 and 2.2 can be written as,

$$0 = \sigma_x - \nu(\sigma_y + \sigma_z) \quad (2.9)$$

$$0 = \sigma_y - \nu(\sigma_x + \sigma_z) \quad (2.10)$$

Solving equation 2.9 and 2.10 gives,

$$\sigma_x = \sigma_y = \frac{\nu}{1 - \nu} \sigma_z \quad (2.11)$$

Substituting equation 2.11 in equation 2.3 generate,

$$M_{eq} = E \frac{1 - \nu}{(1 + \nu)(1 - 2\nu)} = \frac{\sigma_z}{\epsilon_z} \quad (2.12)$$

Where M_{eq} in equation 2.12 is the stress-strain ratio for confined compression and is defined as equilibrium modulus [61] and ν is Poisson's ratio. The above equation was rearranged to calculate Young's Modulus for confined compression as shown in equation 2.13;

$$E = M_{eq} \frac{(1 + \nu)(1 - 2\nu)}{(1 - \nu)} \quad (2.13)$$

Mechanical testing of collagen gels resulted in a force- displacement curve. The curve was converted to a stress-strain curve using pre-defined setting available in Texture Analyser analysis program as illustrated in figure 2.7. The gradient of the elastic region of the curve was defined generating equilibrium modulus, M_{eq} , value in Pascal which was further used to calculate Young's modulus, E, using equation 2.13. Furthermore, poisson ratio, ν , of 0,2 was used to calculate Young's Modulus of collagen on the bases of same values found in previous studies [48, 62] used to calculate Young's Modulus.

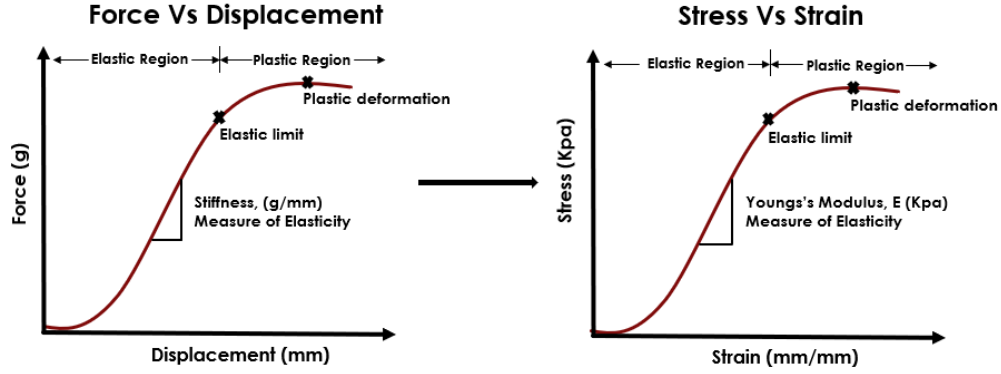


FIGURE 2.7: Illustration of force-displacement and stress-strain curve for calculating Young's modulus as an indication of stiffness of different testing condition of collagen gel.

It is also possible to calculate Young's modulus from force-displacement curve using the gradient value in g/mm by first calculating equilibrium modulus as shown below in formulations under equations 2.14-2.17. Equation 2.17 can be used to first calculate equilibrium modulus and then equation 2.13 can be used to calculate Young's modulus.

$$M_{eq} = \frac{\Delta\sigma_z}{\Delta\epsilon_z} \quad (2.14)$$

$$M_{eq} \cdot \Delta\left(\frac{\Delta L}{L_i}\right) = \Delta\sigma_z \quad (2.15)$$

$$M_{eq} = L_i \cdot \frac{\sigma_{z2} - \sigma_{z1}}{L_1 - L_2} \quad (2.16)$$

$$M_{eq} = \frac{L_i}{A} \cdot \frac{F_{z2} - F_{z1}}{L_1 - L_2} \quad (2.17)$$

2.2.8.2 Structural analysis of collagen gel – Confocal Reflection Microscopy (CRM)

Collagen gel fiber density analysis was done using individual 500-micron slices or stacks of red channel images generated from confocal reflectance microscopy (CRM) for each sample. The pixel intensities of predefined region of interest points were measured by first equalizing the image contrast and then using multiplot function in ImageJ for all sample images per stack as shown in figure 2.6. The resulting pixel

intensity peaks were filtered to include only peaks between the range of 100 and 255. An average of resulting number of peaks for all sample stacks was calculated and divided with image size of 500 micron to get the fibril density of each sample for all ROIs. Resulting values were compared to determine any remodeling and degradation of collagen gel for tested conditions.

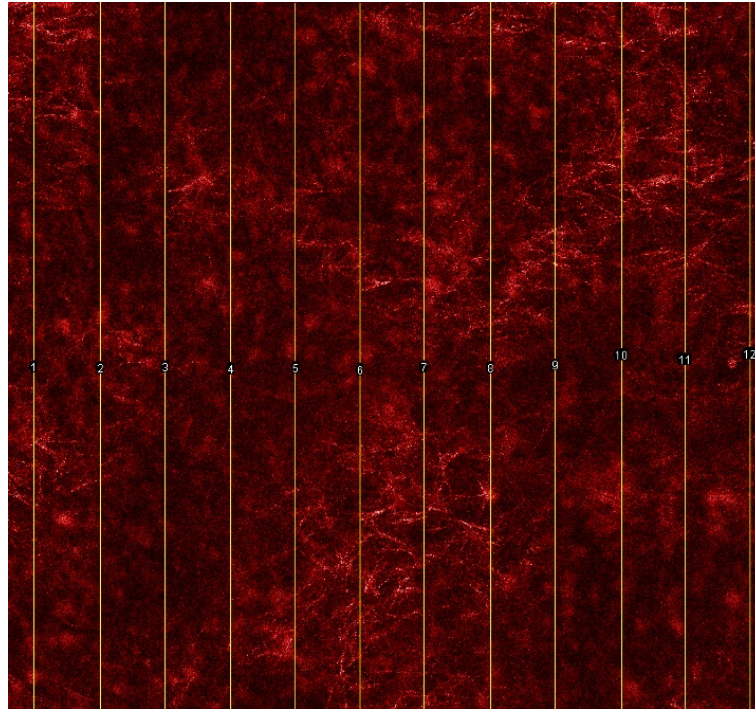


FIGURE 2.8: Quantification of fibril density of collagen gel with confocal reflectance microscopy (CRM) image with 12 regions of interest to calculate pixel intensity peaks

2.2.8.3 Cell-Matrix Interaction Analysis with Collagen Gel Contraction Assay (GCA)

ChemiDoc Touch imaging system was used to take pictures of the wells containing the samples on day 2 and 5. ImageJ was then used to measure the area of floating gel in media of day 2 and day 5 samples. Resulting measurements were then further used to calculate the percentage contraction of collagen gel samples over 5 days.

2.2.8.4 Interstitial Fluid flow and Cell Migration Analysis in 3D Model

2.2.8.4.1 Volumetric flow and permeability Initial volumetric flow, Q_i , was estimated by calculating the values recorded every 30 minutes of the experiment

using equation 2.18.

$$Q_i = \frac{\Delta V_0 - \Delta V_i}{t} \quad (2.18)$$

Where, ΔV_0 is difference in volume in syringes between the media channels at start of experiment, ΔV_i is the difference in volume in syringes between the channels after time, t . values were taken every 30 minutes and estimation of change of pressure was calculated by measuring the change in height of liquid column in syringe over each time interval until the volume equilibrated.

Permeability, k (m^2), was then calculated for each time interval of 30 minutes using the estimated Q_i and ΔP values using equation 2.19.

$$k = -\frac{Q_i \cdot \mu}{A} \times \frac{L}{\Delta P} \quad (2.19)$$

To measure approximate flow of fluid through collagen gel Darcy's equation was used as shown in equation 2.20;

$$Q = -\frac{k \cdot A}{\mu} \times \frac{\Delta P}{L} \quad (2.20)$$

Where, volumetric fluid velocity, Q (m^3/s) is equal to the product of the permeability of collagen gel, k (m^2), the cross-sectional area to flow, A (m^2), and the total pressure drop ΔP (Pascals, Pa), all divided by fluid viscosity, μ (Pa·s) and the length over which the pressure drop is taking place L (m). the negative value denotes the pressure lose through the column.

2.2.8.4.2 Cell migration analysis Quantification of cell migration through collagen gel with different concentrations and test conditions is performed using confocal images acquired at 0 and 48 hours. An image analysis tool called "Icy Bioimage Analysis" is used for fluorescence detection of each channel for individual section image at time point 0 and 48 hrs. thereby enabling differential comparison to access any colorectal cancer cell migration from the media channel in to the collagen gel. Maximum projection was performed on each section image to merge the z-stacks and HK-means tool was used to detect fluorescence for all channels. A defining boundary line between gel region and post was applied manually, 50 microns from the bottom of post as illustrated in figure 2.9. 50 micron was used

as threshold after randomly choosing 5 images and averaging the distance between bottom of post and gel region boundary.

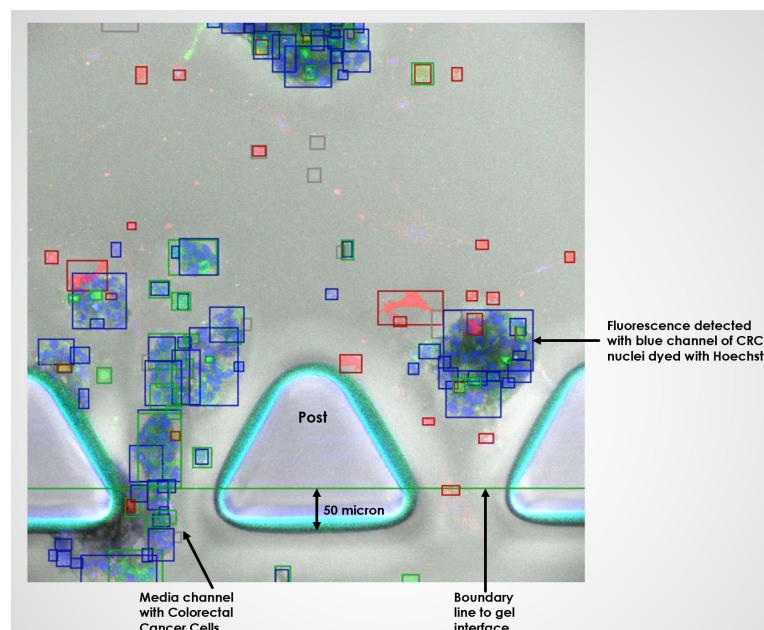


FIGURE 2.9: Illustration of Image analysis using Icy BioImage Analysis. Image presents the detected fluorescence for blue and red channels for cancer cells and fibroblast respectively. The boundary line is the gel interface line over which all the cell were counted as migrated cells.

Acquired green channel fluorescence area of CRC was used to calculate average cell size by randomly choosing 10 single cells in a 0 hr. image section and divided by total detected fluorescence area of CRC over the boundary line in collagen gel to calculate the number of cells, if any, in the gel at 0 hr. Aforementioned process is repeated with 48 hrs images except using blue channel detected fluorescence of CRCs. Difference of migrated cell at 0 and 48 hrs is plotted as the number of migrated cells through the collagen gel over a period of 48 hours.

Chapter 3

Results

3.1 Characterization of Mechanical Properties of Collagen Gel

To understand the underlying biomechanics of collagen and its role in cell and tissue dynamics, a series of mechanical testing (2.2.4) was conducted with varying parameters. Initially, three trial tests with acellular collagen were performed to optimize test settings, configurations and establishing a protocol using the instrument, Texture Analyser. Due to high consumption of collagen for the tests, two more test with acellular collagen gel were done post-optimization and the results were used as control for other tests performed under this section.

3.1.1 Collagen Control Test

The rigidity or stiffness of the extracellular matrix surrounding the cancer cells has been described as a contributing factor to how the tumor grows. The collagen stiffness can be measured by a change in Young's modulus (YM), with higher number indicating increased stiffness. Here this was measured over a period of 5 days and presented in figure 3.1.1. Acellular collagen samples for both 2 and 4 mg/ml concentrations were tested on day 1, 2 and 5 (2.2.4.1.1). In addition to comparison between the two concentrations, the results were also used as control to compare to other mechanical test results. Day 1 results were used to compare mechanical test results with different pH and temperature. Similarly, day 2 and day 5 test results of acellular collagen were used as control to compare with mechanical tests done with co-culture samples of collagen.

Figure 3.1.1 show comparison between 2 and 4 mg/ml collagen gel concentration and revealed a significant difference in Young's modulus between the two tested collagen concentrations. 4 mg/ml collagen gel showed a higher Young's modulus of 88 KPa when compared to 2mg/ml with 44 KPa after day 1 testing giving a significant difference of 50% ($p < 0,02$). Similarly, day 5 results showed higher YM of 71 KPa for 4 mg/ml collagen when compared to 2 mg/ml (32 KPa) with a difference of 55% ($p < 0,005$). 2 mg/ml collagen stiffness decreased nearly by one third (29%) between day 1 and day 5 samples ($p = 0,01$) while no significant different was observed in 4 mg/ml gel samples of 5 days ($p = 0.49$).

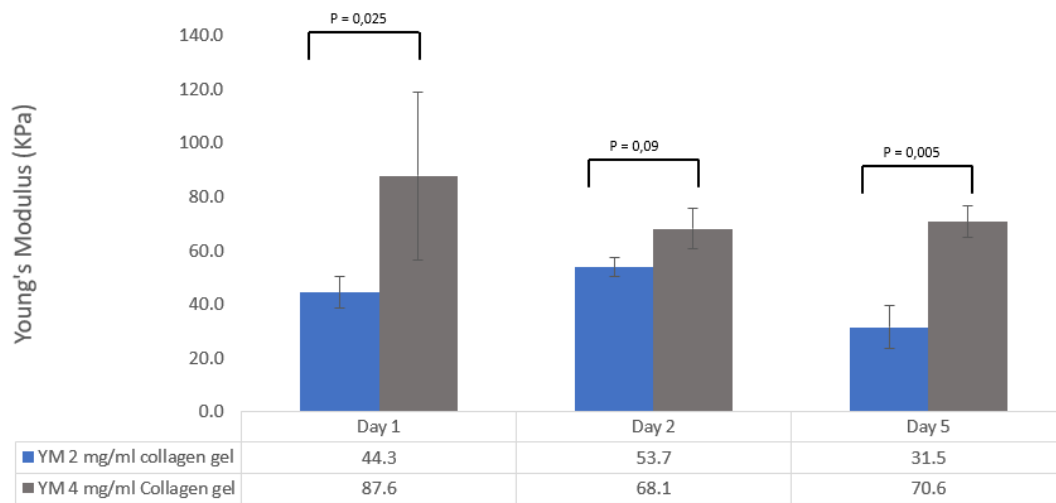


FIGURE 3.1: Measured Young's Modulus (KPa) of acellular collagen gel with concentrations 2 and 4 mg/ml tested after 1, 2 and 5 days of polymerization. All samples tested were prepared at the same time to minimize variance between the samples. Error bars indicate standard deviation of the mean with p value implying significance measured using Student T-Test.

3.1.2 Collagen Gel Polymerization Temperature Test

The temperature at which the collagen polymerizes varies the 3D ECM architecture formation. To test whether this was reflected in mechanical strength of the collagen gels the effect of polymerization temperature on matrix formation of 2 and 4 mg/ml collagen gels were investigated (2.2.4.1.2). The results, as shown in figure 3.2, and 3.3, indicate a trend of decreasing stiffness with increased polymerization temperature for both 2 and 4 mg/ml collagen gels. 2 mg/ml collagen gel with normal polymerization showed higher gel stiffness (22%) when compared to gel polymerized only at higher temperature (37 °C).

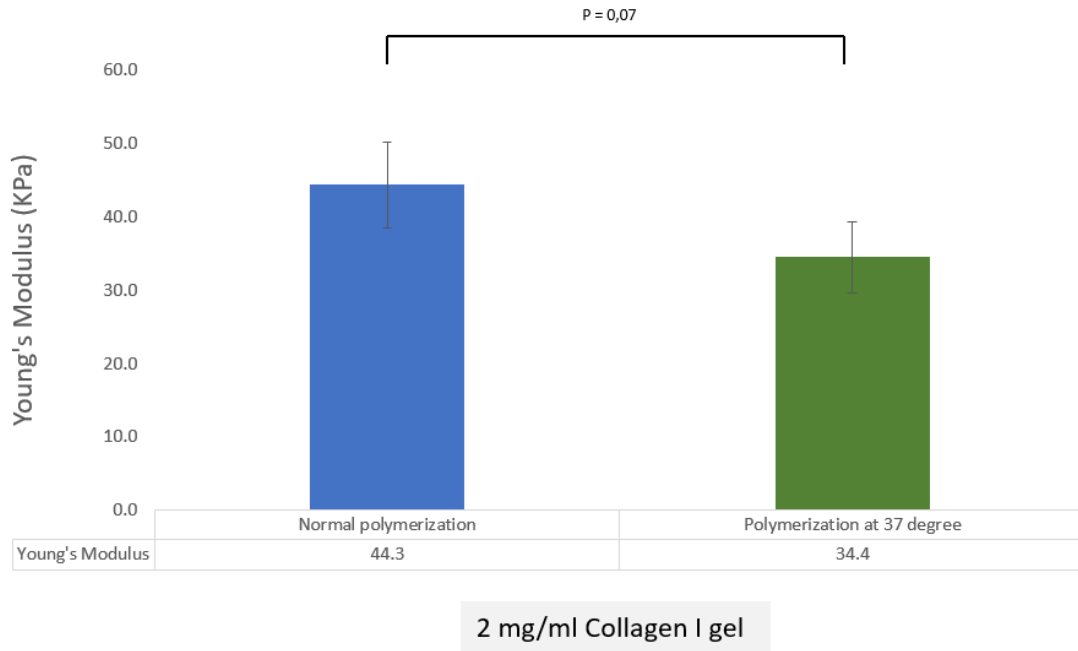


FIGURE 3.2: Measured Young's Modulus (KPa) of 2 mg/ml acellular collagen gel polymerized with two different methods that is normal polymerization for 1 hr. at RT and then for 24 hrs. in incubator at 37 °C and 5% CO₂. The other sample was only polymerized at 37 °C and 5% CO₂. Error bars indicate standard deviation of the mean with p value implying significance measured using Student T-Test.

Similarly, as shown in figure 3.3, 4 mg/ml collagen gel with normal polymerization showed higher YM value (19%) in comparison to gel polymerized at 37°C. Even though the results for both 2 and 4 mg/ml collagen samples show a trend, are not conclusive due to high significance value.

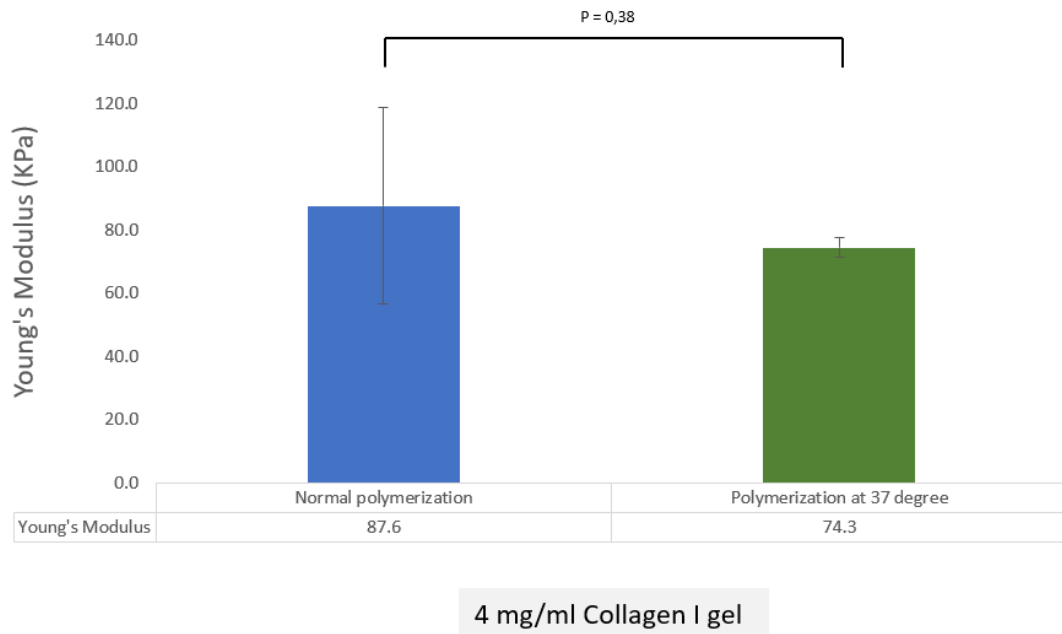


FIGURE 3.3: Measured Young's Modulus (KPa) of 4 mg/ml acellular collagen gel polymerized with two different methods that is normal polymerization for 1 hr. at RT and then for 24 hrs. in incubator at 37 °C and 5% CO₂. The other sample was only polymerized at 37 °C and 5% CO₂. Error bars indicate standard deviation of the mean with p value implying significance measured using Student T-Test.

3.1.3 Collagen Test with Different Polymerization pH

Tumor tissues have been reported to have lower pH (pH 6.0 to 6.5) [42] then what is found in physiological microenvironment (pH 7.4) which may contribute in ECM remodeling and/or degradation. It is therefore investigated in this experiment if acidic environment influences the structural integrity of 2 and 4 mg/ml collagen gel with 3 different polymerization pHs of 7.4, 6.8 and 6.1 (2.2.4.1.3). As shown in figure 3.4, the results showed a significant decrease (73%) in gel stiffness of 2 mg/ml collagen when compared between pH 7.4 and 6.1 ($p < 0.00001$) while the changes between pH 7.4 and 6.8 were not significant ($p = 0.06$).

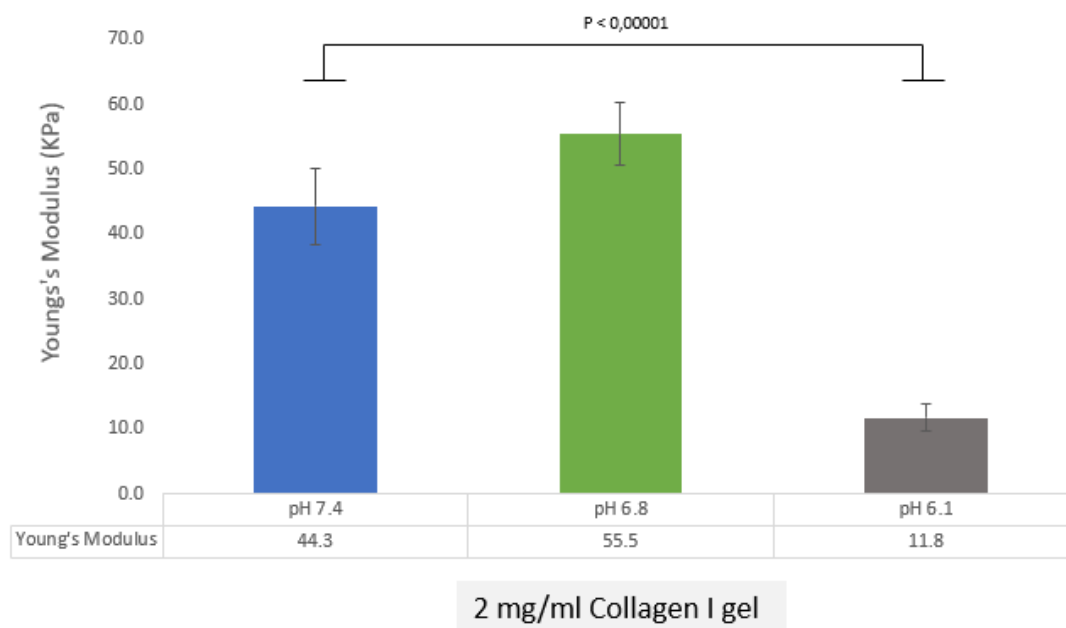


FIGURE 3.4: Measured Young's Modulus (KPa) of 2 mg/ml acellular collagen gel at pH 6.1, 6.8 and 7.4. Error bars indicate standard deviation of the mean with p value implying significance measured using Student T-Test.

Similar trend of decreasing Young's Modulus with decreasing gel pH was observed in 4 mg/ml samples as shown in figure 3.5. In comparison to 2 mg/ml collagen gel, 4 mg/ml gel only showed an overall decrease of 26% from physiological pH 7.4 to acidic pH 6.1 ($p=0,2$) and a decrease of 8% between pH 7.4 and 6.8 ($p=0,8$).

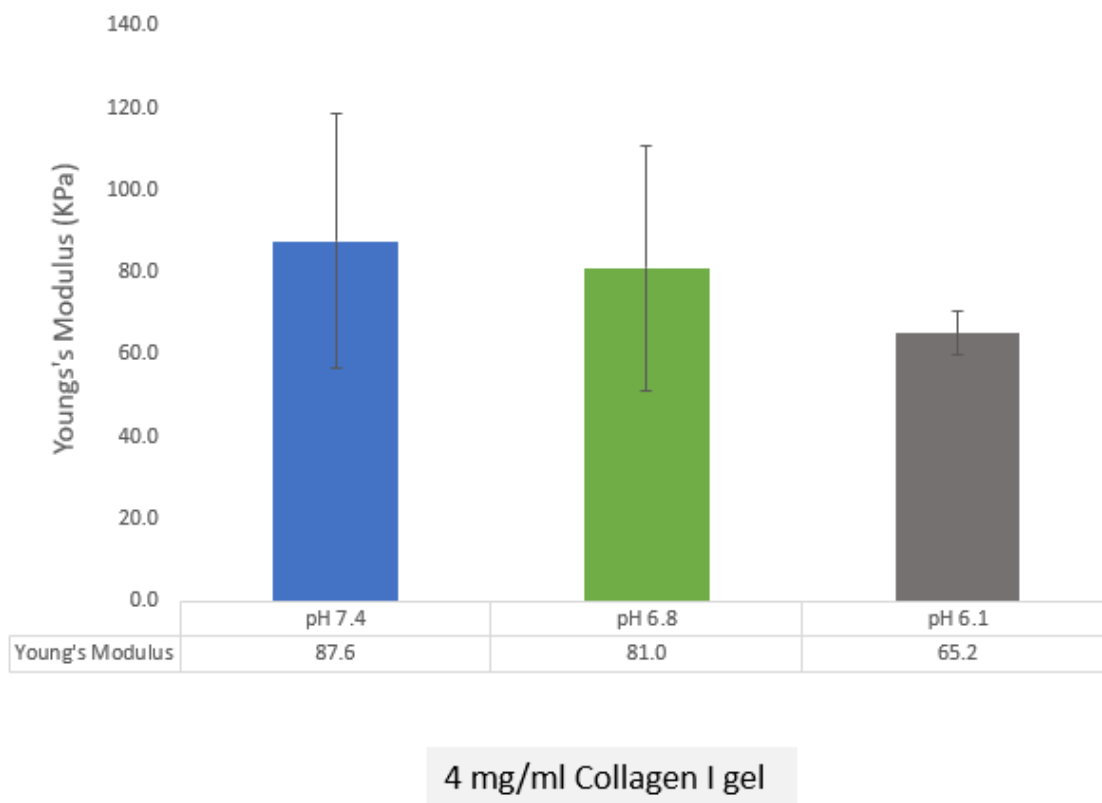


FIGURE 3.5: Measured Young's Modulus (KPa) of 4 mg/ml acellular collagen gel at pH 6.1, 6.8 and 7.4. Error bars indicate standard deviation.

3.1.4 Collagen test with colorectal cancer cell suspension and co-culture

Having performed acellular collagen gel testing for biomechanical properties it was interesting to see how the growth of cancer cells and presence of stromal cells like fibroblast would act on extracellular matrix stiffness in terms of Elastic/Young's modulus (KPa) (2.2.4.1.4). To test this, two different colorectal cancer cell lines (SW948 and SW1116) were independently embedded in the collagen gel 2.1.1. Furthermore, fibroblast is mono-cultured and co-cultured with cancer cell lines in collagen to imitate normal and cancer microenvironment.

Considering acellular collagen as the base value, the results for both day 2 and day 5 were quantitatively compared to cellularized gel samples. The results in figure 3.6 illustrate an overall increase in matrix stiffness with increased Young's Modulus after 2 days in mono and co-culture samples of collagen gel for both colorectal cancer cell lines SW1116/948 and colorectal fibroblast, CCD-18Co when compared to acellular 2mg/ml collagen. Over 5 days a decrease in stiffness in all the acellular

and cellularized collagen samples were observed for 2 mg/ml samples.

Figure 3.6 show that seeding colorectal cancer cell lines SW948 ($p=0,02$) and SW1116 ($p=0,0008$) increase the Young's Modulus (YM) of collagen gel by 65% in both day 2 and 5 samples when compared to 2 mg/ml acellular collagen. Similarly, CCD-18Co cultured collagen gel showed an average increase of YM by 27% in both day 2 and 5 samples ($p=0,0003$) in comparison to acellular gel. Aforementioned trend was also observed in co-culture (SW948 and CCD-18Co) collagen samples when compared to control which showed an average increase ($p=0,0005$) of YM by 39% in both day 2 and 5 samples. Co-cultured collagen with SW1116 and CCD-18Co showed similar trend with average increase in YM by 37% in both day2 and 5 samples when compared to control ($p=0,02$). Independent co-culture of both cell lines SW948 ($p<0,05$) and SW1116 ($p<0,02$) with CCD-18Co, showed a decrease in YM when compared to their respective mono culture YM values.

Over 5 days CCD-18Co mono-culture gel showed the most decrease in stiffness of gel in 2 mg/ml gel concentration among mono culture samples. Moreover, SW948 co-culture gel sample with fibroblast showed a decrease of YM by 41% ($p=0,02$) over 5 days while SW1116 co-culture gel sample showed 19% ($p=0,26$) decrease in YM over 5 days.

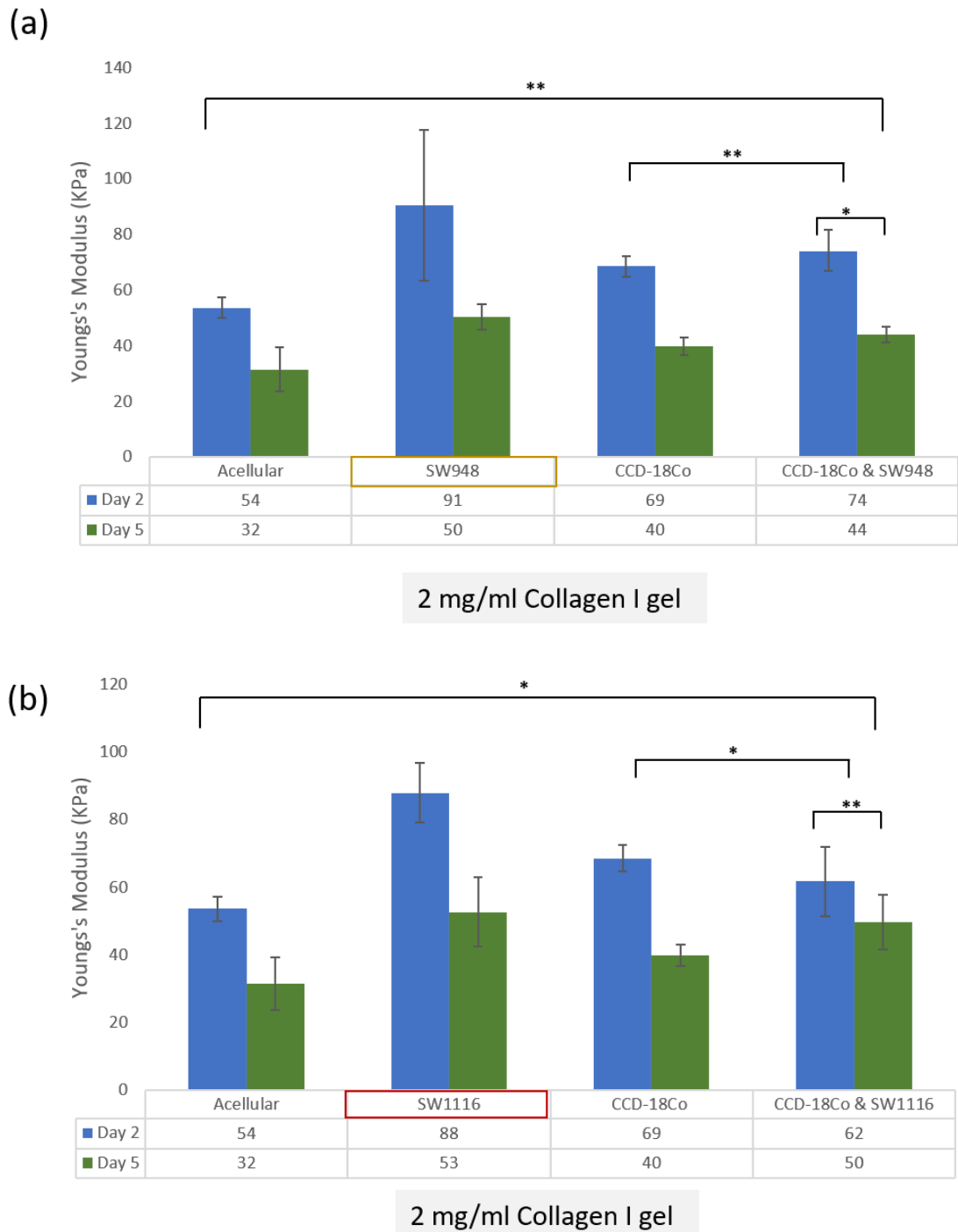


FIGURE 3.6: Measured Young's Modulus (KPa) of 2 mg/ml collagen gel seeded with 1×10^5 cell/ml suspension of colorectal cancer cell lines and colorectal fibroblast after 2 and 5 days of polymerization. The graphs in (a) and (b) present four tested conditions (1) acellular collagen, (2) collagen seeded with mono-culture of colorectal cell lines SW948 (a) and SW1116 (b), (3) collagen seeded with mono-culture of colorectal fibroblast, CCD-18Co and (4) collagen seeded with co-culture of SW948 (a) / SW1116 (b) and CCD-18Co. Error bars indicate standard deviation of the mean with * implying significance value measured using Anova Single Factor and Student T-Test (a) * $p=0.04$, ** $p<0.0006$ (b) * $p<0.02$, ** $p=0.26$

On the contrary, opposite trend can be observed with higher concentration of 4 mg/ml collagen tested with same conditions. The results, as shown in figure 3.7, demonstrate a decline in YM values and stiffness of all mono and co-culture collagen samples with colorectal cells and fibroblast when compared to the control sample of acellular collagen except co-culture gel with SW1116 and CCD-18Co. Furthermore, 4 mg/ml collagen gel seeded with a co-culture of SW948 or SW1116 and FB showed an overall decrease in stiffness over five-day period when compared to acellular control sample. Over five-day period SW948 mono-culture gel showed a nonsignificant ($p=0,3$) increase of 18% in stiffness but when cultured with fibroblast a significant decrease of stiffness by 45% is observed ($p=0,02$). Mono culture gel with SW1116 showed a decrease in YM by 23% ($p=0,07$) for day 2 samples when compared to control but showed a significant increase of 59% ($p=0,0003$) in stiffness when cultured with fibroblast in day 2 sample. While co-culture gels with both cancer cell lines and fibroblast showed a decrease in YM over five days, SW1116 sample showed more significant decrease of 65% in comparison to SW948 co-culture with fibroblast with a decrease of 43% in stiffness ($p<0,02$).

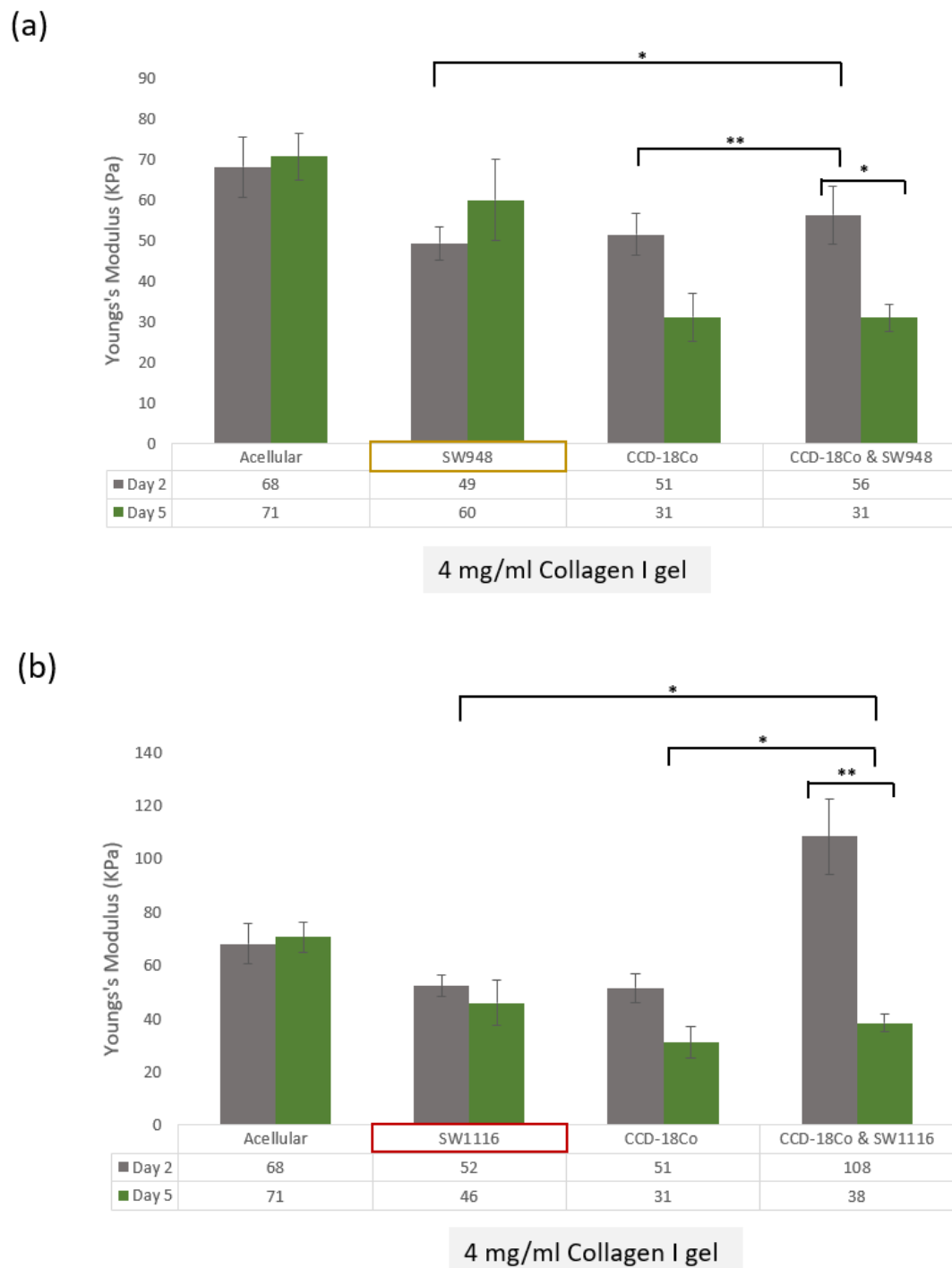


FIGURE 3.7: Measured Young's Modulus (KPa) of 4 mg/ml collagen gel seeded with 1×10^5 cell/ml suspension of colorectal cancer cell lines and colorectal fibroblast after 2 and 5 days of polymerization. The graphs in (a) and (b) present four tested conditions (1) acellular collagen, (2) collagen seeded with mono-culture of colorectal cell lines SW948 (a) and SW1116 (b), (3) collagen seeded with mono-culture of colorectal fibroblast, CCD-18Co and (4) collagen seeded with co-culture of SW948 (a) / SW1116 (b) and CCD-18Co. Error bars indicate standard deviation of the mean with * implying significance value measured using Anova Single Factor and Student T-Test (a) * $p < 0.03$, ** $p = 0.002$ (b) * $p < 0.0002$, ** $p = 0.02$

3.1.5 Structural Analysis of Collagen Gel with Confocal Reflection Microscopy (CRM)

A key feature of tumor cells is to upregulate matrix remodeling (Harjanto et al. 2011). It is therefore important to understand how the cell and matrices interactions modify the stromal cell properties and architecture of surrounding ECM. Therefore, quantification of deposition and/or degradation of collagen fibers is investigated in this study by analyzing any changes in fiber density of 2 and 4 mg/ml concentrations of collagen in physiological condition (acellular with and without fibroblast) and when exposed to pathological environment that is in presence of colorectal cancer (CRC) cells over a period of 6 days using confocal reflectance microscopy (CRM) (2.2.5). A binary image of acellular control sample of 2 and 4 mg/ml collagen gel can be seen in figure 3.8.

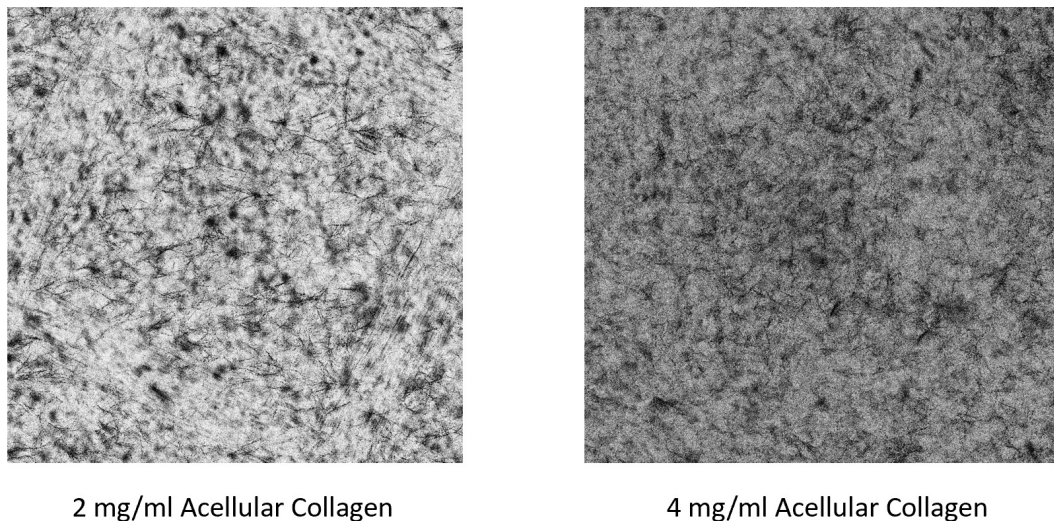


FIGURE 3.8: Visual presentation of confocal reflectance binary image of 2 and 4 mg/ml acellular collagen gel.

As shown in figure 3.9, while a slight decrease in fiber density is observed in colorectal cancer cells SW948 and SW1116 mono-cultured sample in 2 mg/ml, it did not show significant change ($p=0,08$) when compared to both day two and six acellular sample fiber density. Similarly, 2mg/ml collagen gel cultured with fibroblast did not show significant increase in fiber density ($p=0,06$) when compared to control. However, when SW948 co-cultured with CCD-18Co, a decrease of 31% in fiber density was observed in 2mg/ml co-culture sample ($p<0,01$) over six days. SW1116 co-cultured with CCD-18Co showed a decrease of 8% in fiber density over five day ($p<0,003$) over six days

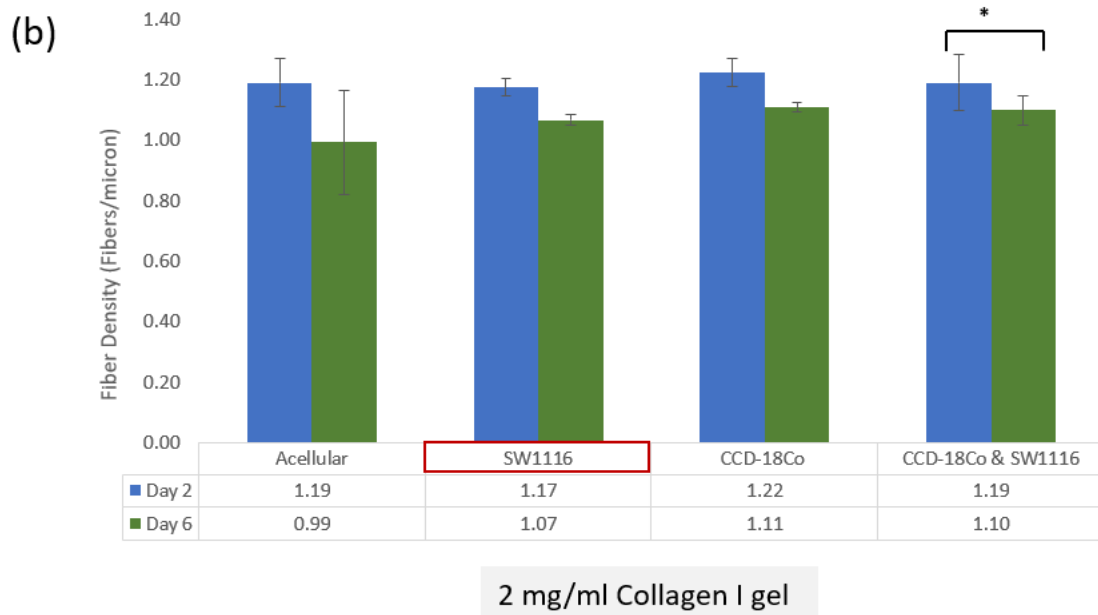
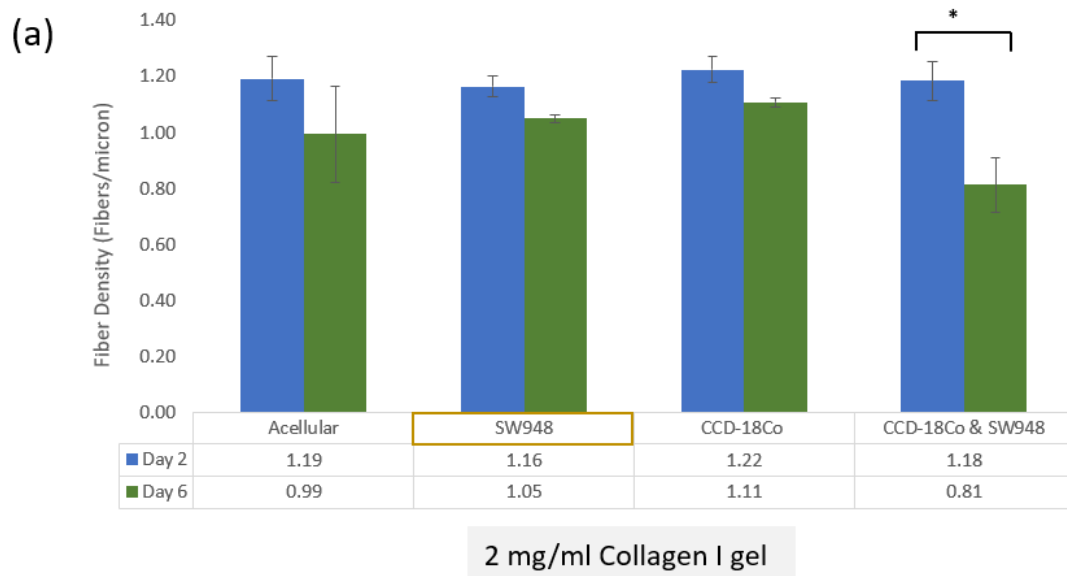


FIGURE 3.9: Measured fiber density/micron of 2 mg/ml collagen gel seeded with 1×10^5 cell/ml suspension of colorectal cancer cell lines and colorectal fibroblast after 2 and 6 days using confocal reflectance microscopy (CRM). The results highlight changes in composition of collagen gel suspended with colorectal cells in terms of fiber/micron. The graphs in (a) and (b) presents four tested conditions (1) acellular collagen, (2) collagen seeded with mono-culture of colorectal cell lines SW948 (a) and SW1116 (b), (3) collagen seeded with mono-culture of colorectal fibroblast, CCD-18Co and (4) collagen seeded with co-culture of SW948 (a) / SW1116 (b) and CCD-18Co. Error bars indicate standard deviation of the mean with * implying significance value measured using Student T-Test (a) and (b) * $p < 0.01$

As shown in figure 3.10, colorectal cancer cells SW948 showed a decrease of 4% ($p < 0,03$) while SW1116 showed a decrease of 8% ($p < 0,002$) in fiber density when mono-cultured in 4 mg/ml gels at day two and six. CCD-18Co when cultured with 4 mg/ml collagen showed significant decrease of 35% in fiber density in comparison to control gel ($p < 0,0000003$). Furthermore, a decrease in fiber density is also observed in co-culture samples, with SW1116 fiber content decreased by 26% ($p = 0,04$) and SW948 ($p = 0,13$) by 20% when cultured with CCD-18Co over 6 days. Overall no significant differences in fiber density between acellular 2 and 4 mg/ml collagen gel were found in this experiment ($p = 0,08$).

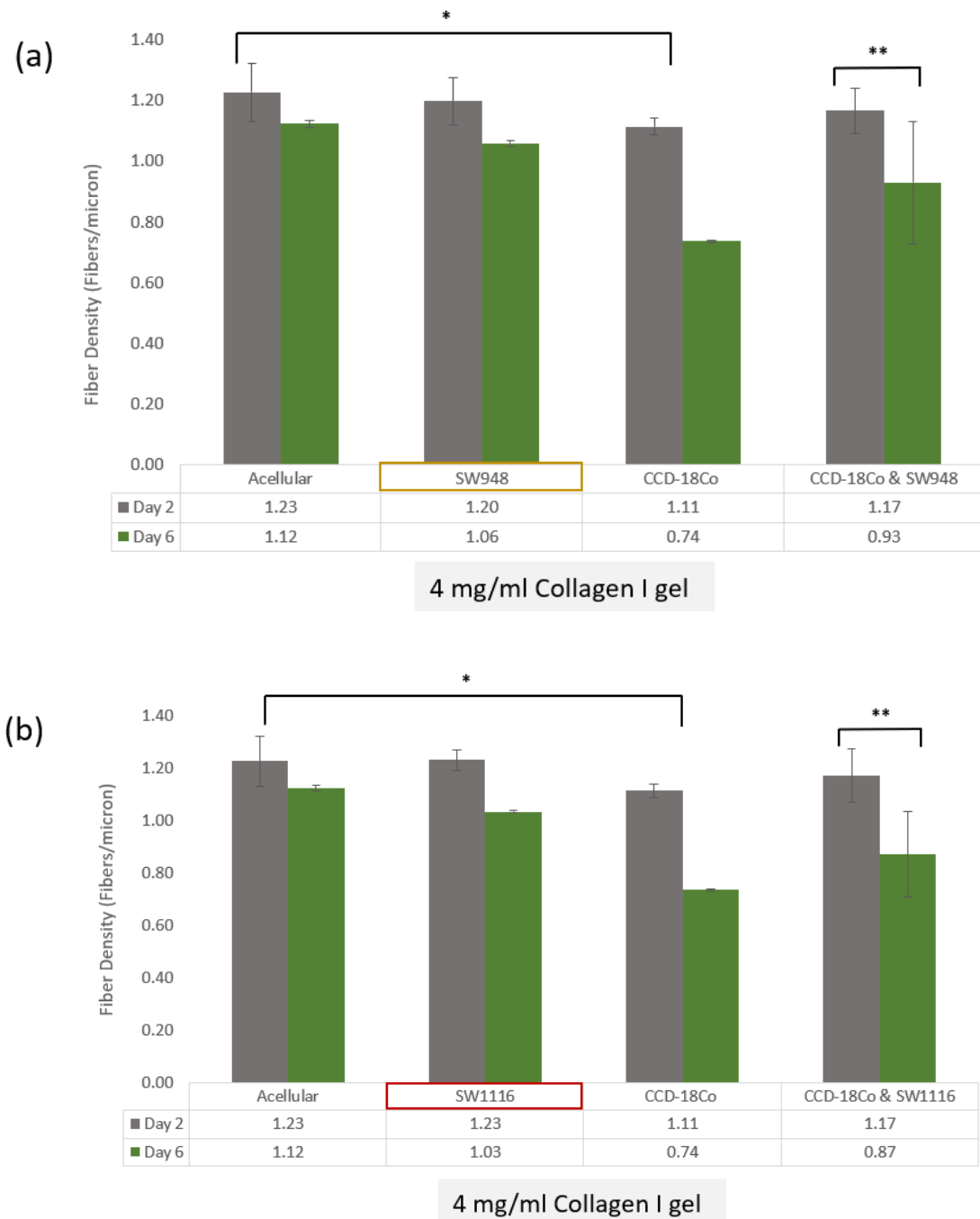


FIGURE 3.10: Measured fiber density of 4 mg/ml collagen gel seeded with 1×10^5 cell/ml suspension of colorectal cancer cell lines and colorectal fibroblast after 2 and 6 days using confocal reflectance microscopy (CRM). The results highlights changes in composition of collagen gel suspended with colorectal cells in terms of fiber/micron. The graphs in (a) and (b) presents four tested conditions (1) acellular collagen, (2) collagen seeded with mono-culture of colorectal cell lines SW948 (a) and SW1116 (b), (3) collagen seeded with mono-culture of colorectal fibroblast, CCD-18Co and (4) collagen seeded with co-culture of SW948 (a) / SW1116 (b) and CCD-18Co. Error bars indicate standard deviation of the mean with * implying significance value measured using Anova Single Factor and Student T-Test (a) * $p < 0,0000003$, ** $p = 0,13$ (b) * $p < 0,0000003$, ** $p = 0,04$

3.2 Cell-Matrix Interaction Analysis with Collagen Gel Contraction Assay

The restructuring of the stromal network is primarily mediated by stromal cells, most prominently fibroblasts, typically in process like wound healing [3, 16]. However, when interacting with tumor cell, the cancer associated fibroblasts also induce tension-dependent matrix remodeling and may increase contraction of extracellular matrix [35, 63, 64]. The degree of matrix reorganization by different cancer cell types can be studied using collagen gel contraction assay (GCA). In this experiment, it was tested at what degree the collagen contracts in the presence of fibroblast and colorectal cancer cells by quantifying the change in gel diameter over time 2.2.6. Visual presentation of gel contraction assay is shown in figure 3.11.

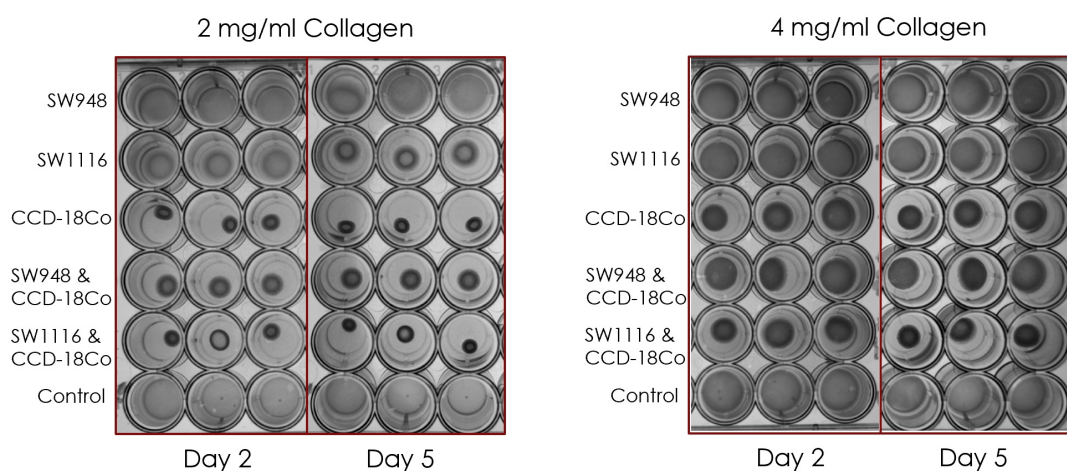


FIGURE 3.11: Visual presentation of gel contraction assay with collagen contracting over 5-day period. Collagen gels were pipetted in 48 well plates and floated after 1 hour of polymerization at RT. Images were taken after 2 and 5 days to investigate gel contraction.

Figure 3.12 present the contraction in percentage % of initial area of 2 mg/ml collagen gel mono and co-cultured with SW948, SW1116 and CCD-18Co over five days. In general, the results indicated that the % contraction of gels observed after two days were mostly consistent with day five results for all samples tested with 2 and 4 mg/ml collagen. 2 mg/ml acellular control gel samples did not show contraction over five days. Collagen gel seeded with SW948 ($p=0,26$) showed no significant contraction over five days while SW1116 mono-culture gel showed an average decrease of 40% when compared to 2 mg/ml acellular control in day two and day five samples ($p<0,000004$). The most significant contraction of collagen gel matrix was observed in 2 mg/ml collagen gels seeded with fibroblast, CCD-18Co, with a substantial decrease of 79% ($p<0,000007$) in both measured samples over five days. Unlike mono culture sample, SW948 when cultured with CCD-18Co showed a

substantial contraction of 60% ($p < 0,000007$) when compared to control. Colorectal cells of SW1116 also co-cultured with CCD-18Co in 2 mg/ml gel showed similar trend, as observed in mono-culture sample, with higher contraction of an average of 78% ($p < 0,000007$) over 5 days when compare to control.

Similar to lower gel concentration, 4 mg/ml acellular gel showed no contraction over five day as shown in figure 3.13 . Furthermore, no significant ($p = 0,9$) change in gel area was observed in SW948 mono-culture 4 mg/ml collagen gel while a slight contraction was observed from results of 9% ($p = 0,05$) in 4 mg/ml gel cultured with SW1116. Fibroblast mono-cultured gel also showed a decrease in gel area by an average of 39% over five days ($p < 0,007$). Similar pattern to 2 mg/ml gel samples is also observed in 4 mg/ml for co-culture samples. SW1116 when cultured with fibroblast showed a significant decrease in gel area by an average of 45% ($p < 0,00004$) over five days while SW948 co-culture showed a decrease of 22% ($p = 0,007$) over five days.

Overall 2mg/ml samples showed higher degree of contraction in comparison to 4 mg/ml.

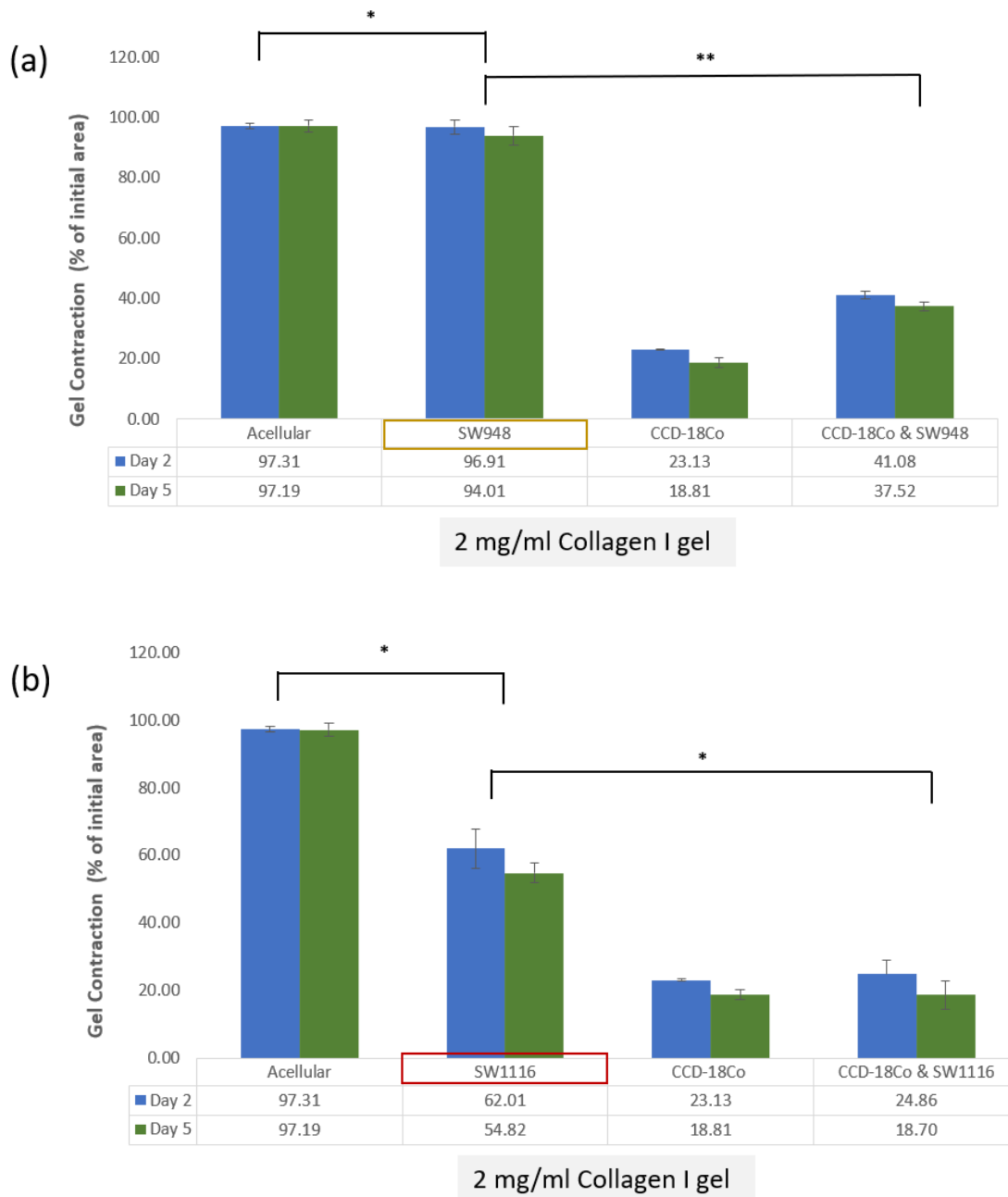


FIGURE 3.12: Measured gel contraction in % of initial area of a 48 well for 2 mg/ml collagen gel with mono and co-culture of SW948, SW1116 with CCD-18Co, fibroblast, 1×10^5 cell/ml suspension at day 2 and day 5 after polymerization. Error bars indicate standard deviation of the mean with * implying significance value measured using Anova Single Factor (a) * $p=0,26$ ** $p<0,000007$ and (b) * $p<0,0000005$

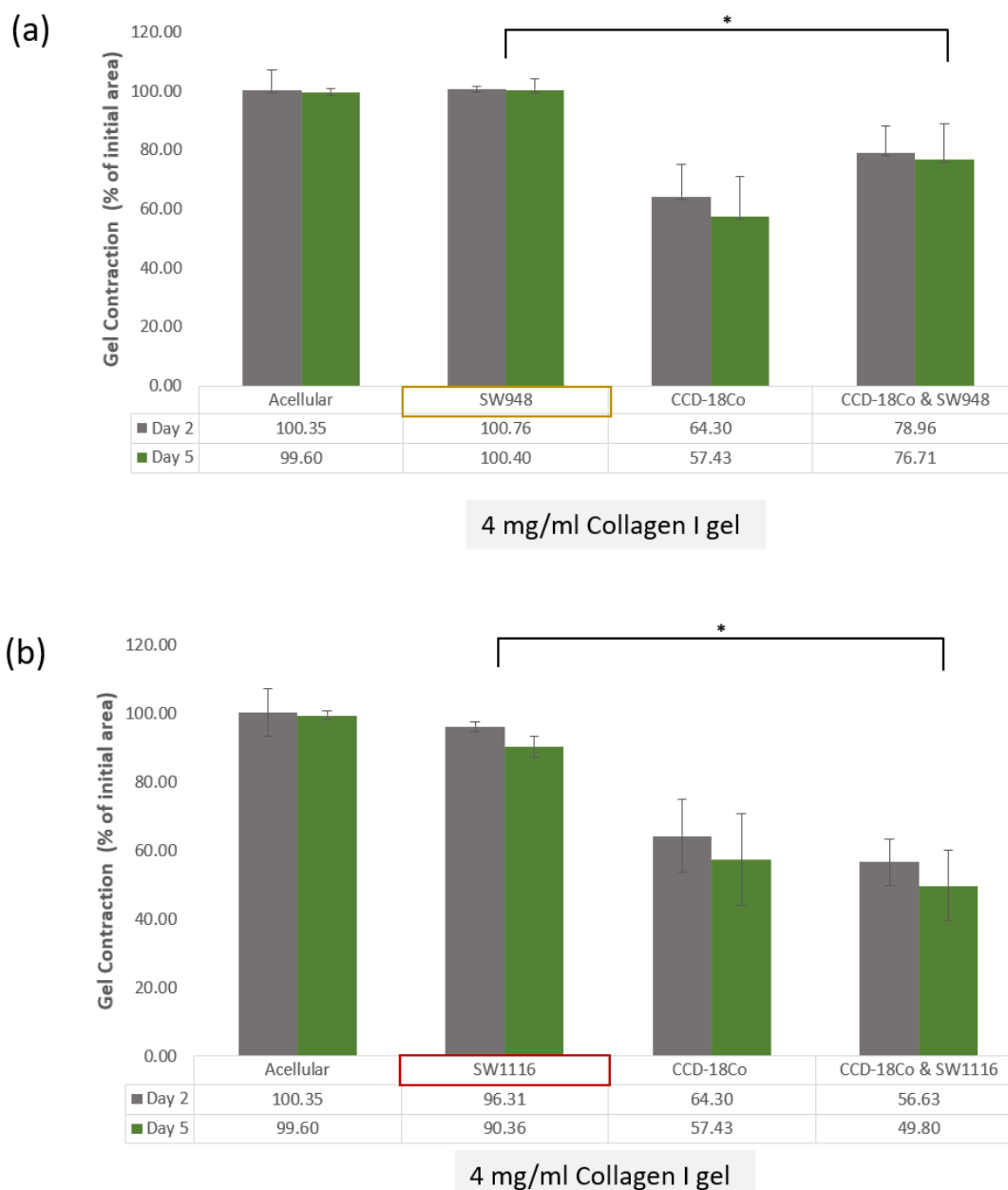


FIGURE 3.13: Measured gel contraction in % of initial area of a 48 well for 4 mg/ml collagen gel with mono and co-culture of SW948 and CCD-18Co, fibroblast, 1×10^5 cell/ml suspension at day 2 and day 5 after polymerization. Error bars indicate standard deviation of the mean with * implying significance value measured using Anova Single Factor (a) and (b) * $p < 0,008$

3.3 Interstitial Fluid Flow and Cell Migration Analysis in 3D Model

In addition to transport and medium for exchange of nutrients, interstitial fluid flow also induces cell and matrix alignment and cell migration due to applied biomechanical forces and pressure. Therefore, in this experiment it was investigated if the interstitial fluid flow plays a role in cancer cell migration. Furthermore, the interaction of fibroblast with cancer cells and its ability of remodeling ECM in the presence of biomechanical forces of interstitial fluid flow is also investigated. A 3D microfluidic cell culture system was used to apply pressure gradients and fluid flow to examine responses of cells seeded next to a 3D type I collagen scaffold over a period of 48 hours to survey the effects of interstitial flow on cancer cell phenotype and migration (2.7, 2.2.7).

3.3.1 Volumetric Fluid Flow & Permeability

Initial volumetric flow was calculated using the change in volume and height of the liquid in syringes over time interval of 30 mins as described in section 2.2.7.2. The resulting individual values for each time point were used further to calculate the permeability over period of 2 hours of flow through 4 mg/ml collagen gel until volume in all the syringes equilibrated. The average permeability value was further used to calculate final volumetric flow using Darcy's equation. Detailed calculations can be seen in Appendix B. Permeability of 4 mg/ml collagen gel was then calculated by rearranging the Darcy's equation and the results are presented in figure 3.14.

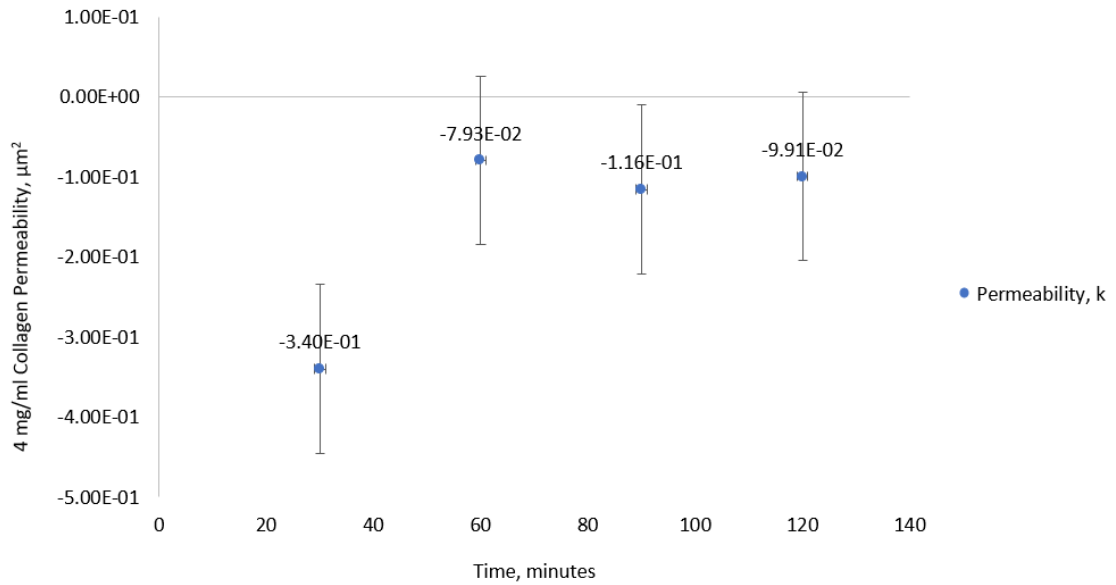


FIGURE 3.14: Measured permeability, k (μm^2) of 4 mg/ml collagen gel with application of fluid flow for a period of 2 hours and measurements taken every 30 mins. Standard deviations (SD) is presented as error bars.

Due to high pressure drop during the first half hour the first value calculated for permeability was omitted when calculating the average k value. From the results the average calculated permeability of 4 mg/ml collagen gel was found to be $9,80 * 10^{-2} \mu m^2$.

Once permeability was estimated Darcy's equation was used to calculate the change in volumetric fluid flow, Q (m^3/s) over a period of 2 hours and is presented in figure 3.15.

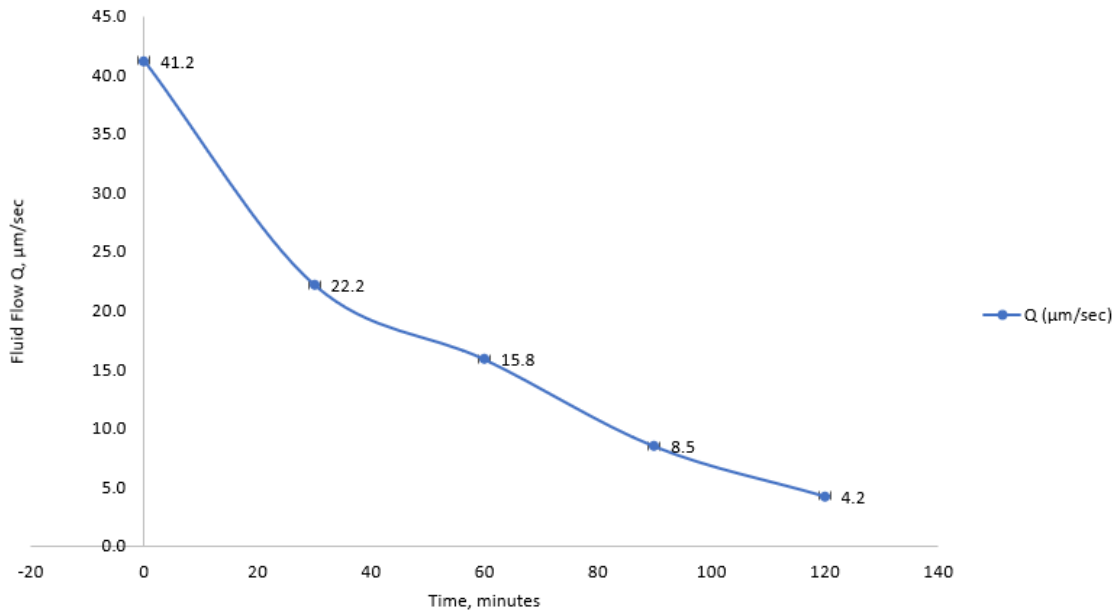


FIGURE 3.15: Measured volumetric fluid flow, $Q(m^3/s)$ through 4mg/ml collagen gel over a period of 2 hours with measurements taken every 30 mins

The flow rate data showed a gradual decrease in fluid velocity with a proportional decrease in pressure. The results were further used to determine the fluid velocity to be used for cell migration experiments thus indicating the volume required in syringes to achieve required flow of cell culture media through different concentrations of collagen. Based on other publicized work [55, 65, 66] where interstitial fluid flow has been investigated it was decided to use a starting velocity of 8.5 μm until the volume equilibrate in the syringes giving a reduced flow rate of 4.2 μm before the syringes with higher volume were filled again to achieve a flow of 8.5 μm .

3.3.2 Interstitial Fluid Flow and Cell Migration

Interstitial fluid flow has shown to affect the tissue architecture and cell organization by regulating morphology and migration of cells in microenvironment. Interstitial fluid flow generated from growing tumor is found to be a promotor of tumor cells invasion. Fibroblast being the key resident of stroma with their contractile

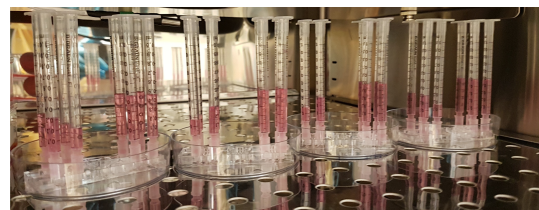


FIGURE 3.16: Interstitial Fluid flow test apparatus

property regulate interstitial fluid volume and pressure via remodeling and contracting the cytoskeletal infrastructure [8, 67, 68]. Therefore, to assess cell migration in cancer progression, an in-vitro 3D model is prepared to investigate the rate of cell migration through different concentrations of collagen with colorectal cell lines SW948 and SW1116 (2.2.7.3).

The results obtained from the experiments done with all conditions as described in table 2.7 showed a substantial difference due to one deciding factor namely, Fibroblast. Condition 1 and 2 with colorectal cancer cell line SW948 and SW1116 embedded in media channel were subjected to flow with cell culture media in the direction of flow (normal) and in the opposite direction of flow (reverse) did not show any migration in either 2 or 4 mg/ml collagen gel on application of flow. Fluorescence images in figures 3.17, 3.18, 3.19 and 3.20 show one section of media channel and gel interface for each of condition 1, 2 and control for both colorectal cell lines and collagen concentrations, before and after flow application. Images clearly indicate no cell migration through the collagen for tested normal and reverse flow in both gel concentrations and for both CRC lines.

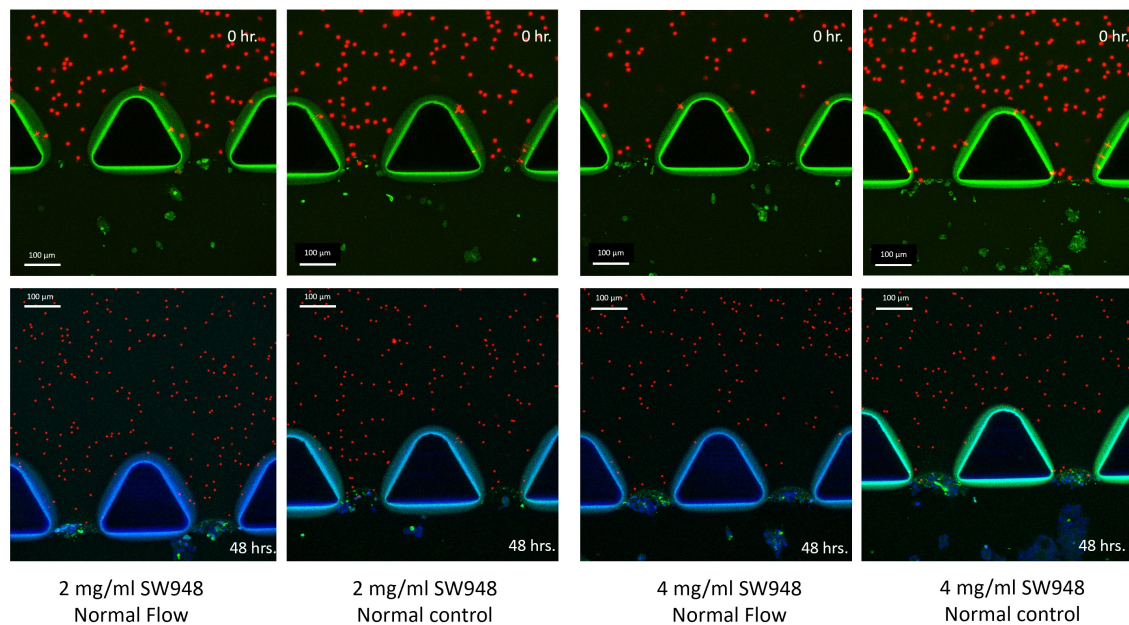


FIGURE 3.17: Confocal fluorescence images of a section of media channel and gel interface when tested with normal flow showing no migration of CRC SW948 at 0 hr. and after application of flow at 48 hrs. in both collagen gel concentrations of 2 and 4 mg/ml. 0 hr. image show SW948 stained with cytosolic CellTracker green while the fluorescent beds are in red suspended throughout collagen. 48 hrs. images show SW948 with additional blue nuclei Hoechst dye.

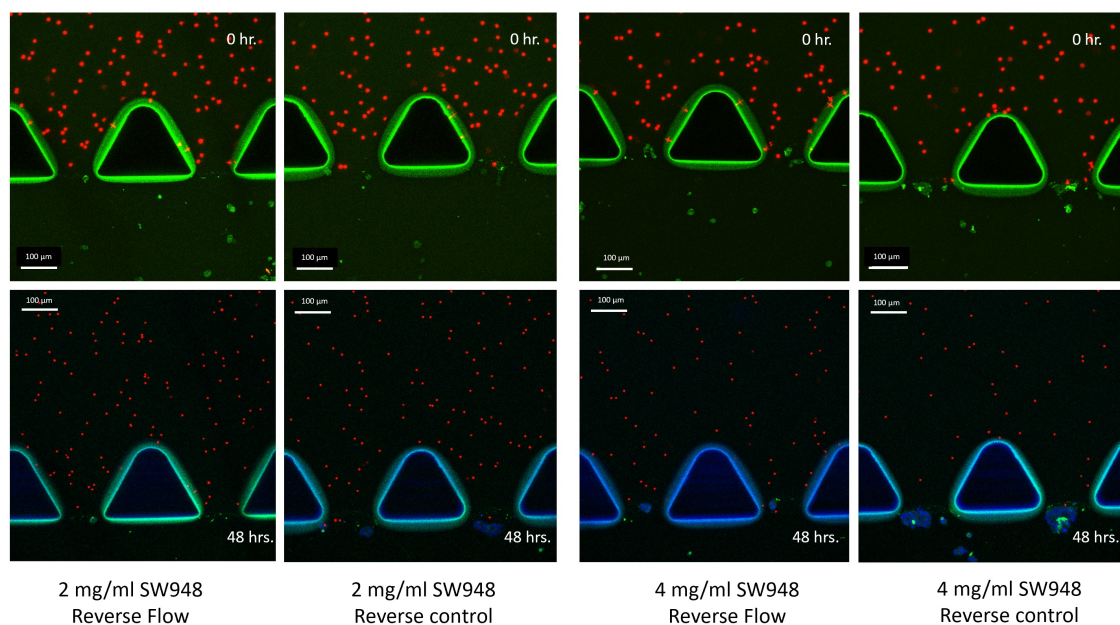


FIGURE 3.18: Confocal fluorescence images of a section of media channel and gel interface when tested with reverse flow showing no migration of CRC SW948 at 0 hr. and after application of flow at 48 hrs. in both collagen gel concentrations of 2 and 4 mg/ml. 0 hr. image show SW948 stained with cytosolic Celltracker green while the fluorescent beds are in red suspended throughout collagen. 48 hrs. images show SW948 with additional blue nuclei Hoechst dye.

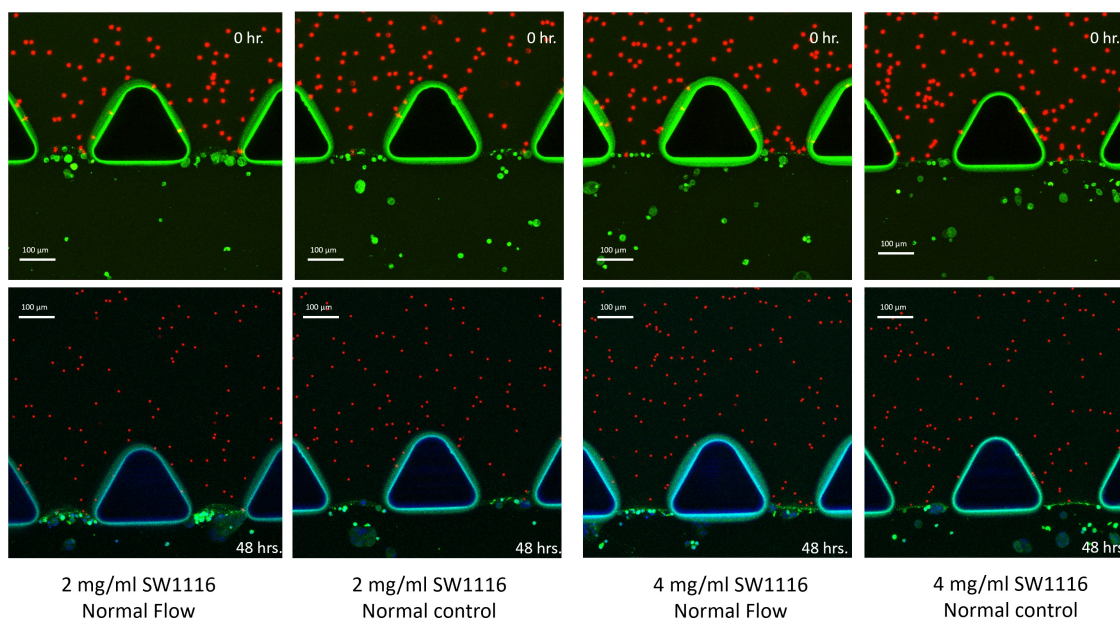


FIGURE 3.19: Confocal fluorescence images of a section of media channel and gel interface when tested with normal flow showing no migration of CRC SW1116 at 0 hr. and after application of flow at 48 hrs. in both collagen gel concentrations of 2 and 4 mg/ml. 0 hr. image show SW1116 stained with cytosolic Celltracker green while the fluorescent beds are in red suspended throughout collagen. 48 hrs. images show SW948 with additional blue nuclei Hoechst dye.

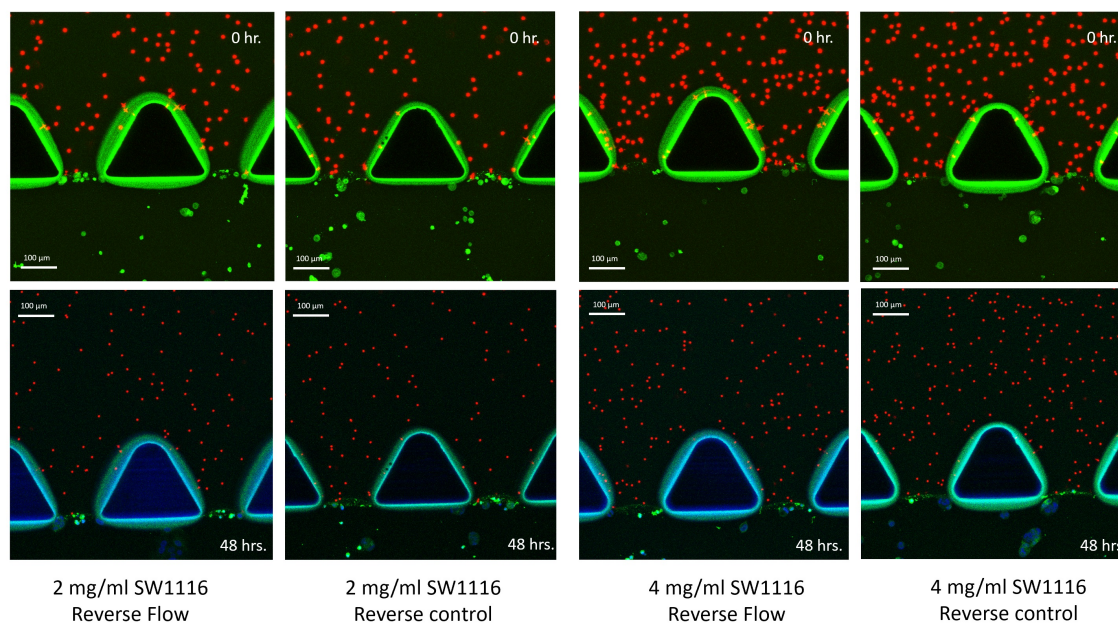


FIGURE 3.20: Confocal fluorescence images of a section of media channel and gel interface when tested with reverse flow showing no migration of CRC SW1116 at 0 hr. and after application of flow at 48 hrs. in both collagen gel concentrations of 2 and 4 mg/ml. 0 hr. image show SW1116 stained with cytosolic Celltracker green while the fluorescent beds are in red suspended throughout collagen. 48 hrs. images show SW948 with additional blue nuclei Hoechst dye.

Contrary to above, an active migration of colorectal cancer cells was observed with both cell lines when subjected to flow in the presence of fibroblast in collagen gel. Tabulated results of cell migration are shown in Appendix B. The results in figure 3.21 show a distribution of amount of cell migration calculated for each section for all tested experiments while figure 3.22 summarize the total migrated cells for each test. Due to time limitation, tests were only carried out with 2 mg/ml collagen concentration as described in table 2.7 for test condition 3. Fluorescence images in figure 3.23 show one section of media channel and gel interface for tested condition 3 with fibroblast-mediated 2 mg/ml collagen and both colorectal cell lines before and after flow application.

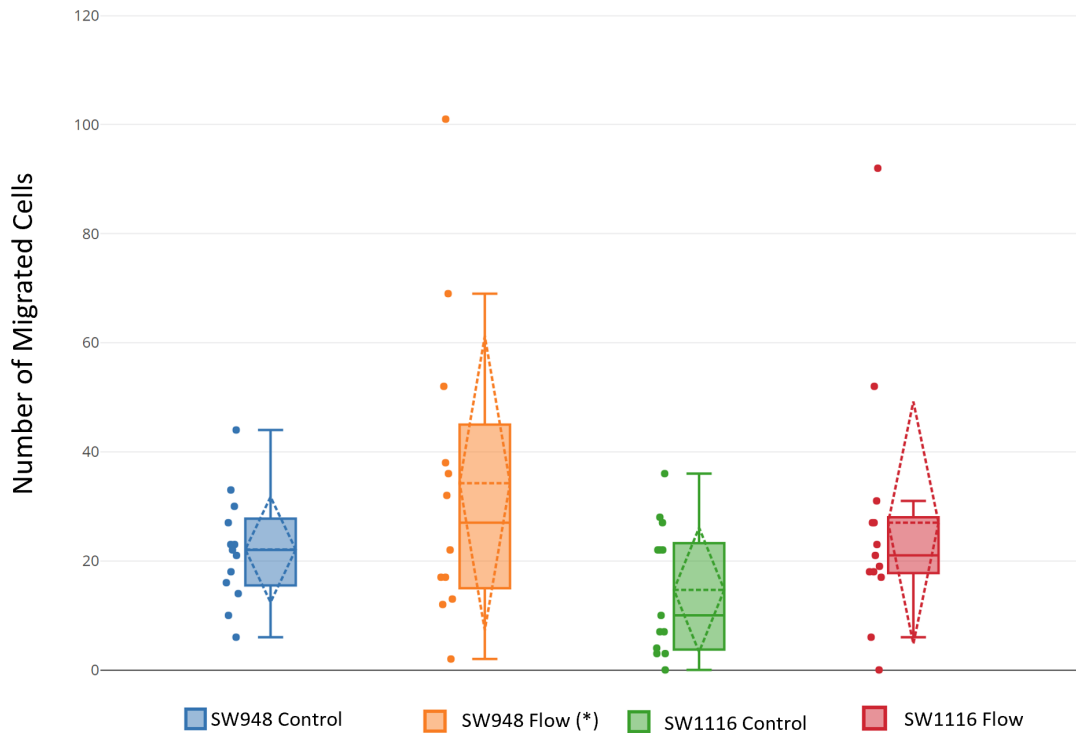


FIGURE 3.21: Distribution of sum of CRCs SW948 and SW1116 migration. Box and Whisker plot show the calculated number of cells that migrated into 2 mg/ml collagen gel region by using fluorescence images of each section of media channel. (*) A data value of 350 migrated cell for one of the sections is not included in the plot for SW948 normal flow test as the number was far out of range in comparison to rest of the data values.

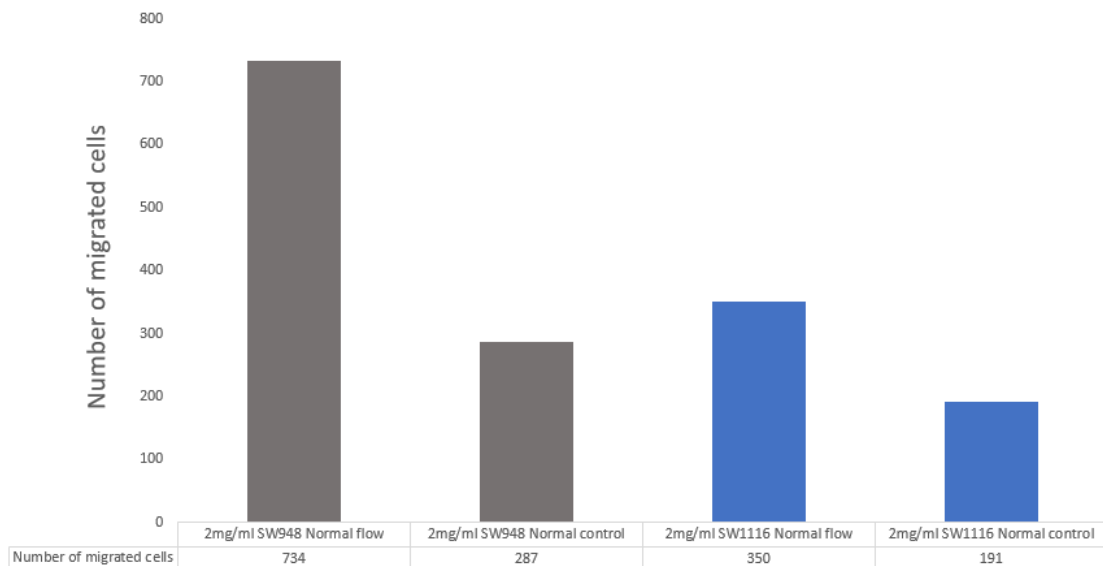


FIGURE 3.22: Sum of total CRCs SW948 and SW1116 migration. Total calculated number of cells that migrated into 2 mg/ml collagen gel region by using fluorescence images. (*) Data value of 350 migrated cell that was not included in the distribution box and whisker plot in figure 3.25 is included in this plot for SW948. Standard deviations (SD) is presented as value in red.

Surprisingly, it can be observed that there was migration of SW948 and SW1116 cells into collagen gel even prior to application of flow. Upon application of flow both cell lines migrated from media channel in to the collagen gel. When considering cell migration per section (figure 3.21), the highest amount of cell migration was observed, during normal flow conditions, by SW948 with migration of 350 cells. This amount was over two times standard deviation of that group and regarded as an outlier and not included in the plotted results. Nevertheless, SW948 still showed highest migration, when compared to SW1116 normal flow, with migration of 101 cells in contrast to 92 cells of SW1116 respectively. As shown in figure 3.21, SW948 control test data is closely distributed showing an even migration throughout the channel while SW1116 does not have a median value indicating uneven cell migration over the channel. Furthermore, SW948 normal flow data show a wide distribution indicating higher difference in number of migrated cells in different sections over the media channel.

Slightly higher amount of cell migration was observed by SW948 (figure 3.22) in control sample in comparison to SW1116 when considering total number of cells migrated from media channel in to the gel. SW948 showed the most significant migration with total of twofold increase in migrated cells then SW1116.

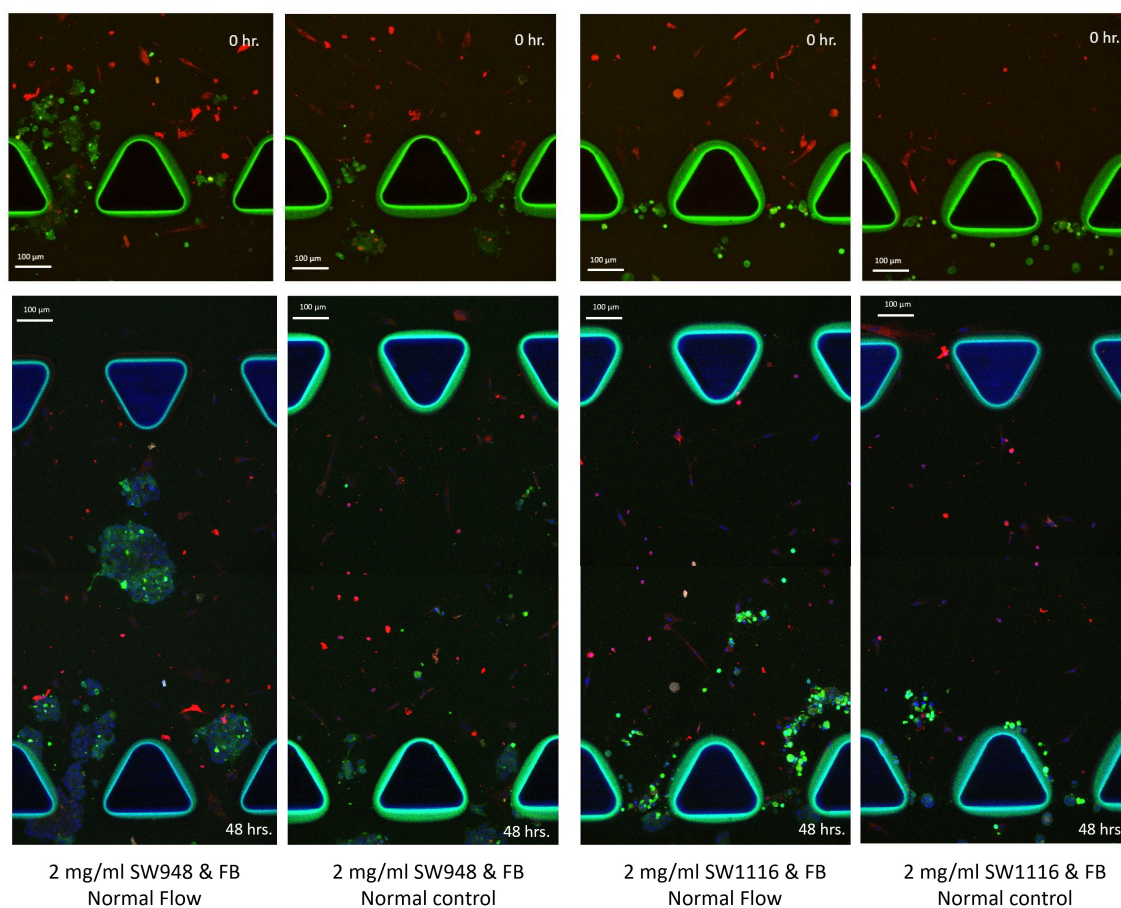


FIGURE 3.23: Confocal fluorescence images of a section of media channel and gel interface when tested with normal flow showing migration of CRC SW948 and SW1116 at 0 hr. and after application of flow at 48 hrs. in 2 mg/ml collagen gel. Zero hour image show CRCs stained with cytosolic CellTracker green while the CCD-18Co, Fibroblast are stained with cytosolic red CellTracker suspended throughout collagen. 48 hrs. images show CRCs and fibroblast with additional blue nuclei Hoechst dye.

Chapter 4

Discussion

4.1 Type I Collagen as model system for ECM, close but not exact.

Initial objective of this study was to understand and assess the structural integrity and composition of the extracellular matrix in the presence of biomechanical forces and to see how remodeling dynamically alters extracellular matrix (ECM) structure.

Two concentrations of type I collagen were tested throughout the study, that is, 2 mg/ml and 4 mg/ml which lay in the range of concentrations previously tested under several publications [48, 57, 61, 69]. 4 mg/ml being twice as high in concentration then 2 mg/ml gives a good margin to emulate stiffer ECM in case of tumor progression.

Several studies [16, 48, 61] have been performed to quantify matrix remodeling by calculating Elastic or Young's modulus which describes the ability of an elastic material to resist deformation on application of stress. A review of literature reveals significant differences in the results due to variations in deformation methods used to interpret the cellular response to biophysical forces [54, 70]. Moreover, some studies [52, 53] used tissue samples instead of biomaterial which would also impact the results. Therefore, better models are needed to replicate what is happening in vivo to be able to understand how this impact cancer growth and response to therapy.

4.1.1 Acellular Collagen Gel Properties

To test whether collagen gel properties are similar and react the same way as previously measured ECM, confined compression test was performed on 2 and 4 mg/ml acellular collagen gels to investigate the different tissue dynamics. The results revealed that gel stiffness increased with increasing collagen concentrations from 44 KPa at the lower concentration to 88 KPa at the highest concentration (day 1 result). This indicates that increased collagen concentration correlates with increased deformation resistance and could be due to increased fibril content of collagen [61, 71]. Although different methods were used, general trend was supported by earlier studies. Cross et al. has made a comparison of equilibrium modulus between different concentrations of collagen ranging from 3 mg/ml to 20 mg/ml using stress compression relaxation confined test and have concluded that the equilibrium modulus is increasing with increased collagen concentration hence increased stiffness of gel with increased concentration [48]. Tensile force test applied to acellular collagen gel to calculate Young's Modulus by Lang et al. showed results that are consistent with finding of this study that gel deformation resistance increase with increasing collagen concentrations [69]. Furthermore, Kawano et al. has investigated the unconfined elastic modulus of colorectal cancer tissue extracted from 106 patients with different clinicopathological characteristics as, tumor size and stage, age and sex of patients and lymph node and distant metastasis and found a median elastic modulus value of 7,51KPa for colorectal cancer tissue [52]. Therefore, collagen having the ability to self-assemble itself when polymerized in vitro into fibrils serves as a good gel model to be used for studying cancer growth in vitro.

To further quantify the above finding, structural analysis of acellular gel was performed to investigate if fibril density in different collagen concentration is the cause of increase stiffness. This was done by quantifying the matrix architecture using confocal reflectance microscopy (CRM). Unfortunately, the results were not quantitative as no significant differences were found in fiber density of acellular 2 and 4 mg/ml collagen gels. Previous literature does support the idea of increase fiber density of collagen gel with increase concentration [48, 69, 72] supporting the argument that increased stiffness of gel could be due to increased fiber content. Line scan [48] method of image analysis was used to calculate the fiber density which seems to be not conclusive. Therefore, other analysis methods need to be considered in future.

4.1.1.1 Acellular collagen gel matrix formation

To find the optimal protocol for collagen matrix formation that would be most similar to *in vivo* situations the acellular 2 and 4 mg/ml collagen gels were also tested for gel stiffness using different polymerization temperature to investigate changes in physical properties of the gel depending on matrix formation. Cells and its surrounding matrix are exposed to variety of mechanical stimuli like hydrostatic pressure, tensile, shear and compression force. *In vivo*, cells exposed to such mechanical forces follow Newton's third law by responding to these alterations and remodeling their matrix resulting in change of its mechanical properties [35]. The results showed a trend of higher gel stiffness in samples polymerized initially at lower temperature then samples polymerized at 37 °C. This indicates that stromal architectures with varying physical characteristics alter the physical organization of the gel. This could be due to changes in matrix formation with varying fiber diameter, fibrillar bundling by cross linking and fiber length [3]. This finding support pervious research done to calculate the gel rigidity of cellularized 3 mg/ml collagen reporting higher gel rigidity in samples polymerized at 21 °C in comparison to gels polymerized at higher temperature of 37 °C ([73]. While the results of this experiment were not significant, a study has reported that collagen polymerized at room temperature resembles fibers found *in vivo* in animal models, in comparison to gels polymerized at 37 °C, due to the type of matrix fiber formation [74].

pH plays a role in the stability of collagen matrix To analyze effect of product of metabolic pathways chosen by normal and tumor cells, on ECM deformation resistance, 2 and 4 mg/ml acellular collagen concentrations were tested with different polymerization pHs of 7.4, 6.8 and 6.1. Normal epithelial cells mostly use oxidative phosphorylation (OXPHOS) for energy production to proliferate and keeping a neutralized microenvironment while tumor cells tend to favor aerobic glycolysis with lactic acid as a product creating an acidic microenvironment and effecting matrix homeostatis [42–44]. The overall results indicated a decrease in gel stiffness or deformation resistance with decrease in pH. A previous study conducted with 2 mg/ml collagen and a range of polymerization pH of 6 – 9 showed similar trend with increased liner modulus with increasing pH [71]. The results indicate that built up of acidic environment plays a role in matrix integrity which could be due to degradation of collagen fibrils and may contribute to enhance growth and invasiveness of tumor cell due to immune destruction (Lyssiotis and Kimmelman 2017, p. 864).

4.1.2 Colorectal cells remodel the matrix dependent on the initial collagen concentration

The key physiological process of extracellular matrix (ECM) to remodel itself creates a three-dimensional structure with physical tension that influences the morphology, behavior and phenotype of cells [48]. Conversely, a key feature of tumor cells is also to upregulate matrix remodelling [51]. Consequently, these cell and matrix interactions modify the cellular properties and architecture of surrounding ECM which then would aid cell migration as cells require intermediate ECM concentrations for optimal cell movement due to their need to balance traction and adhesion forces [75, 76]. The outstanding elastic nature of ECM is altered from soft and compliant, in normal physiological environment, to stiff and rigid due to increased mechanical forces by tumorigenesis. Different mechanism could be a reason of increased matrix stiffness found in solid tumors like preference of metabolic pathways and remodeling of ECM.

The role of metabolism in the ECM interaction is tested by using two colorectal cell lines with differing metabolism that is dependence on glycolysis. SW948 has been found to favor glycolysis and has found to have higher proliferation rate while SW1116 relies more on oxidative phosphorylation (OXPHOS) (Unpublished work from research group at CORE). Interestingly, cellularized collagen gel compression test showed a distinct difference in gel stiffness when seeded in different gel concentration. While cellularized colorectal cancer cells of both metabolic phenotype and stromal fibroblast showed an increase in gel stiffness in 2 mg/ml gel concentration after 2 days of proliferation, a decrease was observed in cellularized gels with 4 mg/ml concentration. These findings support the idea that in low density environment (2 mg/ml collagen), cells deposit more collagen to increase fibril fraction to promote cell adhesion, proliferation and migration [77]. In contrast, cells decompose fibril fraction in highly dense environment [51, 75].

Further quantification of above results was further investigated with structural analysis of both gel concentrations independently cellularized with SW948, SW1116 and fibroblast. 2 mg/ml mono cultured samples didn't show significant increase in fiber density as suggested by mechanical strength test in higher stiffness after 2 days but a decrease in fiber density in 4 mg/ml samples were observed supporting the above hypothesis of fiber decomposition in higher concentration gels [51, 75].

SW948 and SW1116 cells alters the matrix remodeling behavior in presence of fibroblast Morphology, behavior, and phenotype of cells embedded in a 3D environment is significantly influenced by fiber structure and density. Furthermore, fibroblast being

the architect of stromal network are influenced by tumor cells to change extracellular matrix properties by exerting tension on the matrix and influencing the alignment of collagen fibers [11]. Moreover tumor cells can exploit the properties of fibroblast to aid in their proliferation by promoting remodeling and degradation of ECM with increased production of matrix metalloproteinases (MMP) [77].

When comparing mono-culture of SW948 and SW1116 no significant difference can be reported between the two cell lines in 2 mg/ml gel concentration after two days. An increase in gel stiffness of SW948 in 4 mg/ml can be reported in day 5 samples in comparison to SW1116. This could be because of higher cell number of SW948 as they have a higher proliferation rate in comparison to SW1116. This behavior could also suggest that SW948 may have more motile nature and perhaps are more compliant to higher density matrices [75].

While gel mono-culture with fibroblast (CCD-18Co) samples did not show much difference between the two gel concentrations, a change can be observed when co-cultured with different cancer cells. In 2mg/ml co-culture sample, SW948 showed a higher drop in gel stiffness in comparison to SW1116. This could be because of more glycolytic profile of SW948 and higher proliferation aid to acidic environment. As stated by Choi et. al. tumor masses can have a reduced pH of 6.0 to 6.5 [42]. Also, assessment done by Kato et. al. showed that acidic environment results in increased production of proteolytic MMP-9 causing increased invasiveness of the tumor cells. Furthermore, tumor cells having the ability to activate fibroblast which can influence proteolytic activity by production of MMPs causing remodeling and degradation of collagen matrix and enhancing permeability could explain the decrease in stiffness [35, 78, 79]. This indicates that lower pH environment may influence the integrity of ECM cytoskeleton and may influence promotion of tumor growth, invasion and metastasis. [80].

In 4 mg/ml co-culture sample, SW1116 showed significant increase in gel stiffness after 2 days. This could be due to more fibroblastic morphology of SW1116 resulting in increased adhesion forces by pulling on the matrix which is also mediated by the presence of fibroblast [73]. The results therefore suggest that fibroblast with both synthesizing and degrading property of matrix, provide structural integrity to ECM and facilitate functions of resident cells depending on their morphology and phenotypical properties to adhere, proliferate and migrate [3, 8].

Structural analysis of co-cultured collagen gels also suggested similar results as observed above for both cell lines. As expected, in 2mg/ml co-culture sample, SW948 with higher proliferation rate and possibly more MMP production due to presence of fibroblast, showed higher drop in fiber content in comparison to SW1116 over 5 days.

In 4 mg/ml co-culture sample, SW1116 showed slightly higher drop in fiber content in comparison to SW948 over 5 days being consistent to mechanical test findings were SW1116 had a higher drop in YM value indicated possible degradation of fibril content.

Day 5 results for all cellularized collagen samples (except SW948 in 4 mg/ml) show a decrease in YM values which may suggest degradation of collagen contents in consequence of proliferation as the cells have an upper limit on how dense an environment they are able to grow and thrive in [75].

A previous study argues that highly invasive cells favor denser environments while less invasive cell prefer lower dense environments [51, 75]. Another study also suggests that different cell types may interact differently with the extracellular matrix resulting in different stromal activity [81]. These are interesting arguments and could serve as a reasoning for differences found in the results between colorectal cell lines. A future consideration would be to perform cell-type specific analysis and investigate invasion potential of SW1116 and SW948 using different assays and further metabolic and gene profiling to strengthen the explanation of results presented above.

From analysis of acellular and cellularized collagen gel results it can be theorized that ECM is remodeled in a symbiotic manner which is dependent both on initial matrix properties but also on cancer cell migratory behavior [51, 82].

4.2 Fibroblast promotes cell-mediated contraction of Collagen Gel depending on CRCs phenotype

Extracellular matrix has shown to be an important regulator of development, differentiation and organization in many epithelial cells and therefore, organization of cells is dependent upon their ability to interact with extracellular matrix. This epithelial-matrix interaction leads to remodeling of ECM and effecting cell behavior [17, 81]. An important feature of stromal cells, Fibroblast, is to mediate contraction by reorganization of stromal network, typically in process like wound healing [3, 16]. But when interacting with tumor cell, the cancer associated fibroblasts induce tension-dependent matrix remodeling and may increase contraction [35, 63], deformation of ECM and tumor and fibroblast invasion [64, 68, 83, 84].

Cell-mediated contraction of 2 and 4 mg/ml collagen gel was carried out to understand the epithelial-matrix interactions. The most prominent finding was substantial contraction of both fibroblast-mediated collagen concentrations with highest of 81% in 2 mg/ml sample and 42% in 4 mg/ml suggesting the plausible contraction characteristics of fibroblast which could be because of promoted remodeling of collagen fibrils in to thick and stiff fibers by increased crosslinking [3]. A study done as early as in 1989 with the same colorectal fibroblast cell line , CCD-18Co, as this study showed similar results as above with high contractility of collagen gels by fibroblast [85]. This trait of fibroblast play a vital role during biological activities like wound healing but is also modulated by pathological microenvironment for promotion of tumorigenesis [9, 17, 36, 86]. It is suggested that collagen fibrils are organized by fibroblast by exerting tension on the matrix thus influencing the alignment of the collagen [11] leading to increase contractility of ECM [4].

Furthermore, co-cultured collagen gel with both 2 and 4 mg/ml showed most contraction of samples suspended with SW1116 than SW948. This further supports the finding that SW1116 morphologically resembles fibroblasts, which may also include features of a more crosslinking behavior which in the presence of fibroblast could have induced higher traction to matrix thus increasing contraction. On the contrary, SW948 with possibly more motile phenotype could have showed less adhesion and therefore less contraction over 5 days. Thus, cell types with different morphology and proliferation rates may attribute to altered interaction between cells and extracellular matrix [81].

4.3 Interstitial Fluid Flow and Cell Migration Analysis in 3D Model

4.3.0.1 Collagen gel permeability

Collagen gel permeability of 4 mg/ml collagen gel was calculated in 3D fluid flow model to be $9,8 * 10^{-2} m^2$. The hydraulic permeability of 2 mg/mL collagen I gel was determined to be $1 * 10^{1-m^2}$ by Polacheck et al. [57]. Over the years different studies showed a range of permeability values which are inconsistent and not always comparable. This could be due to the biomaterials used in different studies and range of different preparation methods changing the microstructure of the gel samples [48]. In future studies it would be interesting to also apply similar analysis method for calculating permeability with other concentrations of collagen. In addition, it would

also be interesting to investigate if and how change in matrix formation with different polymerization conditions influence permeability of collagen.

4.3.0.2 Fibroblast promote cancer cell migration

The effect of biomechanical force of interstitial flow on cell-cell and cell-matrix interaction was investigated. Normal and reverse flow tests performed with cancer cell lines SW948 and 1116 did not show any migration in to collagen gel region after 48 hrs of application of flow for either 2 or 4 mg/ml concentrations. Fibroblast being the primary mediator of stromal reorganization contributes to change in migratory properties of tumor cells that may later lead to metastasis [3, 87]. This suggests that stromal cells like fibroblast are playing a key role in cell to matrix interaction and may encourage cell migration via cell-cell interaction.

Analysis of images taken at 0 and 48 hours showed that the interface between collagen gel and cancer cells in media channel moved by approximately 50 μm representing slight contraction of collagen gel which was also observed in the acellular sample of gel contraction assay. Similar gel contraction was therefore suspected in the next series of test were fibroblast-mediated collagen is used for testing cell migration.

When considering the normal flow test performed with fibroblast-mediated 2 mg/ml gel conc. and colorectal cancer (CRC) cells, SW948 and SW1116, revealed a significant amount of cell migration. SW948 cell line had the most migration with total of 734 migrated cells while SW1116 had 350 migrated cells. A previous study concluded that fibroblast enhance tumor cell invasion in the presence of interstitial fluid flow by sensing mechanical stress and modulating the biomechanical microenvironment. Study further hypothesized that tumor cell - fibroblast interactions are synergistically effected by interstitial flow due to alteration of cell behavior and 3D matrix through which they communicate and migrate [68]. It has also been proposed that cancer associated fibroblast may induce tumor cells to undergo epithelial to mesenchymal transition (EMT) hence promoting tumor cell motility, invasion and metastasis [8, 31, 88]. Therefore, the results further support the earlier argument suggesting motile morphology of SW948 cell line which is upregulated in the presence of fibroblast.

SW948 have shown to favor moving in clusters while SW1116 showed a more individual or stream like cell migration. More in-depth study in to the morphology of the CRC cell lines would help understand the cells ability or tendency to migrate individually or collectively depending on their phenotype. It has been debated in a study that cells having amoeboid-like morphology tend to migrate individually or in

a stream while other cells like epithelial cells tend to migrate collectively in a cluster [3].

Fluid flow test performed with SW948 and fibroblast mediated collagen showed a higher flow rate on day 2 of flow application with cell culture media equilibration already within approximately 30 mins while other tests performed with fibroblast mediated gel equilibrated in approx. 3 hours. From this observation one can hypothesize that SW948 may have proteolytically active migration mechanism which could be due to degradation of collagen matrix leaving tracks in the gel during migration which can be associated with a previous study proposing similar cell behavior [57].

An unanticipated finding was the resulting cell migration observed at 0 hr. in normal flow samples and migration of cells at 0 and 48 hrs. in the control tests. This can only be explained by presence of physical cell-cell and cell-matrix interactions impacting the migration. Hence, it could conceivably be hypothesized that increased fibroblast migration and physical interactions between tumor cells and fibroblast may influence tumor cell invasion [38, 68]. Moreover, it was also observed from image analysis that fibroblast have travelled upstream and downstream in to the media channel implying their mesenchymal behavior.

On review, several studies suggest a biochemically regulated interaction between fibroblast and CRCs through chemotactic signaling to be the reason of migration in the presence of flow [57, 58]. In flow experiments, any migration due to chemotaxis could only be possible during night as in the presence of flow cancer cells were migrating in the direction of flow and any biochemical signaling from fibroblast would be flowing away from cancer cells. Migration observed at 0 hr. and control sample may have been influenced by the presence of chemotactic signaling from fibroblasts.

4.3.0.3 Data Analysis and limitations

It is important to highlight here that the data analysis process could have an impact on the results. For example, maximum projection (compact) images of z-stack images of each section were made for cell count which may have caused underestimation of migrated cells due to overlapping. Furthermore, the lack of live imaging resulted in no records of cell migrated distance and exact amount of migration. Moreover, as the flow was applied over 2 days there is possibility of normal diffusion of cells overnight which could result in overestimation of migrated number of cells. Considering only time point imaging it is difficult to safely articulate if the sum of migrated cells, in all cases, were entirely due to migration by fluid flow or there

could be possibility of cell proliferation of already existing colonies in the gel from the migrated cells at 0 hr before application of flow.

Troubleshooting of preliminary interstitial fluid flow experiment and time limitation resulted in not performing tests with fibroblast-mediated 4 mg/ml collagen and CRCs. It could be hypothesized that the 3D cancer cell migration would be influenced by properties of collagen matrix as migration velocity and proteolytic requirement would be dependent on the density of the environment [3, 89] as also observed from other mechanical, structural and contraction tests performed as part of this research.

4.4 Challenges and Future Perspectives

4.4.1 Technical Challenges

The most common but limiting challenge of this study was late delivery of type I collagen by the manufacture by overall delays of three months causing time limitation to complete all the experimental work and data analysis. Tests performed to investigate mechanical properties of collagen and fluid flow through collagen were pilot experiments. Collagen mechanical test standardization was challenging as upon reviewing other studies it was evident that deformation method varies between the other studies thus making it difficult to compare when considering test parameters, settings and configurations, data interpretation and processing of results.

When considering 3D fluid flow test, the challenge was handling of 3D cell culture chips with small sample volume. The manufacture protocols were not always clear resulting in a few troubleshooting experiments, which was time consuming, prior to performing experiments with achievable results. Furthermore, data analysis of the images resulting from fluid flow experiments was quite challenging due to generation of over 1000 confocal images for all experiments. Development of automated methods to analyze the images and finding right tools to get the most relevant results needs to be considered going forward. As this field is still new and evolving, the best and standard practice is still to be determined as research progresses.

4.4.2 Future Considerations

Understanding the role of stroma-mediated drug resistance in tumors due to remodeling and alignment of extracellular matrix is an important step in gaining insight

of tumor behaviors in cellular microenvironment and plan of therapeutic interventions. Structural analysis of collagen to investigate how presence of cancer cells change the physical characteristic of matrix could therefore be interesting to further explore. Even though this was investigated in this study with confocal reflectance microscopy, not all the structural analysis results were significant, and further research needs to be carried out to investigate the structural properties of different concentrations of 3D collagen model in the presence of cancer cells, with different image analyzing techniques. These techniques may include more refining of the nonuniform background from the images and trying different software with possible fibril trace features. It would also be interesting to shed light on how cancer cells realign the matrix to help regulate invasion as it is suggested that reorientation of collagen fibrils perpendicular to tumor cell is promoted in tumorous microenvironment by increased fibril cross-linking [9].

Cancer cells with different metabolic phenotype has shown to remodel the matrix differently. To further understand their phenotype, it would be feasible to do gene analysis of the cancer cells by performing protein and gene expression analysis like GLUT1 expression, which is known to be highly expressed in glycolytic tumors [6].

There is abundant room for further progress in determining the effect of interstitial fluid flow on cell migration. Role of fibroblast in cell migration was observed in this study but should be further investigated with different collagen concentrations to see how this will influence cell migration. It would also be interesting to further investigate the effect biochemical stimuli with secretion of chemokines by fibroblast in upstream and downstream cell migration of colorectal cancer cell lines with different phenotype. Another area to explore would be validating the activation of cancer cell stimulated fibroblast in the presence of interstitial fluid flow with use of biomarkers.

When considering the mechanical properties of collagen gel, Poisson's ratio is found to be strongly altered by the network geometrical structure and collagen cross-linking density [62]. It is therefore important to consider calculating Poisson's ratio for different concentrations of collagen gel with unconfined indentation compression method due to its wide-ranging use in in-vitro modeling of ECM.

Over the years many biomechanical, fluid and solid mechanics mathematical models have been established to predict physical and physiological parameters of tumor microenvironment which would in turn help to understand and strategies better methods of drug delivery and treatment [47, 55]. A possible progression of this work would be using in vitro data from this study to give input to an in-silico mathematical model of cancer microenvironment to measure the physical and physiological impacts of tumor on ECM.

Chapter 5

Conclusion

This project was undertaken to design and evaluate the effect of physical and mechanical forces in a 3D model system which may replicate an in-vivo tumor setting. The study showed that pure biophysical forces from cancer and/or fibroblast cells can modulate the mechanical properties of extracellular matrix. The results showed a clear difference in matrix stiffness of 2 and 4 mg/ml concentrations of collagen. The study also extended our knowledge that pH influences collagen matrix stiffness with SW948 showing higher decrease in Young's Modulus/stiffness than SW1116. It was found that cellularized collagen gels with SW948, SW1116 and CCD-18Co showed increased stiffness in 2 mg/ml collagen concentration while a decreased stiffness in 4 mg/ml collagen. Fibroblast, CCD-18Co showed the most contraction of collagen gel in both 2 and 4 mg/ml while SW1116 showed most gel contraction when co-cultured with fibroblast. No cancer cell migration was observed in the absence of fibroblast while in presence of fibroblast-mediated 2 mg/ml collagen gel, SW948 showed the highest degree of cell migration under interstitial fluid flow in comparison to SW1116. The study concludes that extracellular matrix is remodeled in a symbiotic manner in tumor microenvironment which is dependent both on initial matrix properties but also on cancer cell migratory behavior.

References

- [1] A. Jemal *et al.* Global cancer statistics. *CA: a cancer journal for clinicians*, 61(2):69–90, 2011. doi:10.3322/caac.20107.
- [2] I. L. Steffensen, J. E. Paulsen, and J. Alexander. Genetic and environmental factors in colorectal cancer. mutations in the familial adenomatous polyposis gene. *Tidsskrift for den Norske laegeforening : tidsskrift for praktisk medicin, ny raekke*, 117(14):2046–2051, 1997. ISSN 0029-2001.
- [3] A. G. Clark and D. M. Vignjevic. Modes of cancer cell invasion and the role of the microenvironment. *Current opinion in cell biology*, 36:13–22, 2015. doi:10.1016/j.ceb.2015.06.004.
- [4] R. Malik, P. I. Lelkes, and E. Cukierman. Biomechanical and biochemical remodeling of stromal extracellular matrix in cancer. *Trends in biotechnology*, 33(4):230–236, 2015. doi:10.1016/j.tibtech.2015.01.004.
- [5] D. Hanahan and R. A. Weinberg. Hallmarks of cancer: The next generation. *Cell*, 144(5):646–674, 2011. doi:10.1016/j.cell.2011.02.013.
- [6] M. W. Pickup, J. K. Mouw, and V. M. Weaver. The extracellular matrix modulates the hallmarks of cancer. *EMBO reports*, 15(12):1243–1253, 2014. doi:10.15252/embr.201439246.
- [7] B. Weigelt, C. M. Ghajar, and M. J. Bissell. The need for complex 3d culture models to unravel novel pathways and identify accurate biomarkers in breast cancer. *Advanced drug delivery reviews*, 69-70:42–51, 2014. doi:10.1016/j.addr.2014.01.001.
- [8] T. Marsh, K. Pietras, and S. S. McAllister. Fibroblasts as architects of cancer pathogenesis. *Biochimica et biophysica acta*, 1832(7):1070–1078, 2013. ISSN 0006-3002. doi:10.1016/j.bbadis.2012.10.013.
- [9] A. Cho, V. M. Howell, and E. K. Colvin. The extracellular matrix in epithelial ovarian cancer - a piece of a puzzle. *Frontiers in oncology*, 5:245, 2015. doi:10.3389/fonc.2015.00245.

- [10] A. Page-McCaw, A. J. Ewald, and Z. Werb. Matrix metalloproteinases and the regulation of tissue remodelling. *Nature reviews. Molecular cell biology*, 8(3):221–233, 2007. ISSN 1471-0072. doi:10.1038/nrm2125.
- [11] C. Frantz, K. M. Stewart, and V. M. Weaver. The extracellular matrix at a glance. *Journal of Cell Science*, 123(Pt 24):4195–4200, 2010. doi:10.1242/jcs.023820.
- [12] M. Liu *et al.* The effect of mechanical strain on fetal rat lung cell proliferation: Comparison of two- and three-dimensional culture systems. *In vitro cellular & developmental biology. Animal*, 31(11):858–866, 1995. ISSN 1071-2690. doi:10.1007/BF02634570.
- [13] A. J. Engler, S. Sen, H. L. Sweeney, and D. E. Discher. Matrix elasticity directs stem cell lineage specification. *Cell*, 126(4):677–689, 2006. doi:10.1016/j.cell.2006.06.044.
- [14] T. Yeung *et al.* Effects of substrate stiffness on cell morphology, cytoskeletal structure, and adhesion. *Cell motility and the cytoskeleton*, 60(1):24–34, 2005. ISSN 0886-1544. doi:10.1002/cm.20041.
- [15] M. H. Zaman *et al.* Migration of tumor cells in 3d matrices is governed by matrix stiffness along with cell-matrix adhesion and proteolysis. *Proceedings of the National Academy of Sciences of the United States of America*, 103(29):10889–10894, 2006. ISSN 1091-6490. doi:10.1073/pnas.0604460103.
- [16] C. B. Raub, A. J. Putnam, B. J. Tromberg, and S. C. George. Predicting bulk mechanical properties of cellularized collagen gels using multiphoton microscopy. *Acta biomaterialia*, 6(12):4657–4665, 2010. ISSN 1878-7568. doi:10.1016/j.actbio.2010.07.004.
- [17] P. Lu, V. M. Weaver, and Z. Werb. The extracellular matrix: A dynamic niche in cancer progression. *The Journal of cell biology*, 196(4):395–406, 2012. doi:10.1083/jcb.201102147.
- [18] S. Altinay. Is extracellular matrix a castle against to invasion of cancer cells? In K. Xu, editor, *Tumor Metastasis*. InTech, 2016. ISBN 978-953-51-2630-0. doi:10.5772/64495.
- [19] S. Crotti *et al.* Extracellular matrix and colorectal cancer: How surrounding microenvironment affects cancer cell behavior? *Journal of cellular physiology*, 232(5):967–975, 2017. doi:10.1002/jcp.25658.

- [20] J. G. Goetz *et al.* Biomechanical remodeling of the microenvironment by stromal caveolin-1 favors tumor invasion and metastasis. *Cell*, 146(1):148–163, 2011. doi:10.1016/j.cell.2011.05.040.
- [21] D. Radisky, J. Muschler, and M. J. Bissell. Order and disorder: The role of extracellular matrix in epithelial cancer. *Cancer Investigation*, 20(1):139–153, 2002. ISSN 0735-7907. doi:10.1081/CNV-120000374.
- [22] B. R. Lester and J. B. McCarthy. Tumor cell adhesion to the extracellular matrix and signal transduction mechanisms implicated in tumor cell motility, invasion and metastasis. *Cancer and Metastasis Review*, 11(1):31–44, 1992. ISSN 0167-7659. doi:10.1007/BF00047601.
- [23] M. Augsten, C. Hägglöf, C. Peña, and A. Ostman. A digest on the role of the tumor microenvironment in gastrointestinal cancers. *Cancer microenvironment : official journal of the International Cancer Microenvironment Society*, 3(1):167–176, 2010. doi:10.1007/s12307-010-0040-9.
- [24] S. F. Badylak, D. O. Freytes, and T. W. Gilbert. Extracellular matrix as a biological scaffold material: Structure and function. *Acta biomaterialia*, 5(1):1–13, 2009. ISSN 1878-7568. doi:10.1016/j.actbio.2008.09.013.
- [25] O. de Wever, P. Demetter, M. Mareel, and M. Bracke. Stromal myofibroblasts are drivers of invasive cancer growth. *International journal of cancer*, 123(10):2229–2238, 2008. doi:10.1002/ijc.23925.
- [26] B. Depalle, Z. Qin, S. J. Shefelbine, and M. J. Buehler. Influence of cross-link structure, density and mechanical properties in the mesoscale deformation mechanisms of collagen fibrils. *Journal of the mechanical behavior of biomedical materials*, 52:1–13, 2015. doi:10.1016/j.jmbbm.2014.07.008.
- [27] M. K. Gordon and R. A. Hahn. Collagens. *Cell and tissue research*, 339(1):247–257, 2010. doi:10.1007/s00441-009-0844-4.
- [28] J. Myllyharju and K. I. Kivirikko. Collagens, modifying enzymes and their mutations in humans, flies and worms. *Trends in genetics : TIG*, 20(1):33–43, 2004. ISSN 0168-9525. doi:10.1016/j.tig.2003.11.004.
- [29] I. P. Witz. The tumor microenvironment: The making of a paradigm. *Cancer microenvironment : official journal of the International Cancer Microenvironment Society*, 2 Suppl 1:9–17, 2009. doi:10.1007/s12307-009-0025-8.
- [30] C. E. Weber and P. C. Kuo. The tumor microenvironment. *Surgical oncology*, 21(3):172–177, 2012. doi:10.1016/j.suronc.2011.09.001.

- [31] R. Kalluri and R. A. Weinberg. The basics of epithelial-mesenchymal transition. *The Journal of clinical investigation*, 119(6):1420–1428, 2009. doi:10.1172/JCI39104.
- [32] M. J. Paszek *et al.* Tensional homeostasis and the malignant phenotype. *Cancer cell*, 8(3):241–254, 2005. ISSN 1535-6108. doi:10.1016/j.ccr.2005.08.010.
- [33] E. Cukierman and D. E. Bassi. Physico-mechanical aspects of extracellular matrix influences on tumorigenic behaviors. *Seminars in Cancer Biology*, 20(3):139–145, 2010. doi:10.1016/j.semcancer.2010.04.004.
- [34] H. F. Dvorak. Tumors: Wounds that do not heal. *New England Journal of Medicine*, 315(26):1650–1659, 1986. ISSN 0028-4793. doi:10.1056/NEJM198612253152606.
- [35] D. T. Butcher, T. Alliston, and V. M. Weaver. A tense situation: Forcing tumour progression. *Nature reviews. Cancer*, 9(2):108–122, 2009. doi:10.1038/nrc2544.
- [36] M. A. Wozniak, R. Desai, P. A. Solski, C. J. Der, and P. J. Keely. Rock-generated contractility regulates breast epithelial cell differentiation in response to the physical properties of a three-dimensional collagen matrix. *The Journal of cell biology*, 163(3):583–595, 2003. doi:10.1083/jcb.200305010.
- [37] R. Kalluri and M. Zeisberg. Fibroblasts in cancer. *Nature reviews. Cancer*, 6(5):392–401, 2006. doi:10.1038/nrc1877.
- [38] S.-Y. Jeong, J.-H. Lee, Y. Shin, S. Chung, and H.-J. Kuh. Co-culture of tumor spheroids and fibroblasts in a collagen matrix-incorporated microfluidic chip mimics reciprocal activation in solid tumor microenvironment. *PLoS one*, 11(7):e0159013, 2016. ISSN 1932-6203. doi:10.1371/journal.pone.0159013.
- [39] M. Herrera *et al.* Functional heterogeneity of cancer-associated fibroblasts from human colon tumors shows specific prognostic gene expression signature. *Clinical cancer research : an official journal of the American Association for Cancer Research*, 19(21):5914–5926, 2013. ISSN 1078-0432. doi:10.1158/1078-0432.CCR-13-0694.
- [40] M. G. Vander Heiden, L. C. Cantley, and C. B. Thompson. Understanding the warburg effect: The metabolic requirements of cell proliferation. *Science*, 324(5930):1029, 2009. doi:10.1126/science.1160809.

- [41] A. R. Grassian, J. L. Coloff, and J. S. Brugge. Extracellular matrix regulation of metabolism and implications for tumorigenesis. *Cold Spring Harbor symposia on quantitative biology*, 76:313–324, 2011. doi:10.1101/sqb.2011.76.010967.
- [42] S. Y. C. Choi, C. C. Collins, P. W. Gout, and Y. Wang. Cancer-generated lactic acid: A regulatory, immunosuppressive metabolite? *The Journal of pathology*, 230(4):350–355, 2013. doi:10.1002/path.4218.
- [43] A. Brand *et al.* Ldha-associated lactic acid production blunts tumor immunosurveillance by t and nk cells. *Cell metabolism*, 24(5):657–671, 2016. doi:10.1016/j.cmet.2016.08.011.
- [44] O. R. Colegio *et al.* Functional polarization of tumour-associated macrophages by tumour-derived lactic acid. *Nature*, 513(7519):559–563, 2014. doi:10.1038/nature13490.
- [45] C. A. Lyssiotis and A. C. Kimmelman. Metabolic interactions in the tumor microenvironment. *Trends in cell biology*, 27(11):863–875, 2017. ISSN 1879-3088. doi:10.1016/j.tcb.2017.06.003.
- [46] L. Graziano and L. Preziosi. Mechanics in tumor growth. In F. Mollica, L. Preziosi, and K. R. Rajagopal, editors, *Modeling of biological materials*, Modeling and simulation in science, engineering, and technology, pages 263–321. Boston Mass.: Birkhäuser, 2007. ISBN 978-0-8176-4410-9. doi:10.1007/978-0-8176-4411-6{\textunderscore}7.
- [47] T. Stylianopoulos, L. L. Munn, and R. K. Jain. Reengineering the physical microenvironment of tumors to improve drug delivery and efficacy: From mathematical modeling to bench to bedside. *Trends in cancer*, 4(4):292–319, 2018. doi:10.1016/j.trecan.2018.02.005.
- [48] V. L. Cross *et al.* Dense type i collagen matrices that support cellular remodeling and microfabrication for studies of tumor angiogenesis and vasculogenesis in vitro. *Biomaterials*, 31(33):8596–8607, 2010. ISSN 0142-9612.
- [49] K. Stuart and A. Panitch. Influence of chondroitin sulfate on collagen gel structure and mechanical properties at physiologically relevant levels. *Biopolymers*, 89(10):841–851, 2008. ISSN 0006-3525. doi:10.1002/bip.21024.
- [50] R. Q. Erkamp, P. Wiggins, A. R. Skovoroda, S. Y. Emelianov, and M. O’Donnell. Measuring the elastic modulus of small tissue samples. *Ultrasonic imaging*, 20(1):17–28, 1998. ISSN 0161-7346. doi:10.1177/016173469802000102.

- [51] D. Harjanto, J. S. Maffei, and M. H. Zaman. Quantitative analysis of the effect of cancer invasiveness and collagen concentration on 3d matrix remodeling. *PLoS one*, 6(9):e24891, 2011. ISSN 1932-6203. doi:10.1371/journal.pone.0024891.
- [52] S. Kawano *et al.* Assessment of elasticity of colorectal cancer tissue, clinical utility, pathological and phenotypical relevance. *Cancer science*, 106(9):1232–1239, 2015. ISSN 1349-7006. doi:10.1111/cas.12720.
- [53] M. Griffin, Y. Premakumar, A. Seifalian, P. E. Butler, and M. Szarko. Biomechanical characterization of human soft tissues using indentation and tensile testing. *Journal of visualized experiments : JoVE*, (118), 2016. doi:10.3791/54872.
- [54] C. T. McKee, J. A. Last, P. Russell, and C. J. Murphy. Indentation versus tensile measurements of young’s modulus for soft biological tissues. *Tissue engineering. Part B, Reviews*, 17(3):155–164, 2011. ISSN 1937-3376. doi:10.1089/ten.TEB.2010.0520.
- [55] M. Sefidgar and M. Soltani. Interstitial flow in cancerous tissue: Effect of considering remodeled capillary network. *Journal of Tissue Science & Engineering*, 01(S4), 2014. ISSN 21577552. doi:10.4172/2157-7552.S4-003.
- [56] C. P. Ng and M. A. Swartz. Fibroblast alignment under interstitial fluid flow using a novel 3-d tissue culture model. *American journal of physiology. Heart and circulatory physiology*, 284(5):H1771–7, 2003. ISSN 0363-6135. doi:10.1152/ajpheart.01008.2002.
- [57] W. J. Polacheck, J. L. Charest, and R. D. Kamm. Interstitial flow influences direction of tumor cell migration through competing mechanisms. *Proceedings of the National Academy of Sciences of the United States of America*, 108(27):11115–11120, 2011. ISSN 1091-6490. doi:10.1073/pnas.1103581108.
- [58] J. D. Shields *et al.* Autologous chemotaxis as a mechanism of tumor cell homing to lymphatics via interstitial flow and autocrine ccr7 signaling. *Cancer cell*, 11(6):526–538, 2007. ISSN 1535-6108. doi:10.1016/j.ccr.2007.04.020.
- [59] S.-F. Chang *et al.* Tumor cell cycle arrest induced by shear stress: Roles of integrins and smad. *Proceedings of the National Academy of Sciences of the United States of America*, 105(10):3927–3932, 2008. ISSN 1091-6490. doi:10.1073/pnas.0712353105.
- [60] M. Hofmann *et al.* Lowering of tumor interstitial fluid pressure reduces tumor cell proliferation in a xenograft tumor model. *Neoplasia (New York, N.Y.)*, 8(2):89–95, 2006. doi:10.1593/neo.05469.

- [61] G. A. Busby, M. H. Grant, S. P. MacKay, and P. E. Riches. Confined compression of collagen hydrogels. *Journal of Biomechanics*, 46(4):837–840, 2013. ISSN 0021-9290. doi:10.1016/j.jbiomech.2012.11.048.
- [62] B. Lee *et al.* A three-dimensional computational model of collagen network mechanics. *PLoS one*, 9(11):e111896, 2014. ISSN 1932-6203. doi:10.1371/journal.pone.0111896.
- [63] S. Rhee and F. Grinnell. Fibroblast mechanics in 3d collagen matrices. *Advanced drug delivery reviews*, 59(13):1299–1305, 2007. doi:10.1016/j.addr.2007.08.006.
- [64] P. P. Provenzano *et al.* Collagen reorganization at the tumor-stromal interface facilitates local invasion. *BMC medicine*, 4(1):38, 2006. doi:10.1186/1741-7015-4-38.
- [65] W. A. Farahat *et al.* Ensemble analysis of angiogenic growth in three-dimensional microfluidic cell cultures. *PLoS one*, 7(5):e37333, 2012. ISSN 1932-6203. doi:10.1371/journal.pone.0037333.
- [66] C. P. Ng, B. Hinz, and M. A. Swartz. Interstitial fluid flow induces myofibroblast differentiation and collagen alignment in vitro. *Journal of Cell Science*, 118(Pt 20):4731–4739, 2005. doi:10.1242/jcs.02605.
- [67] H. Wiig, K. Rubin, and R. K. Reed. New and active role of the interstitium in control of interstitial fluid pressure: Potential therapeutic consequences. *Acta anaesthesiologica Scandinavica*, 47(2):111–121, 2003. ISSN 0001-5172.
- [68] A. C. Shieh, H. A. Rozansky, B. Hinz, and M. A. Swartz. Tumor cell invasion is promoted by interstitial flow-induced matrix priming by stromal fibroblasts. *Cancer research*, 71(3):790–800, 2011. ISSN 1538-7445. doi:10.1158/0008-5472.CAN-10-1513.
- [69] N. R. Lang *et al.* Biphasic response of cell invasion to matrix stiffness in three-dimensional biopolymer networks. *Acta biomaterialia*, 13:61–67, 2015. ISSN 1878-7568. doi:10.1016/j.actbio.2014.11.003.
- [70] K. L. Billiar. The mechanical environment of cells in collagen gel models. In A. Gefen, editor, *Cellular and Biomolecular Mechanics and Mechanobiology*, vol. 4 of *Studies in Mechanobiology, Tissue Engineering and Biomaterials*, pages 201–245. Berlin, Heidelberg: Springer Berlin Heidelberg, 2011. ISBN 978-3-642-14217-8. doi:10.1007/978-3-642-14217-8_30.
- [71] B. A. Roeder, K. Kokini, J. E. Sturgis, J. P. Robinson, and S. L. Voytik-Harbin. Tensile mechanical properties of three-dimensional type I collagen extracellular

- matrices with varied microstructure. *Journal of Biomechanical Engineering*, 124(2):214, 2002. ISSN 01480731. doi:10.1115/1.1449904.
- [72] R. M. Kuntz and W. M. Saltzman. Neutrophil motility in extracellular matrix gels: Mesh size and adhesion affect speed of migration. *Biophysical journal*, 72(3):1472–1480, 1997. ISSN 1542-0086. doi:10.1016/S0006-3495(97)78793-9.
- [73] A. D. Doyle, N. Carvajal, A. Jin, K. Matsumoto, and K. M. Yamada. Local 3d matrix microenvironment regulates cell migration through spatiotemporal dynamics of contractility-dependent adhesions. *Nature communications*, 6:8720, 2015. doi:10.1038/ncomms9720.
- [74] S. Geraldo *et al.* Do cancer cells have distinct adhesions in 3d collagen matrices and in vivo? *European journal of cell biology*, 91(11-12):930–937, 2012. doi:10.1016/j.ejcb.2012.07.005.
- [75] D. Harjanto, M. H. Zaman, and E. Katz. Modeling extracellular matrix reorganization in 3d environments. *PLoS one*, 8(1):e52509, 2012. ISSN 1932-6203. doi:10.1371/journal.pone.0052509.
- [76] S. P. Palecek, J. C. Loftus, M. H. Ginsberg, D. A. Lauffenburger, and A. F. Horwitz. Integrin-ligand binding properties govern cell migration speed through cell-substratum adhesiveness. *Nature*, 385(6616):537–540, 1997. doi:10.1038/385537a0.
- [77] E. Makareeva *et al.* Carcinomas contain a matrix metalloproteinase-resistant isoform of type i collagen exerting selective support to invasion. *Cancer research*, 70(11):4366–4374, 2010. ISSN 1538-7445. doi:10.1158/0008-5472.CAN-09-4057.
- [78] O. Nagakawa *et al.* Effect of chromogranin a (pancreastatin) fragment on invasion of prostate cancer cells. *Cancer letters*, 147(1-2):207–213, 1999. ISSN 0304-3835.
- [79] O. Nagakawa *et al.* Expression of membrane-type 1 matrix metalloproteinase (mt1-mmp) on prostate cancer cell lines. *Cancer letters*, 155(2):173–179, 2000. ISSN 0304-3835.
- [80] Y. Kato *et al.* Acidic extracellular ph induces matrix metalloproteinase-9 expression in mouse metastatic melanoma cells through the phospholipase d-mitogen-activated protein kinase signaling. *The Journal of biological chemistry*, 280(12):10938–10944, 2005. ISSN 0021-9258. doi:10.1074/jbc.M411313200.

- [81] S. C. Kirkland, K. Henderson, D. Liu, and M. Pignatelli. Organisation and gel contraction by human colonic carcinoma (hca-7) sublines grown in 3-dimensional collagen gel. *International Journal of Cancer*, 60(6):877–882, 1995. ISSN 00207136. doi:10.1002/ijc.2910600626.
- [82] J. Fenner *et al.* Macroscopic stiffness of breast tumors predicts metastasis. *Scientific reports*, 4:5512, 2014. ISSN 2045-2322. doi:10.1038/srep05512.
- [83] P. P. Provenzano, D. R. Inman, K. W. Eliceiri, S. M. Trier, and P. J. Keely. Contact guidance mediated three-dimensional cell migration is regulated by rho/rock-dependent matrix reorganization. *Biophysical journal*, 95(11):5374–5384, 2008. ISSN 1542-0086. doi:10.1529/biophysj.108.133116.
- [84] C. Gaggioli *et al.* Fibroblast-led collective invasion of carcinoma cells with differing roles for rhoGTPases in leading and following cells. *Nature cell biology*, 9(12):1392–1400, 2007. ISSN 1465-7392. doi:10.1038/ncb1658.
- [85] A. MichaelV. Human colon cancer and fibroblast cell lines cultured in and on collagen gels. *Australian and New Zealand Journal of Surgery*, 59(5):415–420, 1989. ISSN 0004-8682. doi:10.1111/j.1445-2197.1989.tb01598.x.
- [86] T. Kobayashi *et al.* Matrix metalloproteinase-9 activates tgf-b and stimulates fibroblast contraction of collagen gels. *American journal of physiology. Lung cellular and molecular physiology*, 306(11):L1006–15, 2014. doi:10.1152/ajplung.00015.2014.
- [87] M. Egeblad, M. G. Rasch, and V. M. Weaver. Dynamic interplay between the collagen scaffold and tumor evolution. *Current opinion in cell biology*, 22(5):697–706, 2010. doi:10.1016/j.ceb.2010.08.015.
- [88] S. A. Mani *et al.* The epithelial-mesenchymal transition generates cells with properties of stem cells. *Cell*, 133(4):704–715, 2008. doi:10.1016/j.cell.2008.03.027.
- [89] K. Wolf *et al.* Physical limits of cell migration: Control by ecm space and nuclear deformation and tuning by proteolysis and traction force. *The Journal of cell biology*, 201(7):1069–1084, 2013. doi:10.1083/jcb.201210152.

Appendix A

Characterization of Mechanical Properties of Collagen Gel

Measurement of the rupture stress, depression depth at failure and elasticity of an agar... Page 1 of 3



REF: GEL3/PK
Issued: June 12

Application Study for

TA.XT^{plus} TA.HD^{plus} TA.XT^{Express}

Product: AGAR GEL
Objective : Measurement of the rupture stress, depression depth at failure and elasticity of an agar gel

Introduction

There is reference to the Kobe method in Industrial Gums, Polysaccharides and Their Derivatives, 3rd Edition, Edited by Roy L. Whistler and James N. BeMiller - Chapter 5, Agar, H. H. Selby & Roy L. Whistler, p87 – 104

Page 101 explains the sample preparation and test from which this project has been prepared.

"A 1cm2 cylindrical plunger is pressed into the gel without lateral movement at 2mm/s. Load and depth of gel depression are simultaneously recorded to rupture. Rupture stress is a measure of strength; depression depth at failure varies as tenacity; and curve slope is a function of elasticity."

TA Settings:	<i>Mode:</i>	Measure Force in Compression
	<i>Option:</i>	Return to Start
	<i>Pre-Test Speed:</i>	1.0 mm/s
	<i>Test Speed:</i>	2.0 mm/s
	<i>Post-Test Speed:</i>	10.0 mm/s
	<i>Target Mode:</i>	Distance
	<i>Distance:</i>	15 mm (or greater to cause rupture)
	<i>Trigger Type:</i>	Auto - 3g
	<i>Tare Mode:</i>	Auto
	<i>Data Acquisition Rate:</i>	500pps

LOAD PROJECT

Accessory: 1cm2 Kobe Probe ([P/1KD](#) or [P/1KSS](#)) using a 5 kg load cell

Sample Preparation:

Fill 65ml ointment jars to the 50ml level with a 1.6% solids solution at a 45 degree angle. Seal and store for 1 hour in a stirred water bath at 19.5-20.5 degrees C.

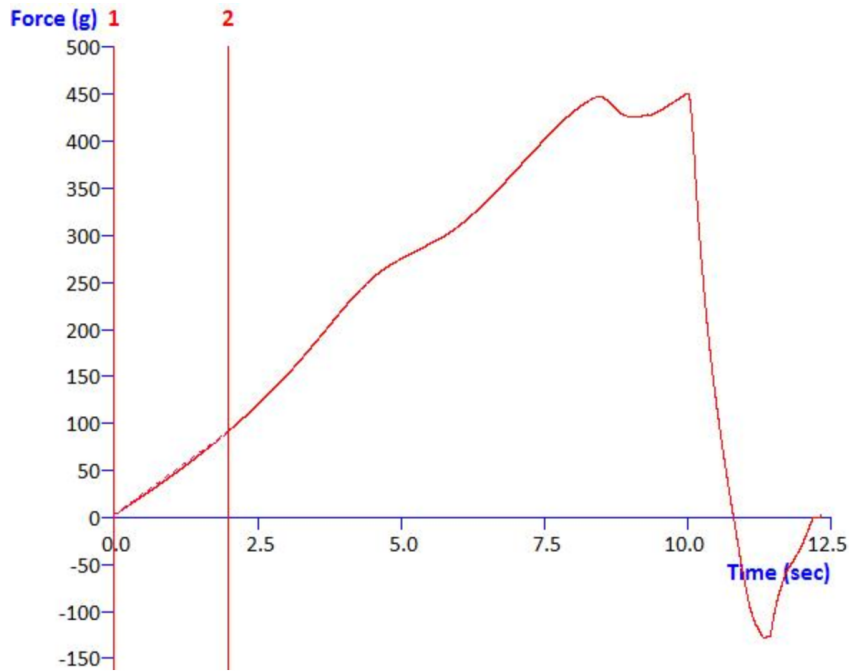
Test Set Up:

Remove a jar from the water bath just prior to testing and position centrally under a 1cm2 cylindrical probe (Kobe Probe). Commence the test.

Test Settings:

The sample must rupture in this test. A distance of 15mm is set in this project. If this is not enough to cause the sample to rupture simply increase this value.

mk:@MSITStore:C:\Program%20Files%20(x86)\Exponent\Teguide.chm::/GEL3_PK.... 15.09.2017



Observations:

The test begins with the probe moving at the pre-test speed. When the probe reaches the surface of the gel and the trigger force is reached the probe speed changes to the test speed and data is recorded. As the probe deflects the gel the force increases until the sample ruptures. The peak force is recorded as the Rupture Stress or Gel strength at Failure and the distance to rupture is recorded as the Depression Depth at Failure. The gradient is taken at the initial linear region of the curve and recorded as 'Elasticity'.

Data Analysis:

Once tests have been performed, values of particular interest for sample analysis can be automatically obtained by a MACRO, e.g.

Clear Graph Results
 Redraw
 Search Forwards
 Go to Min. Time
 Drop Anchor
 Advance Cursor 2s
 Drop Anchor
 Gradient 'Elasticity'
 Go to Abs. +ve Value Force
 Mark Value Force Rupture Stress/Gel Strength at Failure
 Mark Value Distance Depression Depth at Failure

This macro is a general example for the analysis of a curve such as the one above. Any changes made to the test parameters or significant differences to the shape of the curve profile may require optimisation of this

Measurement of the rupture stress, depression depth at failure and elasticity of an agar... Page 3 of 3

macro.

The macro may also include analytical features which are not present in all versions of Stable Micro Systems software. The above macro is supported by:



N.B. This application study has been designed for a specific sample(s) and it therefore must be noted that any deviation from this sample in terms of sample size, shape, formulation etc. may cause large deviations or indeed may require a different testing method.

Copyright 2002-2016 Stable Micro Systems Ltd. All Rights Reserved
Stable Micro Systems Ltd, Vienna Court, Lammas Road, Godalming, Surrey, UK. GU7 1YL
Tel: +44 1483 427345. Fax: +44 1483 427600
<http://www.stablemicrosystems.com>
Support: app.support@stablemicrosystems.com

FIGURE 1: Measurement of Young's Modulus with Kobe method. Image from data library of Texture Analyser. Property of Stable Micro Systems

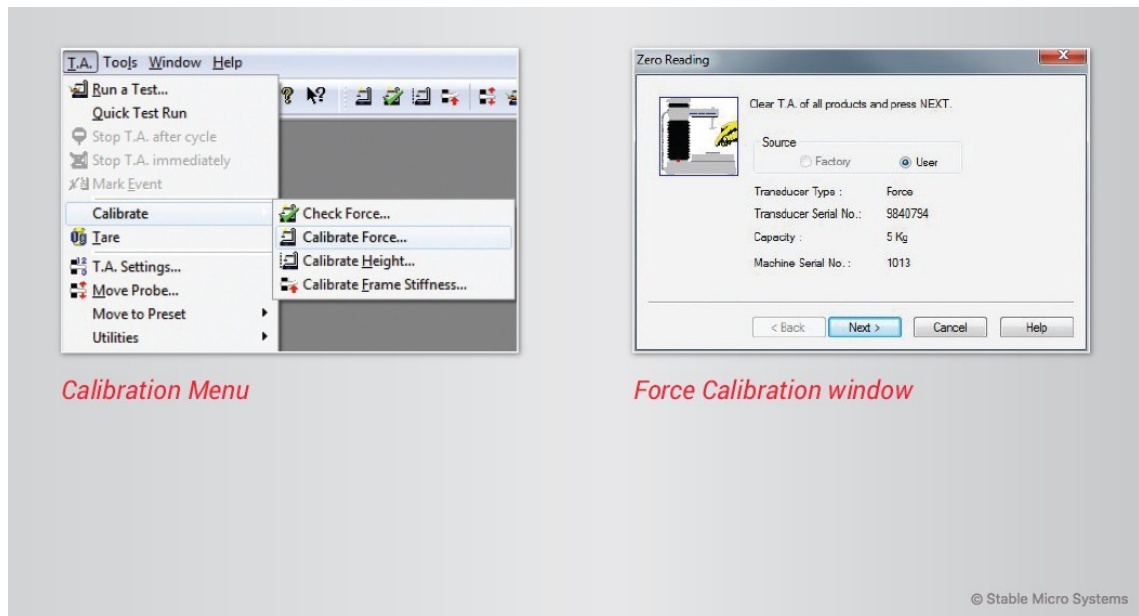


FIGURE 2: Texture Analyser calibration of height and force. Image from Texture Analyser. Property of Stable Micro Systems

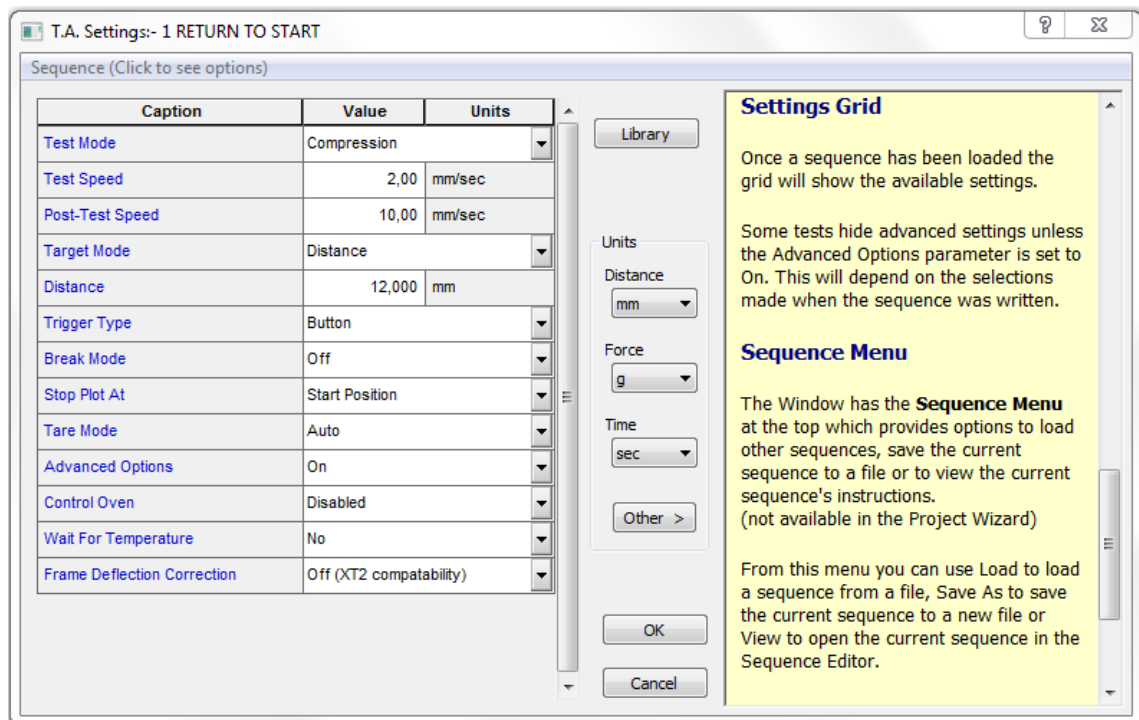


FIGURE 3: Texture Analyser test settings. Image from Texture Analyser. Property of Stable Micro Systems

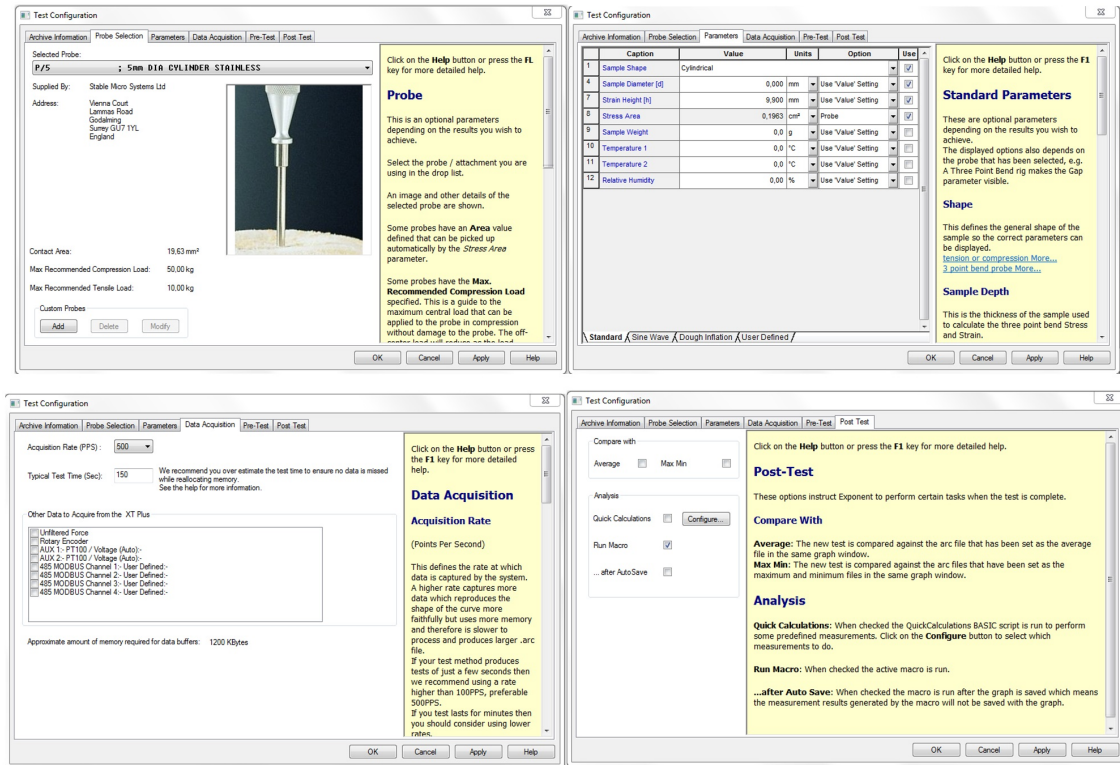


FIGURE 4: Texture Analyser test configuration. Image from Texture Analyser. Property of Stable Micro Systems

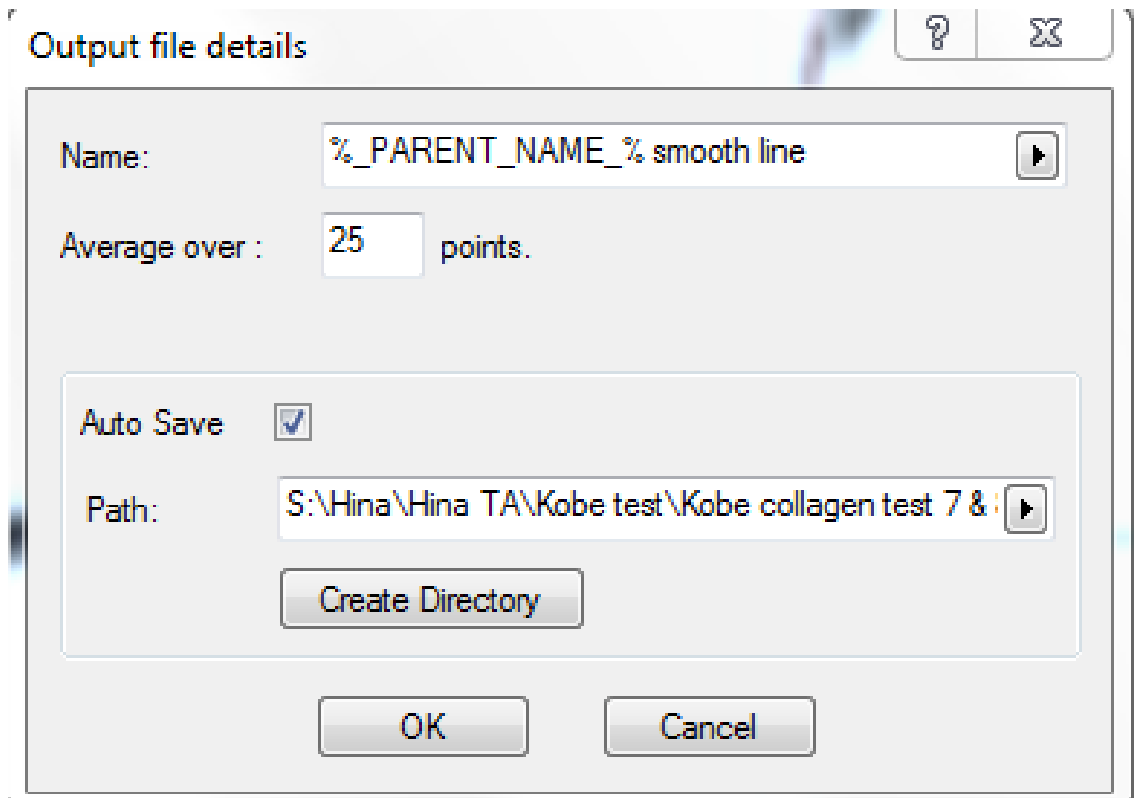


FIGURE 5: Texture Analyser test smooth line feature. Image from Texture Analyser. Property of Stable Micro Systems

Command	Program	Flags	Comment
Mark Value	1: Clear Graph Results		
Drop Anchor	2: Redraw		
Select Anchor	3: Search Forwards		
Search Forwards	4: Change X Axis Type Distance		
Search Backwards	5: Go to Min. Time		
Go to Min. Time	6: Go to Distance 5,794 mm		
Go to Max. Time	7: Drop Anchor		
Set Threshold	8: Go to Distance 5,954 mm		
Go to Peak +ve Value	9: Drop Anchor		
Go to Peak -ve Value	10: Gradient(Active vs Active) As Gradient	R g	
Area	11: Go to Absolute +ve Value Force Current Units	A	
Gradient	12: Mark Value(Stress (g/cm ²)) As Stress	R g	
Mean	13: Mark Value(Distance (Current Units)) As Depression Depth at Failure	R g	
	14: Mark Value(Force (Current Units)) As Depression rupture force	R g	
	15: Open Chart Window %_PARENT_FOLDER_%Chart template.vtc	-F	
	16: Open Chart Window %_PARENT_FOLDER_%Chart template 2.vtc	-F	
	17: Open Chart Window %_PARENT_FOLDER_%Chart template 3.vtc	-F	

FIGURE 6: Texture Analyser Youngs’s Modulus test macro settings. Image from Texture Analyser. Property of Stable Micro Systems

Young's Modulus

In order to calculate the Modulus the Stress and the Strain need to be calculated.
 Stress (Compression) = Force (N) / Area (Cross sectional area of the probe (m²))
 Strain (Compression) = Distance compressed (mm) / Height of sample (mm)

The archive files that you have already obtained may not have this information previously added. You need to add this information to the file.

For example:

It has been noted that an 8 mm Perspex probe has been used. This is not a standard probe but the cross sectional area is calculated as being 50.3 mm². There is no indication of the height of the sample so a nominal height of 10 mm has been used. If the true height is known then this should be substituted.

In put these values into the file as follows;

Menu - View - InfoList and tick

A blue box appears underneath the graph.

Choose the second Tab - Parameters and the box will turn pale yellow.

Double Click with the mouse anywhere in the box and a Parameters window appears (see below).

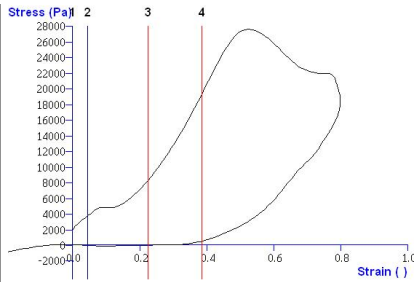
Type 50.3 in the Contact Area and type 10 in the Product Height. Make sure the right hand boxes (Use) are ticked.

1	2	3	4	5	6	7	8
1	2	3	4	5	6	7	8
Contact Area	50.3	mm ²		<input checked="" type="checkbox"/>			
Product Width	0	mm		<input type="checkbox"/>			
Product Length	0	mm		<input type="checkbox"/>			
Product Height	10	mm		<input checked="" type="checkbox"/>			
Delta 1	0	°C		<input type="checkbox"/>			
Delta 2	0	°C		<input type="checkbox"/>			
Product Weight	0	kg		<input type="checkbox"/>			
Relative Humidity	0	%		<input type="checkbox"/>			

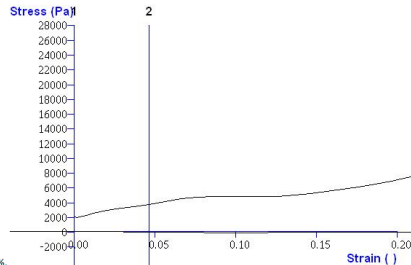
Now click on OK and the values will appear in the yellow box.

Now look at the graph. Change the vertical axis to units of Stress (Pa) and change the horizontal axis to units of Strain (%).

The Graph looks like the one below.



Modulus is the slope of the line of Stress and Strain and with a pure elastic material it should be a straight line through the origin. The graph above does not show a good straight line through the origin so a compromise must be found. Consider a parameter called Initial Modulus. This value is at the beginning of the curve and is probably the closest value to the Young's Modulus. Note that the graph above is measured in compression and Young's Modulus is conventionally measured in tension.



By zooming in to the curve there seems to be a linear part between 0 and 5%.

By zooming in to the curve there seems to be a linear part between 0 and 5%.

Initial Modulus Macro - LOAD MACRO

After a bit of a bump at around 10% Strain there is another linear region between 30% Strain and 70% Strain. This could be considered to be the High Strain Modulus. A macro to calculate this is detailed below.

High Strain Modulus Macro - LOAD MACRO

The two macros can be combined to measure both results at the same time if both results are required for comparison.

Initial and High Strain Macro - LOAD MACRO

FIGURE 7: Texture Analyser Young's Modulus test macro project. Image from data library of Texture Analyser. Property of Stable Micro Systems

Appendix B

Interstitial Fluid Flow and Cell Migration Analysis in 3D Model

Parameters	Units						Average
Time	T (min)	0	30	60	90	120	
Time	T (sec)	0	1800	3600	5400	7200	
Volume channel 1	V1 (ml)	1	0,82	0,76	0,66	0,6	
Volume channel 2	V2 (ml)	0,22	0,4	0,46	0,5	0,52	
Height channel 1	H1 (mmH2O)	56	46	42	37	33	
Height channel 2	H2 (mmH2O)	12	22	26	28	29	
Radius of syringe	R (mm)	2,39					
Δ in vol. btw channels	ΔV (ml)	0,78	0,42	0,30	0,16	0,08	
Δ in pressure btw channels	ΔP (pa)	-426	-230	-164	-87	-44	
Initial Flow	Q_i (m ³ /sec)		2,00E-10	3,33E-11	2,59E-11	1,11E-11	
Viscosity of DMEM media	μ (Pa.s)	0,00078					
Length of channel	L (m)	0,0013					
Cross sectional area of gel sec.	A (m ²)	2,60E-06					
Permeability of collagen	K (m ²)		-3,40E-13*	-7,93E-14	-1,16E-13	-9,91E-14	-9,80E-14
Volumetric Flow rate	Q_f (m ³ /sec)	1,07E-10	5,77E-11	4,12E-11	2,20E-11	1,10E-11	
Velocity	Q_f (m/sec)	4,12E-05	2,22E-05	1,58E-05	8,45E-06	4,23E-06	
Velocity	Q_f (μ m/sec)	41,2	22,2	15,8	8,5	4,2	

* Ignored the first K value due to high pressure drop variations when calculating the average

FIGURE 8: Fluid flow test calculations for initial flow, permeability and volumetric flow rate of 4 mg/ml collagen gel

Test Condition	Number of Migrated Cells per Section													Sum	SD
	1	2	3	4	5	6	7	8	9	10	11	12	13		
2 mg/ml with FB and SW948 control	10	14	6	27	22	23	18	21	30	33	23	44	16	287	9.75
2 mg/ml with FB and SW948 Flow	101	36	13	17	22	350	38	69	32	52	17	2	12	733	89.36
2 mg/ml with FB and SW1116 control	3	22	7	28	0	3	10	22	7	4	22	27	36	191	11.37
2 mg/ml with FB and SW1116 Flow	0	27	6	18	19	27	17	18	92	52	31	21	23	350	22.10

FIGURE 9: Interstitial fluid flow cell migration test calculations